

國立交通大學

電信工程學系

博士論文

高頻、高品質因素
及低相位雜訊壓電振盪器之研究

Investigation of High Frequency,
High Quality Factor and Low Phase Noise
Oscillators with Piezoelectric Resonators

研究生：林炯宏

指導教授：高曜煌

中華民國九十八年一月

高頻、高品質因素及低相位雜訊壓電振盪器之研究

Investigation of High Frequency, High Quality Factor
and Low Phase Noise Oscillators with Piezoelectric
Resonators

研究生：林炯宏

Student: Jon-Hong Lin

指導教授：高曜煌 博士

Advisor: Dr. Yao-Huang Kao

國立交通大學

電信工程學系

博士論文

A Dissertation

Submitted to Institute of Communication Engineering
College of Electrical and Computer Engineering

National Chiao Tung University

in Partial Fulfillment of the Requirements
for the Degree of Doctor of Philosophy

in

Communication Engineering

Hsinchu, Taiwan

2009 年 1 月

高頻、高品質因素及低相位雜訊壓電振盪器之研究

學生：林炯宏

指導教授：高曜煌 博士

國立交通大學電信工程學系博士班

摘 要

在高速數位通訊系統中，為解決不同傳輸速率設備間訊號之連結與訊號在長距離傳輸後之衰減，系統之寬頻收發器須具備時脈恢復電路對訊號作頻率轉換及波形重整以維持資料完整性。上述電路中均須使用高性能之壓控振盪器，因此具高穩定性之高品質因素壓控壓電振盪器成為最佳選擇。若以壓電共振器的製程限制及工作頻率來區分，當工作振盪頻率低於 200 MHz 時，石英晶體共振器為最佳選擇；當工作頻率低於 3000 MHz 時，表面聲波共振器(SAWR)為目前主流元件；而薄膜體波共振器(FBAR)則適用於微波頻段。

本論文共提出四種高品質因素壓電振盪器，分別為：2488 MHz 壓控聲橫波(STW)振盪器，2488 MHz 壓控薄膜體波(FBAR)振盪器，622 MHz 修正式皮爾斯(Pierce)振盪器及 433 MHz 平衡式表面聲波(SAW)振盪器。

本文中 2488 MHz 壓控聲橫波振盪器之可調頻率範圍可達 ± 200 ppm，其相位雜訊在 100 kHz 偏移時，相較於一般市售同類產品低 8 分貝；在振盪器設計階段藉由分析元件的殘餘相位雜訊(residual phase noise)，發現聲橫波共振器為本振盪器主要雜訊來源，而非主動元件。振盪器之相位雜訊可經由元件之殘餘相位雜訊及回路轉換函數預測且預測值與量測結果相當接近。本 2488 MHz 壓控薄膜體波振盪器之可調頻率範圍可達 $\pm 6\%$ ，其振盪頻率之溫度係數大約為 -34.5 ppm/ $^{\circ}\text{C}$ 。

我們藉由在傳統皮爾斯振盪器之回授 π 電路上增加一相移器來降低回授電路之插入損失，以改善其在高頻應用不易起振之缺點。本振盪器核心電路僅銷耗

+1.2V, 10.2 mA，其相位雜訊在距中心載波 10 kHz 處可達-136 dBc/Hz。

我們藉由一般商用表面聲波共振器來製作平衡式表面聲波振盪器，其對偶特性經由量測獲得驗證，並增加一 180 度反相功率耦合器來完成 push-push 架構振盪器，其相位雜訊相對於單端輸出可獲 6 分貝之改善。




Investigation of High Frequency, High Quality Factor and Low Phase Noise Oscillators with Piezoelectric Resonators

Student : Jon-Hong Lin

Advisors : Dr. Yao-Huang Kao

Institute of Communication Engineering
National Chiao Tung University

ABSTRACT



The increasing demand for high speed digital communication applications motivates a growing interest in the high data rate transceivers. In these transceivers, clock recovery circuits are used for data integrity. The clock is usually extracted from a phase-lock-loop circuit with low phase noise voltage-controlled oscillator (VCO). For the requirements on the high frequency and low phase noise voltage-controlled oscillators, the highly stable VCOs with piezoelectric resonators are the hopeful candidates. In the frequency below 200 MHz, the crystal resonators are the best choice. In the ultrahigh-frequency (UHF) band, surface acoustic wave resonators (SAWR) play the important roles now. In the band of UHF and microwave frequency, the film bulk acoustic resonators (FBAR) are the future stars. There are four different types oscillators are presented in this thesis. They are VCO with STW resonator, VCO with FBAR, modified Pierce SAW oscillator, and balanced SAW oscillator.

Both the surface transverse wave (STW) resonator and FBAR are applied for the low phase noise 2488 MHz voltage-controlled oscillators. The tuning ability of the 2488 MHz voltage-controlled oscillator with STW resonator achieves ± 200 ppm and

its phase noise performance is 8 dB better than the other commercial products at offset 100 kHz frequency. The white phase-noise floor is about -170 dBc/Hz. In the design phase of the oscillator with STW resonator, by examining the residual phase noises of the main components in the oscillator, we found that the STW resonator dominates the phase noise of the oscillator, instead of active devices. The behavior of the phase noise of the oscillator is shaped by the important factor of group delay. The tuning capability of the voltage-controlled FBAR oscillator achieves $\pm 6\%$. The temperature coefficients factor is about -34.5 ppm/ $^{\circ}\text{C}$ which is dominated by FBAR.

An extra phase shifter is used to reduce the insertion loss of the π -feedback network in the conventional Pierce SAW oscillator. The modified Pierce oscillator provides 4.0dBm of output power and the core circuit consumes 10.2 mA from +1.2V DC power supply. The phase noise level of the oscillator is approximately -136 dBc/Hz at 10 kHz offset.

With a popular commercial one-port SAW resonator, the behavior of the balanced SAW oscillator is presented. The balanced SAW oscillator provides pure antiphase signals without balun. By using an 180° power combiner, a push-push topology SAW oscillator is presented and results in 6dB phase noise improvement in comparison with the single-end output.

誌 謝

長時間在職場工作後，心中漸漸有被掏空的感覺，體會到再進修的必要，在內人的支持下暫別職場來到交大。非常感謝高曜煌教授這幾年的指導與教誨，除學習高頻電路及積體電路的知識外，還有機會一窺壓電振盪器設計的堂奧。學習的過程雖然艱辛，也充滿了挑戰與挫折，但在師長及同學的陪伴協助下，最終否極泰來，心靈與知識也在磨練中更上一層樓。

我要感謝立朗科技、台灣晶技、台灣嘉碩及希華晶體等幾家公司在我求學期間所提供的表面聲波元件、製程及量測設備，尤其要感謝吳朗教授讓我在立朗科技任職期間能有機會以材料的觀點來重新認識壓電材料特性及表面聲波元件。同時要感謝 Dr. B. Temple (Agilent Technology, Spokane, WA) 協助驗證量測系統及比對振盪器量測結果並提供相當多有關於雜訊量測的寶貴經驗。

我還要感謝國家晶片中心(CIC)提供晶片設計及製作的環境，讓晶片能順利製作完成；並感謝中科院提供的 FBAR 的設計、量測與製程，讓我有機會接觸到 FBAR 並完成壓控振盪器的製作。

最後，我要感謝一直在背後默默支持的內人，沒有她的支持，我就沒有辦法順利完成學業。並在此衷心祝福所有陪伴我走過求學之路的師長、同學及朋友。

林炯宏

書於風城

2009 年 1 月

目 錄

中文摘要	i
英文摘要	iii
誌謝	v
目錄	vi
表目錄	viii
圖目錄	ix
Chapter 1	Introduction.....	1
1.1	Motivation.....	1
1.2	Feedback Loop Oscillators with Piezoelectric Resonators.....	3
1.3	Modified Pierce Oscillator with One-port SAW Resonator.....	4
1.4	Balanced Oscillator with One-port SAW Resonator.....	5
1.5	Organization of this thesis.....	5
Chapter 2	Feedback Loop Oscillators with Piezoelectric Resonators....	7
2.1	Piezoelectric Resonators.....	7
2.1.1	SAW Resonators.....	7
2.1.2	Film Bulk Acoustic Resonators.....	9
2.2	Voltage-Controlled Oscillator with STW Resonator.....	13
2.2.1	Design Method.....	13
2.2.2	STW Resonator.....	14
2.2.3	Loop Amplifier.....	18
2.2.4	Power Splitter.....	18
2.2.5	Electronic Phase Shifter.....	19
2.2.6	Oscillator Performance.....	20
2.3	Voltage-Controlled Oscillator with FBAR Resonator.....	25
2.3.1	FBAR Design and Fabrication.....	26
2.3.2	Oscillator Design.....	31
2.3.3	Measurement and Discussion.....	33
Chapter 3	Measurement and Prediction of Phase Noise in Oscillator with STW Resonator.....	36
3.1	Introduction.....	36
3.2	Residual Phase Noise of Devices.....	37
3.2.1	Residual Noise.....	37
3.2.2	Measurement Process of Residual Phase Noise.....	39
3.2.3	Residual Phase Noise of Main Components in Oscillator.....	41
3.3	Absolute Phase Noise of Oscillators.....	44
3.3.1	Phase techniques of absolute phase noise measurements.....	45
3.3.2	Theory of FM discriminator.....	48
3.3.3	Frequency Discriminator System Setup.....	51
3.4	Prediction of Phase Noise.....	53

Chapter 4	Modified Pierce Oscillator with One-port SAW Resonator..	58
4.1	Introduction.....	58
4.2	One-port SAW Resonator.....	59
4.3	Oscillator Design.....	60
4.4	Oscillator Performance.....	68
Chapter 5	Balanced Oscillator with One-port SAW Resonator.....	72
5.1	Introduction.....	72
5.2	Oscillator Design.....	72
5.3	Measurement and Discussion.....	77
Chapter 6	Conclusions.....	84
References	86



表 目 錄

2.1	Measured results for the voltage-controlled STW oscillator and comparison with the other commercial products.....	23
2.2	Physical properties of representative materials for FBAR.....	27
2.3	Measured results for the FBAR oscillator.....	33
4.1	Measurement results for the SAW oscillator.....	68
5.1	Parameters of the transistor.....	74
5.2	Performance of balanced SAW oscillator.....	77
5.3	Harmonics before and after the 0° or 180° power combiner.....	82



圖 目 錄

1-1	Frequency translation circuit.....	3
1-2	Clock recovering circuit.....	4
2-1	(a) Structure, and (b) equivalent circuit model for one-port SAW resonator.....	8
2-2	(a) Structure, and (b) equivalent circuit model for two-port SAW resonator.....	9
2-3	Thin film resonator configurations (a) membrane formed by etching a VIA in the substrate. (b) air gap isolated resonator. (c) solidly mounted resonator (SMR) using a reflector array to isolate the resonator from the substrate.....	10
2-4	Butterworth Van Dyke (BVD) equivalent circuit.....	12
2-5	Block diagram of a feedback loop oscillator.....	14
2-6	(a) Picture, and (b) structure of the STW Resonator, (c) insertion loss from 2468 to 2508 MHz, and (d) insertion loss and transmission phase responses 2486.32 - 2490.32 MHz.....	16
2-7	Wilkinson power splitter.....	18
2-8	Electronic phase shifter.....	19
2-9	Total phase shifter and the open loop gain at the oscillation frequency.....	20
2-10	(a) Measured output spectrum for the 2488.32 MHz and (b) harmonics spectrum.....	21
2-11	Dependence of the oscillation frequency on tuning voltage.....	22
2-12	Dependence of the oscillation frequency on temperature.....	23
2-13	Measured phase noise spectrum for the oscillator with STW resonator.....	24
2-14	Process flow of FBAR.....	27
2-15	Picture for the film bulk acoustic resonator.....	29
2-16	Cross-sectional SEM photograph of (002)-oriented AlN film with SiN _x buffer layer (a) 30000X, (b) 60000X.....	29
2-17	Z-parameters of the FBAR.....	31
2-18	Block diagram of a feedback loop oscillator.....	32
2-19	Results of linear simulation using ADS.....	32
2-20	(a) Output fundamental spectrum, and (b) harmonics spectrum for the oscillator.....	34
2-21	Measured variation of fundamental frequency with temperature for FBAR and oscillator.....	35
2-22	Output frequency vs. tuning voltage.....	35
3-1	Additive noise component.....	38
3-2	Multiplicative noise component.....	38
3-3	The basic setup for residual phase noise measurement.....	40

3-4	The E5503B connection diagram for residual phase noise measurement.....	40
3-5	Measured noise floor for residual phase noise measurement system.....	41
3-6	Residual phase noise of STW resonator.....	42
3-7	Residual phase noise of loop amplifier.....	43
3-8	Residual phase noise of electronic phase shifter.....	44
3-9	General block diagram described in NIST technical note 1337.....	46
3-10	Basic block diagram for frequency discriminator.....	48
3-11	Connect diagram of Agilent E5503B for FM discriminator technique.....	52
3-12	The measured system noise floor and the null points for FM discriminator.....	53
3-13	Measured phase noise for the 2488.32 MHz STW oscillator.....	54
3-14	The open loop gain and phase shift of the STW oscillator at the oscillation frequency.....	55
3-15	Transfer functions in open loop circuit.....	55
3-16	The transfer function vs. Fourier frequency.....	57
4-1	Conventional Pierce oscillator.....	58
4-2	Equivalent circuit for SAW resonator.....	60
4-3	Reactance of SAW resonator.....	60
4-4	Phase shift and insertion loss of open-loop simulation for conventional Pierce oscillator.....	62
4-5	Modified pierce oscillator.....	63
4-6	Phase shift and insertion loss of open-loop simulation for Modified Pierce oscillator.....	63
4-7	The ABCD matrix for T-circuit.....	65
4-8	The ABCD matrix for π -circuit.....	65
4-9	The 90 degree phase shifter at 622.08 MHz.....	65
4-10	Circuit diagram of active device of SAW oscillator.....	66
4-11	Results of linear simulation using ADS.....	67
4-12	Picture of the active part of the SAW oscillator.....	68
4-13	(a) Fundamental spectrum, and (b) harmonics spectrum of oscillator.....	69
4-14	Phase noise comparison for different SAW oscillators.....	70
5-1	Oscillator with one-port SAW resonator.....	73
5-2	Equivalent circuit model for one-port SAW resonator.....	73
5-3	Balanced Oscillator with one-port SAW resonator.....	75
5-4	Principle of push-push oscillator.....	76
5-5	Photograph of balanced SAW oscillator.....	77
5-6	Circuit diagram of balanced SAW oscillator with ASK switch..	78
5-7	Measured output waveforms of the balanced SAW oscillator....	79

5-8	Harmonic spectrum of the output Q+.....	80
5-9	Harmonic spectrum of the output Q-.....	80
5-10	Harmonic spectrum of the subtraction (Q+, Q-).....	81
5-11	Harmonic spectrum of the sum (Q+, Q-).....	81
5-12	Measured phase noise of SAW oscillator at 433 MHz.....	83



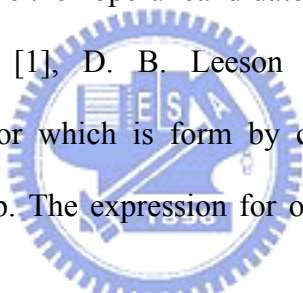
Chapter 1

Introduction

1.1 Motivation

The increasing demand for high speed wire (or wireless) communication applications, such as optical communications, cellular phone, wireless data networks, global positioning systems, etc., motivates a growing interest in the high data rate transceivers. In these transceivers, clock recovery circuits are used for data integrity. The clock is usually extracted from a phase-lock-loop circuit with low jitter voltage-controlled oscillator (VCO). For the requirements, the highly stable VCOs with piezoelectric resonators are the hopeful candidates.

In a benchmark letter [1], D. B. Leeson summarized the phase noise characteristics of the oscillator which is form by cascading the amplifier with a resonator and closing the loop. The expression for oscillator single side band noise from Leeson is


$$L(f_m) = 10 \log \left[\frac{1}{2} \left(1 + \left(\frac{f_0}{2Q_l f_m} \right)^2 \right) \left(\frac{f_c}{f_m} + 1 \right) \frac{FkT}{P_s} \right] \quad (1.1)$$

Where

Q_l = loaded quality factor of the resonator

F = effective noise factor

P_s = signal level at the oscillator active element input

f_m = offset frequency

f_c = flicker frequency

f_0 = center frequency

k = Boltzmann's constant

T = temperature

According to Leeson's model above, we can find the parameters which include Q_l , P_S , F , and f_c are important when designing the low phase noise oscillator. For low phase noise design, the piezoelectric resonators which normally have high quality factor are chosen as the tanks of the oscillators in UHF band.

The existence of the surface acoustic wave (SAW) was first discussed in 1885 by Lord Rayleigh. [2] Till 1965, White suggested that SAWs can be excited and detected efficiently by using an inter-digital transducer (IDT) placed on the piezoelectric substrate. [3] This is because very fine IDTs can be mass-produced by using photolithography, which has been well developed for semiconductor device fabrication, and proper design of the IDT enables the construction of transversal filters with outstanding performance. [4] The width of the IDT is proportional to the velocity of the acoustic wave. The wave velocity and the resolution of the photolithography are the important limits for the mass production SAW devices. For example, quartz is widely used to fabricate the resonators for use in stable oscillators because of its low temperature coefficient. The wave velocity in quartz is about 3100 m/s for Rayleigh wave mode. The width of the IDT which is about quarter wavelength of acoustic wave will be as fine as $0.31\mu\text{m}$ for 2500 MHz SAW devices. This width is much smaller than the resolution of photolithography which is about $0.5\mu\text{m}$ for mass production SAW devices. [5] It needs high investments in the fabricated equipments to achieve this resolution. So, several higher wave velocity materials and wave modes are developed in recent years. Here, we present four types of oscillators for different piezoelectric resonators application. They are 2488 MHz voltage-controlled oscillator with surface transverse wave (STW) resonator, 2488 MHz voltage-controlled oscillator with film bulk acoustic resonator (FBAR), 622 MHz modified Pierce oscillator with one-port SAW resonator, and balanced oscillator with one-port SAW resonator.

1.2 Feedback Loop Oscillators with Piezoelectric Resonators

For Synchronous Optical Network (SONET) Optical Carrier level 12 (OC-12) applications, the VCOs were mostly fabricated at 622 MHz either by the fourth harmonic of 155 MHz crystal oscillator (VCXO) or directly 622 MHz SAW oscillator (VCSO). For OC-48 applications which are shown in Fig. 1-1 and Fig. 1-2, due to the availability of high frequency and high quality resonator, the VCOs were mostly fabricated at 2488 MHz by the fourth harmonic of 622 MHz SAW oscillator (VCSO). [6, 7] But it will suffer from the degradation factor of $20\log N = 12\text{dB}$ on the phase noise as applications to OC-48. Seldom studies on 2488 MHz have been presented. [8-10] To fulfill this requirement, the STW resonator and the FBAR working directly at 2488.32 MHz are developed for the tanks of the VCOs.

The high-Q STW resonator on quartz was demonstrated in 1987 [11]. Its advantages over the conventional Rayleigh waves are the very high velocity and low propagation loss [4]. The wave velocity of STW is approximately 5000m/s. High wave velocity makes the width of IDT larger and then reduces the requirement of the photolithography process. A coupled-mode resonator with unloaded $Q = 5500$ has been carefully designed to accommodate the request of wide band tuning and low phase noise applications. By using this STW resonator, a STW resonator based oscillator was developed in response to SONET OC-48 application.

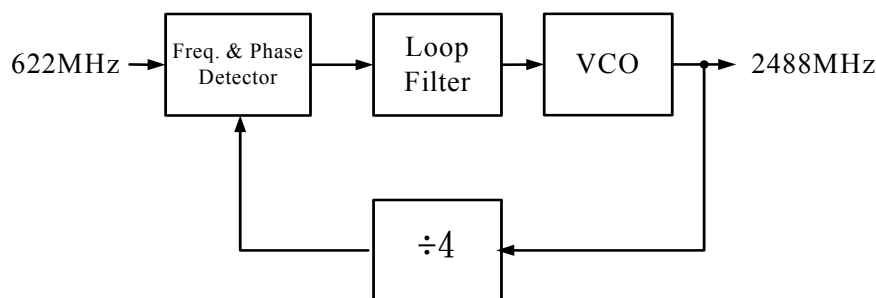


Fig. 1-1 Frequency translation circuit.

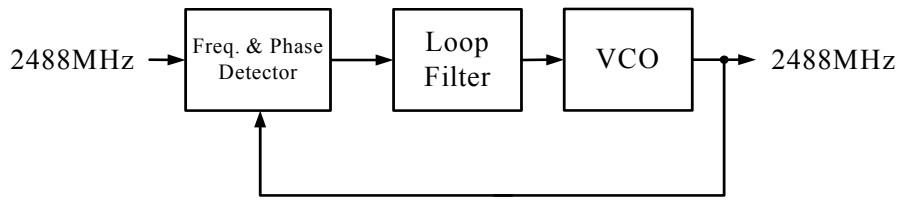


Fig. 1-2 Clock recovering circuit.

After the success on the development of 2488 MHz voltage-controlled oscillator with STW resonator, we try to use the FBAR to replace the STW resonator. Because the high investments in the fabrication equipments for the SAW resonator which working at the frequency above 2500 MHz, the FBAR is the hopeful candidate for the resonators used in microwave oscillators. A 2488 MHz FBAR based on AlN thin film process was developed for this work. By using this resonator, a FBAR based oscillator was developed in response to SONET OC-48 application.

1.3 Modified Pierce Oscillator with One-port SAW Resonators

The Pierce oscillator is one of the more popular circuits for the crystal oscillator today. In comparison with feedback loop oscillator, the component counts of Pierce oscillator will be lower. While applying this circuit working with a one-port SAW resonator at UHF frequency, the shunting capacitance has a serious bad effect on the high frequency oscillation. The shunting capacitance increases the insertion loss of the π -feedback network in the Pierce oscillator which constructed by one-port SAW resonator and two capacitors. This feature makes the oscillator hard to start oscillation

and the efficiency to degrade. To prevent these disadvantages, we modified the conventional Pierce oscillator circuits by adding an extra phase shifter. This modification successfully solves the problem above.

1.4 Balanced Oscillator with One-port SAW Resonator

The balanced circuits are widely used to enhance the circuit's performance, which like differential amplifier and balance mixer. The improvement of the circuit's performance relies on the availability of the antiphase signal sources, which is often the difficult part of the circuit design. Traditionally, the antiphase signals are obtained by using passive or active balun. The balanced oscillator can provide the antiphase signals without balun. Several balanced oscillator circuits using different type resonators have been reported. [12-16] But the balanced oscillator with one-port SAW resonator is hard to find. Here, we use a popular 433 MHz one-port SAW resonator to present the circuit and discuss the behavior of the balanced SAW oscillator.

1.5 Organization of this thesis

It is the aim to investigate the problems while applying piezoelectric resonators to build the high frequency, high quality factor, and low phase noise oscillators and provide some useful solutions.

In chapter 2, the structure and equivalent circuits for SAW resonator and FBAR are introduced. By using these resonators, we present two feedback loop oscillators: 2488 MHz voltage-controlled oscillator with STW resonator and 2488 MHz voltage-controlled oscillator with FBAR. The designs of oscillators and performances will be measured and discussed.

In chapter 3, the basic theory and measurement method for the residual phase

noise of the two-port devices will be introduced. After that, we will discuss the different measurement techniques for absolute phase noise measurement and chose the frequency discriminator method to measure the phase noise of the oscillators with piezoelectric resonators. By examining the residual phase noise of the devices, we can find the main noise contributors in the oscillator quickly and accurately. The method to predict the phase noise of the feed-back loop oscillator based on the residual phase noise of devices will be introduced. The prediction of the phase noise of the oscillator has a good agreement with the measured results.

In chapter 4, Pierce oscillator which is widely used in low-frequency crystal oscillators is applied for 622 MHz application. For solve difficulty of the oscillation start-up in this band, an extra phase shifter is added. The oscillator design method and how to choose a proper phase shifter are discussed.

In chapter 5, the balanced oscillator with a 433 MHz one-port SAW resonator is presented. We use a commercial one-port SAW resonator which is made by ftech Co. to demo this circuit. Based on this balanced oscillator, a push-push SAW oscillator is constructed and achieves 6dB improvement in phase noise of oscillator in comparison with one-side oscillator.

In chapter 6, there are the short conclusion of our work and the view of the future work.

Chapter 2

Feedback Loop Oscillators with Piezoelectric Resonators

2.1 Piezoelectric Resonators

2.1.1 SAW Resonators [4]

Both one-port and two-port SAW resonators are used for the tanks of oscillators in this thesis. Fig. 2-1(a) shows a typical configuration of the one-port SAW resonator where two grating reflectors are replaced at both ends of the inter-digital transducers (IDT). Very steep resonance can be detected by the IDT when the device is designed so that resonance frequencies of the IDT and reflectors coincide with each other. The width of the IDT is about quarter wavelength of the acoustic wave. The length of the gaps between the IDT and reflectors significantly influence the resonance characteristics. Fig. 2-1(b) shows the equivalent circuit near resonance, where $C1$ and $L1$ are the motional capacitance and inductance, respectively, corresponding to the contributions of elasticity and inertia. $R1$ is the motional resistance corresponding to the contribution of damping. $C0$ is the capacitance of the IDT. The capacitance ratio γ is given by:

$$\gamma = \frac{C0}{C1} = \frac{1}{\left(\frac{\omega_a}{\omega_r}\right)^2 - 1} \quad (2.1)$$

where ω_r and ω_a are the resonant frequency and anti-resonant frequency, respectively. The smaller γ enable us to control the oscillation frequency over a wider range by a capacitance parallel-connected to the resonator. This feature is preferable for use in a voltage controlled oscillator where the varactors are employed as a voltage adjustable

capacitance.

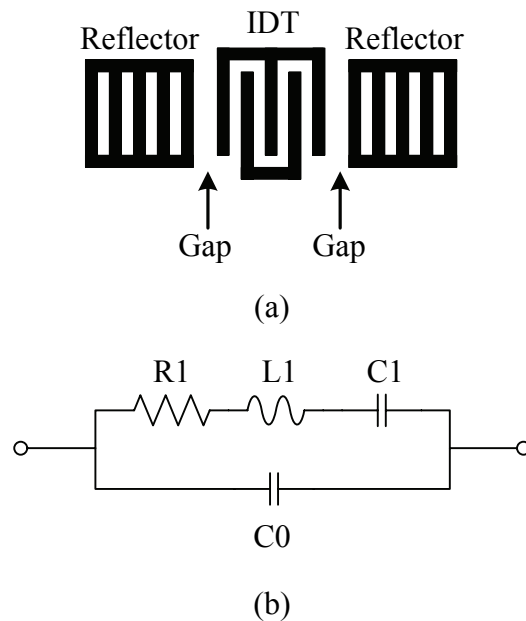


Fig. 2-1 (a) Structure, and (b) equivalent circuit model for one-port SAW resonator.

Fig. 2-2(a) shows a two-port SAW resonator where the grating reflectors are replaced at both sides of a conventional transverse filter. When the devices are designed so that the reflectors resonate at IDT resonance frequency, the transfer admittance becomes very large at resonance and a very narrow but low-pass passband is realized. Fig. 2-2(b) shows the equivalent circuit near resonance. The resonance circuit is involved as a shunt element between two IDTs because the structure is equivalent to a one-port SAW resonator when the two IDTs are parallel-connected. The oscillator can be constructed by using two-port SAW resonator as a feedback element. This configuration is widely used for operation in the UHF range because of its insensitivity to parasitic circuit elements.

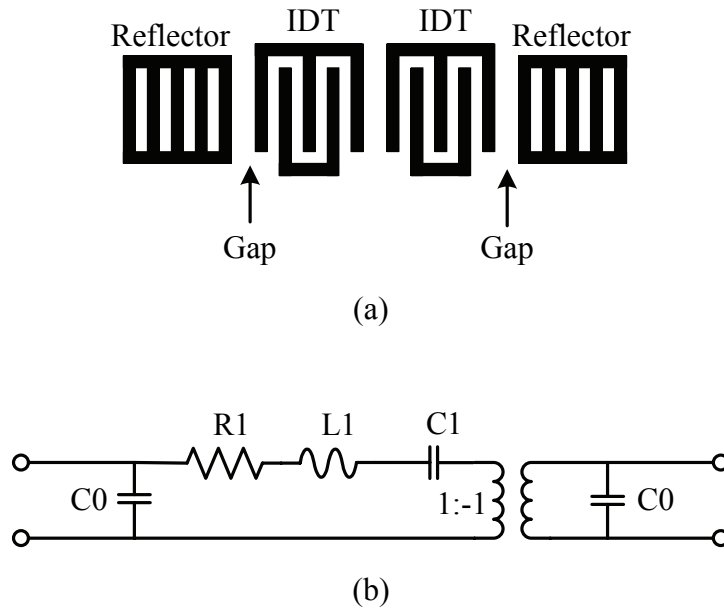
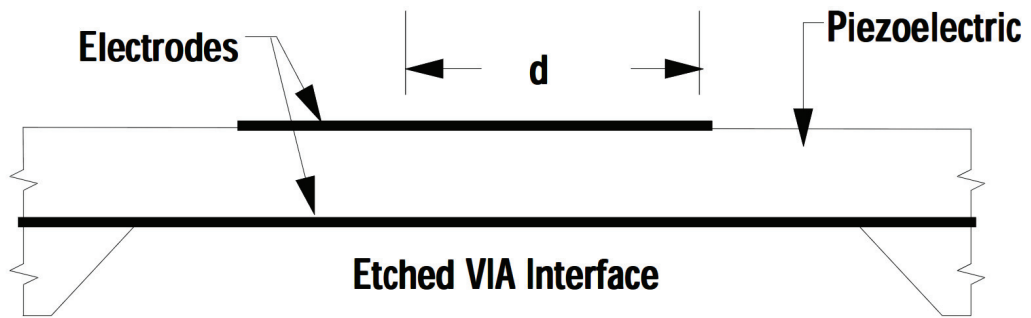


Fig. 2-2 (a) Structure, and (b) equivalent circuit model for two-port SAW resonator.

2.1.2 Film Bulk Acoustic Resonators

Another high frequency bulk wave approach is to obtain a specified thickness by thin film deposition techniques rather than by thinning crystal plates. There is considerable breadth to the thin film resonator technology, both in device types and applicable frequency spectrum. Much of this is due to the fact that the technology is based upon thin films that can be fabricated, by various means, on a variety of substrates employing integrate circuit type wafer scale processing. Bulk wave resonators require that both surfaces be free to vibrate, even though vibration amplitudes are fractions of a nanometer, in order to sustain a resonance. This condition is supplied by mechanically free surfaces such air or vacuum. Resonator geometries suitable for use with piezoelectric thin film resonators are shown in Fig. 2-3. The resonators in Fig. 2-3(a) and (b) have mechanically low impedance material interfaces of air or vacuum while the one in Fig. 2-3(c) is solidly attached to the substrate. The configuration of Fig. 2-3(a) is a membrane structure supported by the edge of the substrate [17-30].

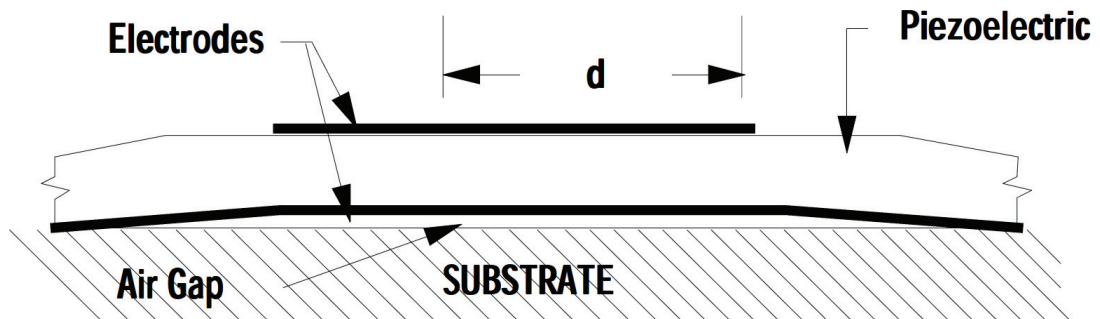
VIA ISOLATED RESONATOR



(a)



AIR GAP ISOLATED RESONATOR



(b)

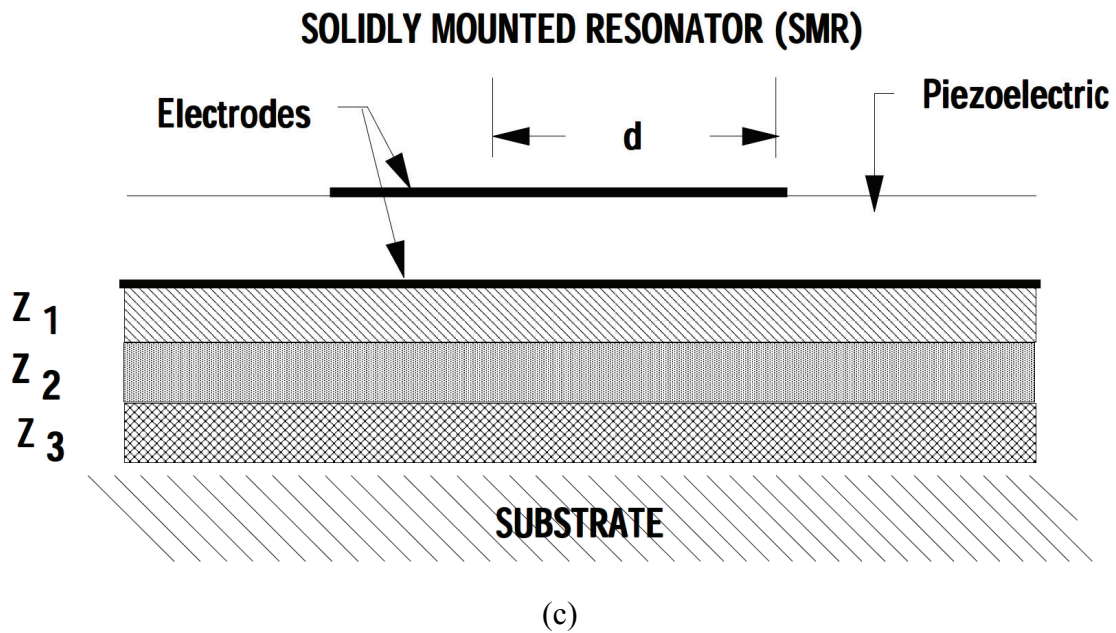


Fig. 2-3 Thin film resonator configurations (a) membrane formed by etching a VIA in the substrate. (b) air gap isolated resonator. (c) solidly mounted resonator (SMR) using a reflector array to isolate the resonator from the substrate.

Typical fabrication involves deposition of a piezoelectric film on a supporting substrate followed by removal of a portion of the substrate to form the membrane and thereby define the resonator. The configuration is similar to that used in inverted mesa quartz crystals where a thin piezoelectric membrane is surrounded by a more rigid supporting structure. The difference is in the details of how the membranes are formed. The second configuration involves fabricating an air gap under the resonator [31,32]. This may be accomplished by first depositing and patterning an area of temporary support material, next depositing and patterning an overlay piezoelectric resonator with electrodes, and finally removing the temporary support. The approach in Fig. 2-3(a) has seen greater work of the two membrane configurations and is known generally as the FBAR (Film Bulk Acoustic Resonator) configuration [19].

Advances in thin film processing have allowed the fabrication of membrane devices with high width to thickness ratios. Within one membrane of AlN multiple

resonators have been fabricated and electrically interconnected to form complex ladder filters [22]. Resonators have an electrical response that is modeled quite accurately by the Butterworth Van Dyke (BVD) equivalent circuit shown in Fig. 2-4. [23,27].

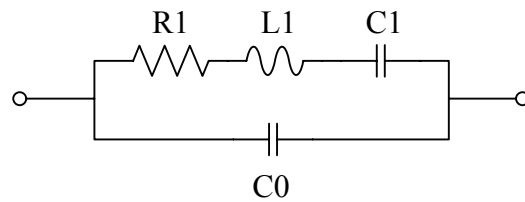


Fig. 2-4 Butterworth Van Dyke (BVD) equivalent circuit.



2.2 Voltage-Controlled Oscillator with STW Resonator

2.2.1 Design Method

In this section, a highly stable VCSO with STW resonator working directly at 2488.32 MHz is developed. The high-Q STW resonator on quartz was demonstrated in 1987 [11]. Its advantages over the conventional Rayleigh waves are the very high velocity and low propagation loss [4]. The wave velocity of STW is approximately 5000m/s, which relaxes slightly the requirement of the photolithography process. A coupled-mode resonator is carefully designed to accommodate the request of wide band tuning and low phase noise applications. The unloaded quality factor equal to 5500 was realized in this work.

It is noted that the oscillator with one-port SAW resonator suffers from large parasitic capacitance from inter-digit transducers. Here, the architecture with two-port resonator forming a feedback loop is chosen as shown in Fig. 2-5. It consists of a single loop amplifier, an electronic phase shifter, a lump element reactive Wilkinson power splitter, a lumped element reactive phase adjusting, and a two-port STW resonator. The resonator acts as a short circuit with zero phase-shift at the desired frequency. No output buffer amplifier is used because it may degrade the oscillator's white phase noise floor. The oscillation starts as the closed loop gain satisfies Barkausen's criteria. The total loop gain is larger than unity at the frequency of oscillation and the phase shift is equal to $2\pi N$ radians, N is an integer. The conditions are written as

$$\sum (G_a, G_p, G_s) \geq 1 \quad (2.2)$$

and

$$\theta_a + \theta_p + \theta_s = 2\pi N \quad (2.3)$$

where, G_a : Gain of Loop Amplifier, G_p : Loss of Phase Shifter and Loop Phase Adjust, G_s : Loss of STW Resonator, θ_a : Phase change in Loop Amplifier, θ_p : Phase change in Phase Shifter and Loop Phase Adjust, and θ_s : Phase change in STW Resonator. During design phase, the open loop gain is evaluated by breaking the loop at the appropriate plane with equal input and output impedance, such as line AB noted in Fig. 2-5. Here, the impedances seen are 50ohm network analyzer measurement. Actually the input/output impedances in each module are all set to 50ohm for convenience. This approach has the advantage that the noise characteristics of the individual component as measured in an open-loop configuration have a direct bearing on the closed-loop phase noise of the oscillator.

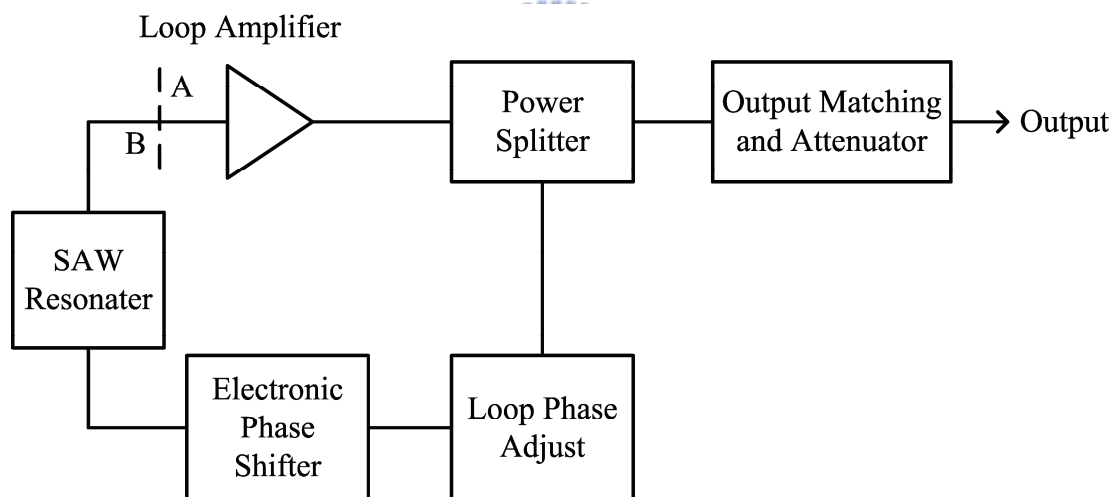


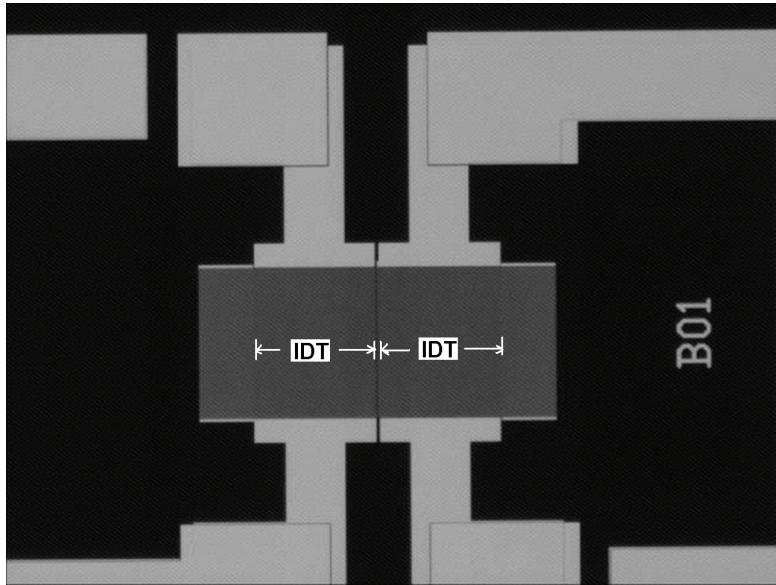
Fig. 2-5 Block diagram of a feedback loop oscillator.

2.2.2 STW Resonator

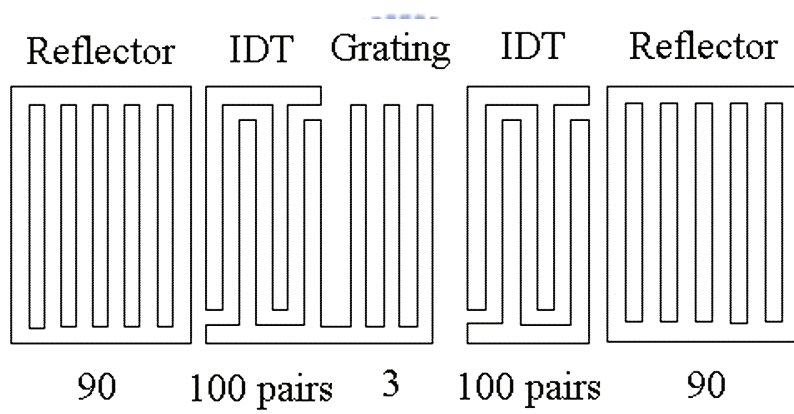
To achieve low insertion loss, high frequency, and high quality factor, the SAW resonator with STW is employed.[5] The picture of the resonator is shown as Fig. 2-6(a). The STW is a shear wave with very high velocity and energy trapping reduces the diffraction of the shallow bulk wave into the substrate, thus reduce in device

insertion loss and increase in resonator Q. The width of the transducer is approximately $0.5\mu\text{m}$. The overlap aperture is about $250\mu\text{m}$. This larger transducer width also makes it possible that the resonator could be manufactured in mass production with acceptable yield. Since STW also do not associate volume charge with propagation, its propagation loss is small. [4] To achieve the proper turnover temperature, the 90° rotated ST-cut quartz is employed to be as substrate of the resonator, which has the turnover temperature approximately at 45°C . This work simplifies the circuit design without using extra temperature compensation circuit for the real environment and lowers the cost.

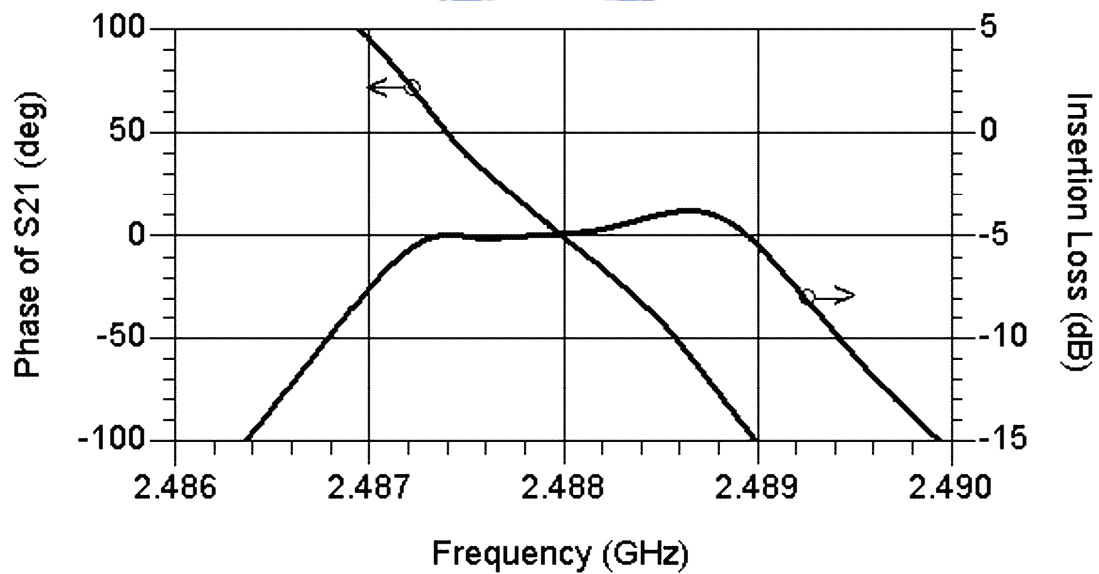
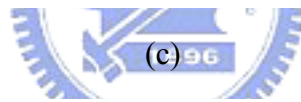
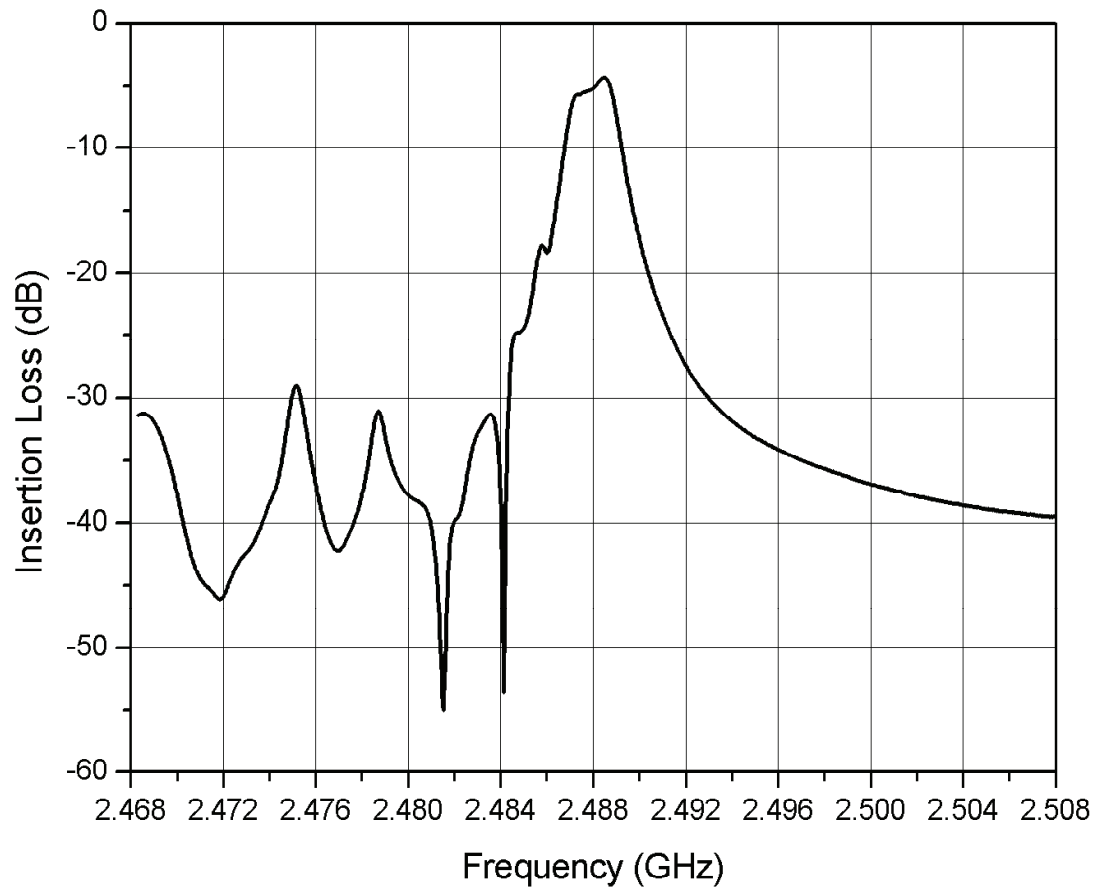
The IDTs are detailed in Fig. 2-6(b) with die size of $1.8\text{mm} \times 1.2\text{mm}$. The input and output IDTs have 100 fingers are placed between two shorted reflectors, which has 90 fingers, and are separated by a shorted grating with 3 fingers. The resonant modes formed by input and output IDTs are coupled just as two coupled parallel LC resonators. The coupling is carefully tuned by the central grating. This results in a two-mode wideband response such as that shown in Fig. 2-6(d). Due to the grounding grating the insertion loss is reduced to $4\sim 5\text{dB}$, which is much smaller than that of $10\sim 15\text{dB}$ in conventional SAW or STW delay line. [10] The approximately linear phase change with slope equal to $1.713 \times 10^{-6}\text{rad/Hz}$ is obtained within the 3dB frequency band. The up and down limits of the phase change are above $\pm 90^\circ$. The loaded Q factor $Q_L = \frac{\omega_o}{2} \cdot \frac{d\phi}{d\omega}$ is estimated equal to 1537. The group delay is about $1.713 \times 10^{-6}\text{rad/Hz}$. High insertion loss out of the pass band is revealed in Fig. 2-6(c). The spurious are suppressed under 30dB. The center frequency is trimmed to 2488.32 MHz.



(a)



(b)



(d)

Fig. 2-6 (a) Picture, and (b) structure of the STW resonator, (c) insertion loss from 2468 to 2508 MHz, and (d) insertion loss and transmission phase responses 2486.32 - 2490.32 MHz.

2.2.3 Loop Amplifier

The HBT monolithic amplifier is selected as the loop amplifier because of low noise figure and high dynamic range. The P1dB is at +17dBm and the bandwidth is 4 GHz. Its bandwidth was properly selected to prevent high 2nd harmonics. The nominal gain of 17dB is much greater than that required to overcome the total loop losses to insure the stable oscillation. The magnitude of gain variation over temperature is approximately 0.005dB/°C and this feature can prevent the AM-PM noise induced with the temperature variation.

2.2.4 Power Splitter

Because resistive attenuator in the feedback loop will degrade of white phase noise floor, an unequal Wilkinson power splitter is employed to adjust the excess small signal loop gain instead of resistive attenuator. [33] The Wilkinson power splitter can be realized as lump component or transmission line designs. To save the volume, the circuit is realized by the lump reactive components instead of microstrip line as shown in Fig. 2-7.

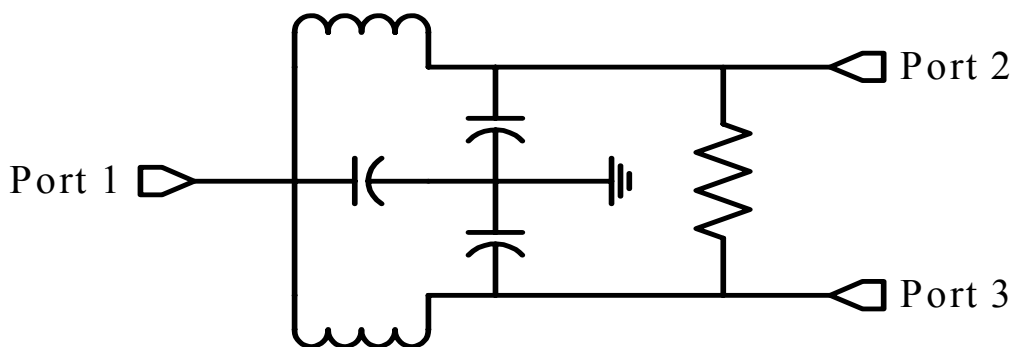


Fig. 2-7 Wilkinson power splitter.

2.2.5 Electronic Phase Shifter

The electronic phase shifter is used to tune electronically the oscillation frequency. The electronic phase shifter is constructed with silicon tuning diodes and inductors using T-circuit as shown in Fig. 2-8. It is basically a tunable high pass filter which, except for providing variable phase shifter in the loop, suppresses the excess gain of the loop amplifier at low frequency, preventing it from spurious oscillation. The phase noise and tuning linearity will be affected by the tuning diodes. High residual phase noise of tuning diodes will degrade the phase noise of voltage-controlled oscillator. With proper selection of varactor diodes, the high tuning linearity and low phase noise are achieved at the same time.

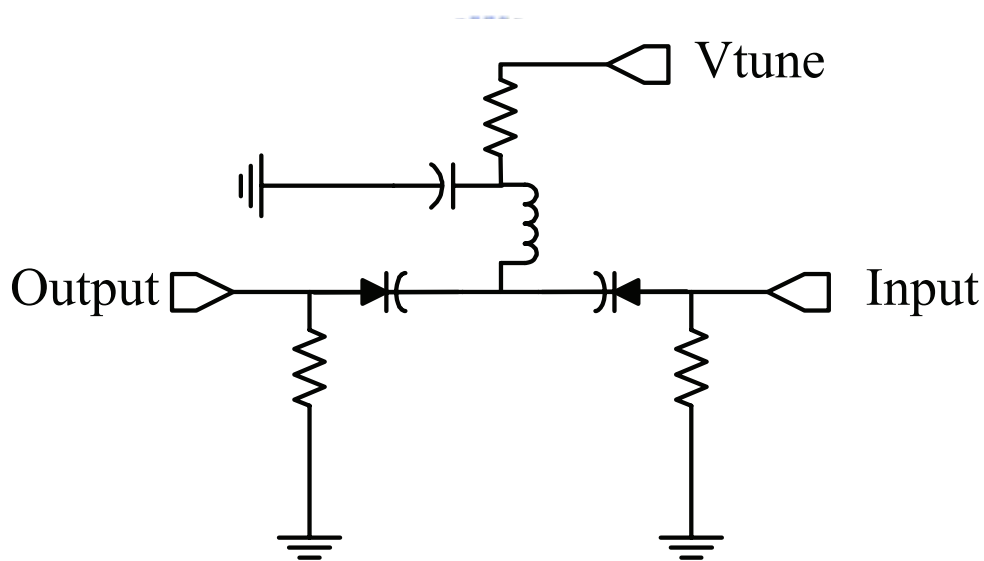


Fig. 2-8 Electronic phase shifter.

The phase shift of loop amplifier and power splitter is about equal to -80° and 90° , respectively. The electronic phase shifter is about 40° . Because the total phase shift around the loop must be $2\pi N$ radians, another 10° is required, which is from the loop phase adjust constructed with fixed lumped reactive components. The frequency dependences of total phase shifter and open loop gain seen from the reference plane

A-B line indicated in the Fig. 2-5 are shown in Fig. 2-9. Curve X and Curve Y are the total phase shift with $V_{\text{tune}} = 0\text{Volts}$ and $V_{\text{tune}} = 5\text{Volts}$, respectively. Curve M and curve N are the respective open loop gain with $V_{\text{tune}} = 0\text{Volts}$ and 5Volts , respectively. The group delay is about $1.74 \times 10^{-6}\text{rad/Hz}$. As compared to Fig. 2-6(d), we see that the SAW resonator dominates the phase shift. The slight increase in group delay may be from the tunable phase shifter with varactors. The oscillation frequency is predicted at the zero-crossing point with enough gain margins about 2dB. This gives us the benefit of low flicker noise from the amplifier without deep gain compression. The tuning bandwidth is approximately equal to the resonator's 1dB bandwidth. It is approximately from 2487.85 MHz to 2488.85 MHz. The tuning bandwidth is approximately equal to the resonator's 1dB bandwidth.

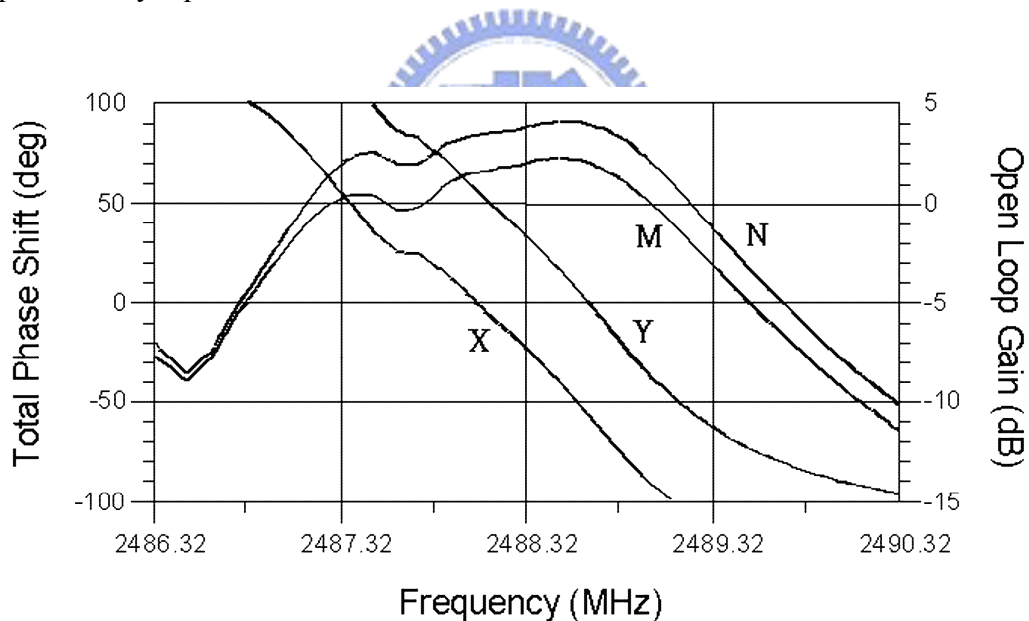
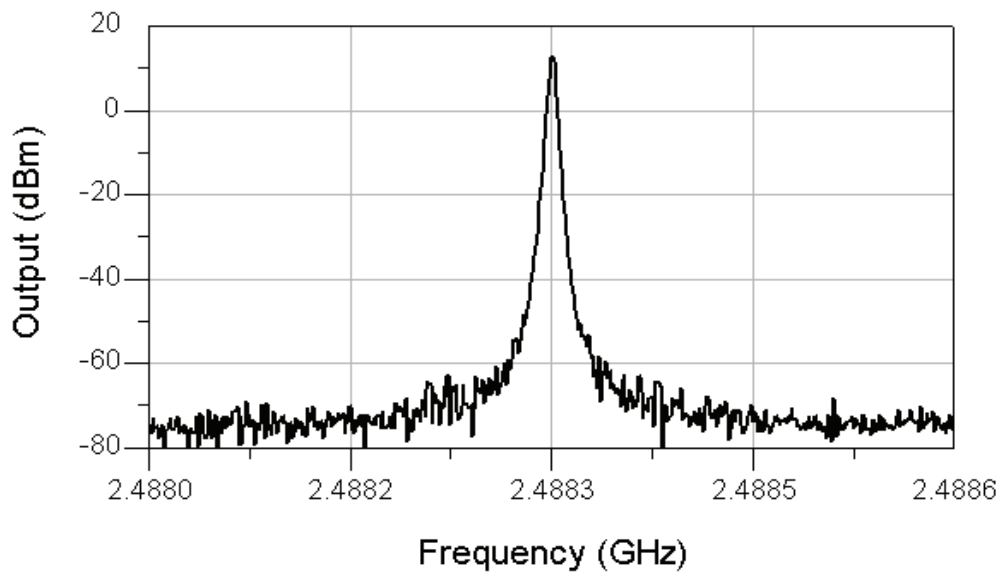


Fig. 2-9 Total phase shifter and the open loop gain at the oscillation frequency.

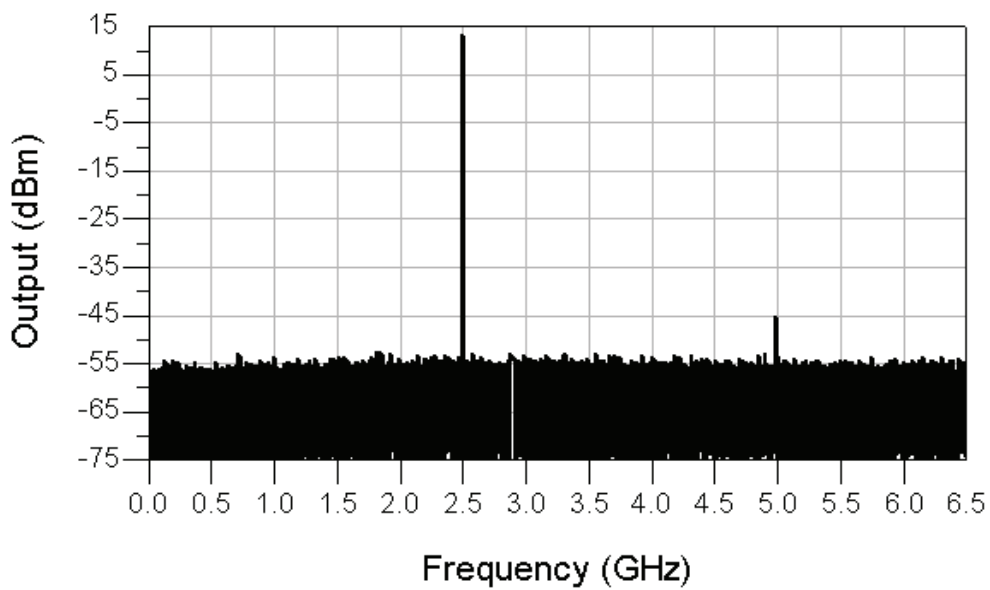
2.2.6 Oscillator Performance

The performances of the oscillator with STW resonator are measured. The narrow and wide scan of output spectrum and relative levels of harmonic are shown in Fig. 2-10(a) and (b), respectively. Because the STW resonator do not have 2nd harmonic response and the bandwidth of the loop amplifier is limited at 4 GHz, the

2nd harmonics of oscillator is suppressed below 58 dB as shown in Fig. 2-10(b) without any output low pass filter. The tuning characteristic is shown in Fig. 2-11 with ± 200 ppm range and good linearity. The frequency dependence on temperature is illustrated in Fig. 2-12. The turnover temperature is approximately 45°C, which is mainly determined by the SAW resonator.



(a)



(b)

Fig. 2-10 (a) Measured output spectrum for the 2488.32 MHz and (b) harmonics spectrum.

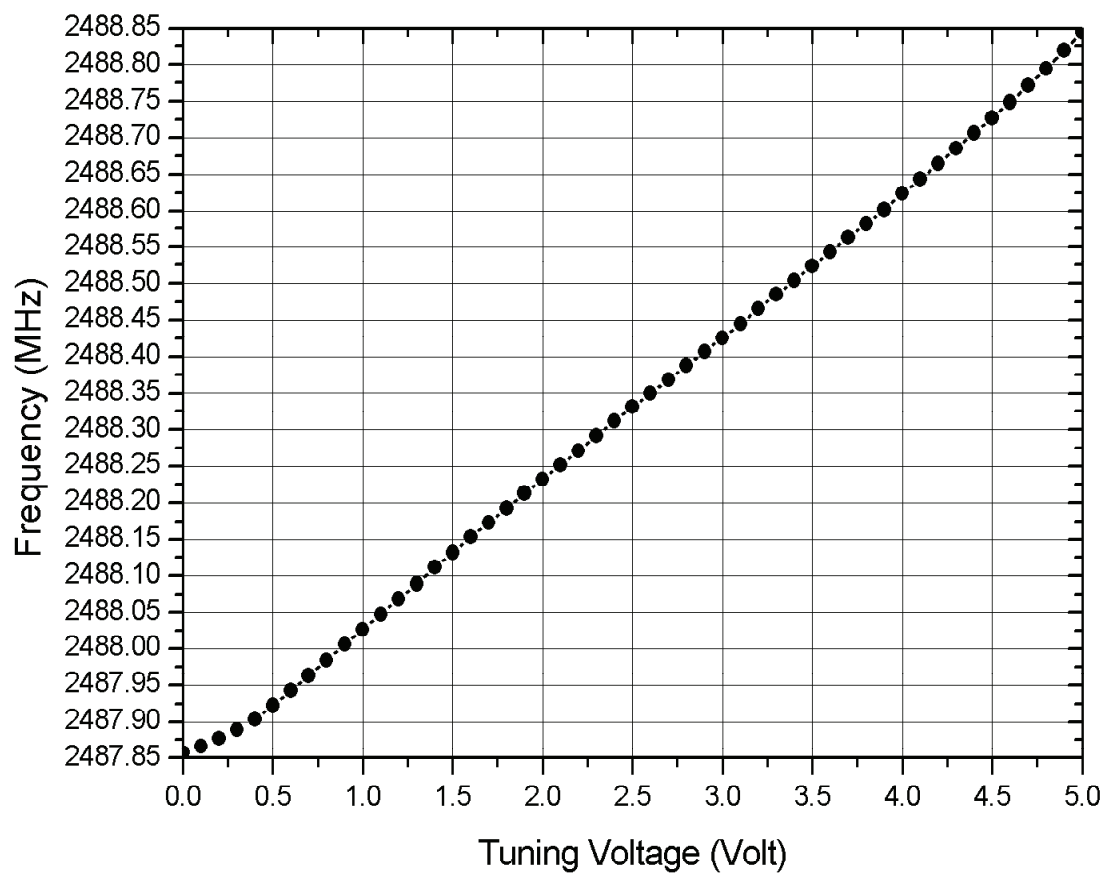


Fig. 2-11 Dependence of the oscillation frequency on tuning voltage.



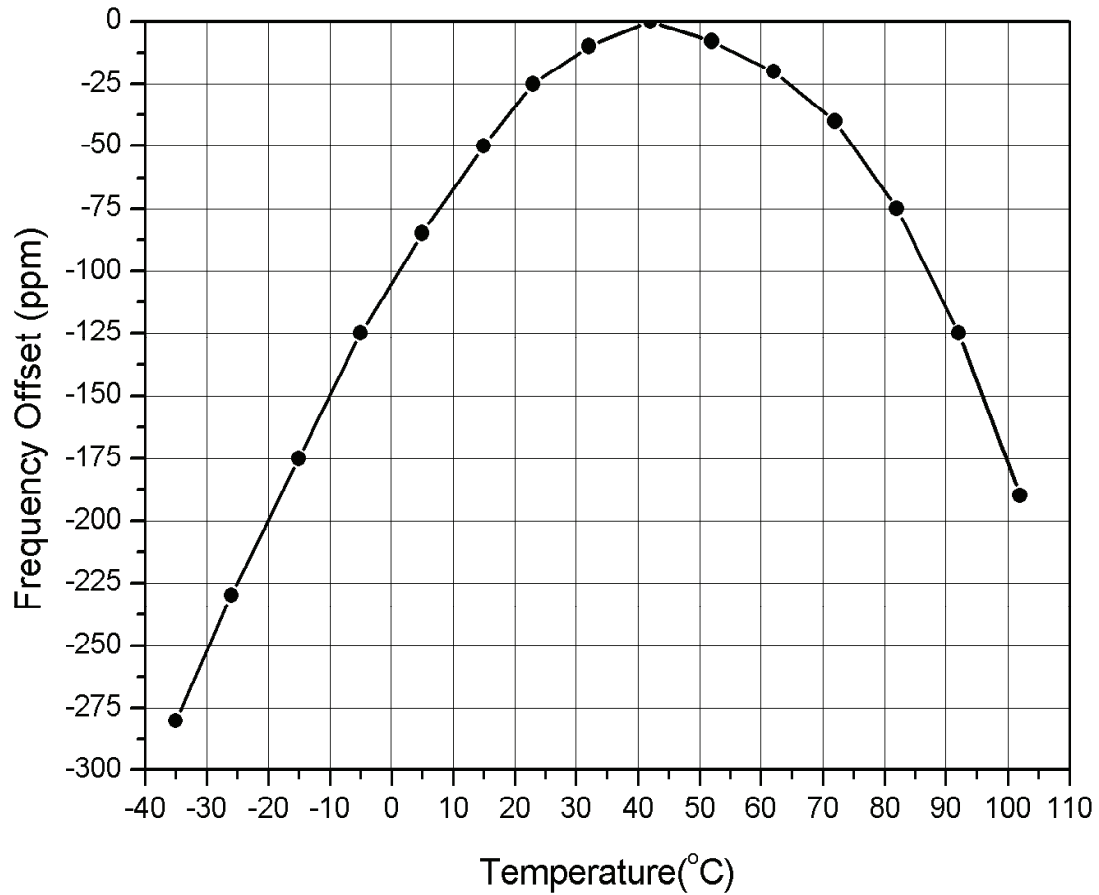


Fig. 2-12 Dependence of the oscillation frequency on temperature.

The phase noise of the oscillator is measured as shown in Fig. 2-13. The measured parameters of the STW oscillator and the specifications of the other commercial products are summarized in Table 2.1.

Table 2.1: Measured results for the voltage-controlled STW oscillator and comparison with the other commercial products.

Item	Value			
	This Work	Synergy	M-tron	SAWTEK
Supply Voltage (Volts)	+5	+5	+5	+5
Supply Current (mA)	65	60	100	55
Output Power (dBm)	+13	+3	+7	+10
Tuning voltage (Volts)	0-5	1-4	0-5	N/A
Tuning Range (ppm)	±200	250	±50	80
Sub Harmonic (dBc)	-58	-30	-26	N/A
Phase Noise @ offset 100 kHz (dBc/Hz)	-153	-142	-145	-145

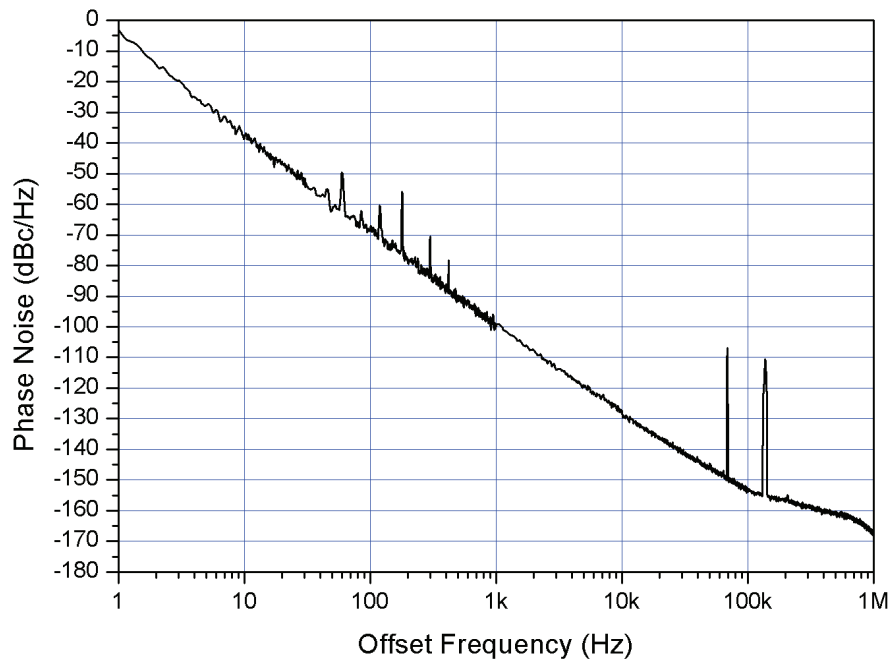
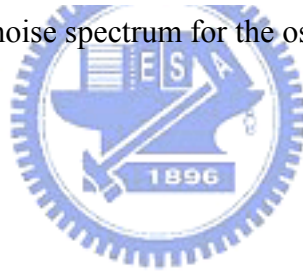


Fig. 2-13 Measured phase noise spectrum for the oscillator with STW resonator.



2.3 Voltage Controlled Oscillator with FBAR

After the success development of 2488 MHz voltage-controlled oscillator with STW resonator, we try to use the FBAR to replace the STW resonator. Basically, the suspended FBAR device is a three-layer structure with the top and bottom electrodes sandwiching a middle layer of oriented piezoelectric material. Air interfaces are used on both outer surfaces to prevent acoustic energy leaking out of the device; as the solid membrane and air boundary form high impedance to acoustic wave, functioning as high-Q acoustic reflectors at all frequency. When RF signals are applied near the mechanical resonant frequency, the piezoelectric transducer excites the fundamental bulk compress wave traveling perpendicular to the films. Resonators for use in stable oscillators need low temperature coefficient (TC), which needs composite structures for positive and negative coefficient compensation. On the contrary, for temperature sensing, a higher degree of TC is required for sensitivity, which is achieved also through composite structure containing all positive (or negative) coefficient material.

Here, AlN is employed for the potential integration. AlN has a crystal structure of hexagonal wurtzite where aluminum and nitrogen atoms are combined. AlN film is grown along (002) direction to achieve high piezoelectric coupling to the required extensional mode. AlN lattice extends and retracts toward c-axis orientation creating vibration if an alternating field is applied cross the crystal.

In this section, a high quality factor FBAR was designed and fabricated. Using this resonator, a high frequency voltage-controlled FBAR oscillator is designed and realized with hybrid circuits.

2.3.1 FBAR Design and Fabrication

It was reported that the lower the full width at half maximum (FWHM) value of a piezoelectric material has, the better the performance characteristics of the resonators and filters has. [34] Thus, the AlN piezoelectric film needs to have highly c-axis oriented columnar structure. [35] To achieve this requirement, a SiN_x thin film is added between AlN and bottom electron. [36] The SiN_x layer also serves as an etching stop layer to protect bottom electron while patterning the AlN layer.

The resonant frequency of FBAR is predominantly determined by half wavelength of standing acoustic wave in the resonator. The fundamental resonant frequency is then inversely proportional to the thickness (d) of the piezoelectric material used, and is equal to $V_a/2d$, where V_a is an acoustic velocity at the resonant frequency. The Nth harmonic frequency of the FBAR can be approximated as

$$f_r \approx \frac{N}{2\left(\frac{d_{elec_t}}{V_{elec_t}} + \frac{d_{piezo}}{V_{piezo}} + \frac{d_{SiN}}{V_{SiN}} + \frac{d_{elec_b}}{V_{elec_b}}\right)} \quad (2.4)$$

where d_{elec_t} , d_{piezo} , d_{SiN} , and d_{elec_b} are the thickness of top electrode (Al), piezoelectric material (AlN), buffer layer (SiN_x), and bottom electrodes (Cr/Au), respectively. V_{elec_t} , V_{piezo} , V_{SiN} , V_{elec_b} are the acoustic velocities of top electrode (Al), piezoelectric material (AlN), buffer layer (SiN_x), and bottom electrodes (Cr/Au) respectively. According to equation (2.4), the thickness of each layer in the FBAR for fundamental frequency (N=1) at 2.48 GHz for unlicensed application was designed and listed in Table 2.2.

Table 2.2: Physical properties of representative materials for FBAR. [37-39]

Layer	Metal	Piezoelectric	Buffer	Metal
Layer material	Al	AlN	SiN _x	Cr/Au
Density (kg/m ³)	2700	3255	3270	19700
Acoustic velocity (m/s)	6420	10400	11000	3240 (Au)
Designed thickness (Å)	3500	11000	1000	1000
Thermal expansion coefficient (ppm/°C)	23.6	4.6	0.8	14.4

It is well known that AlN films must be grown orientated in the (002) direction to achieve high piezoelectric coupling to the required extensional mode. Therefore columnar AlN grains whose c-axes are perpendicular to the substrate are needed. The four layered composite structure Al/AlN/SiN_x/Au of FBAR is shown in Fig. 2-14.

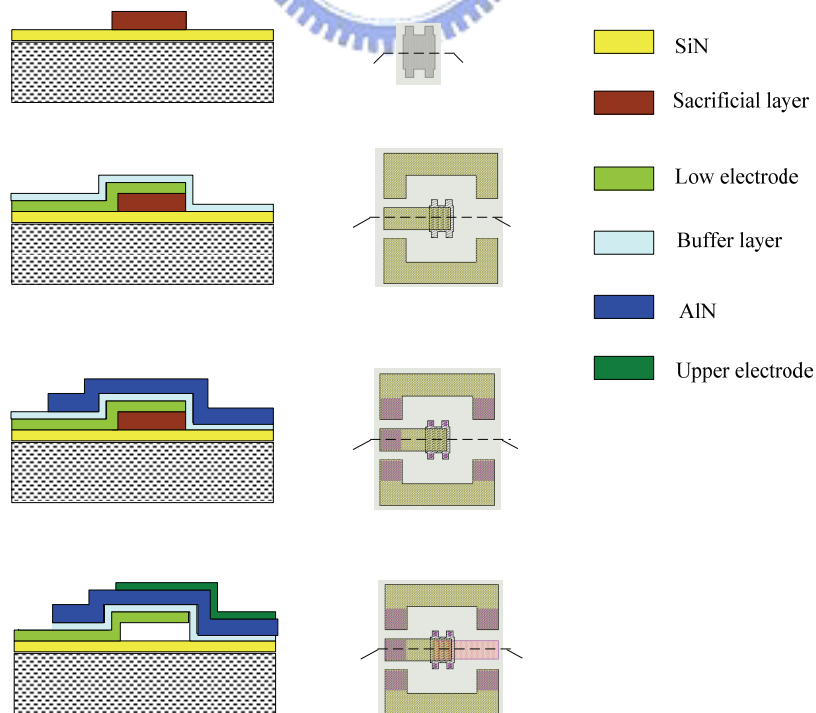


Fig. 2-14 Process flow of FBAR.

AlN was fabricated on (100) crystallographic oriented epitaxial silicon wafers. After RCA cleaning, silicon wafer was deposited with low stress silicon nitride (Si_3N_4) using Low Pressure Chemical Vapor Deposition (LPCVD) and the thickness is 1200\AA . The Si_3N_4 layer served both as a high resistivity substrate to eliminate any parasitic contributions from mobile charges or a highly boron-doped epitaxial layer and an etch obstruction layer. Temporary support (sacrificial layer: Cu) is formed by E-gun on top of Si_3N_4 followed by electrode and piezoelectric layer. Then, a thin layer of Cr/Au film which thickness is 1000\AA was fabricated by electron beam evaporation and patterned using lift-off process and serves as the bottom electrode. The AlN film deposited on bottom electrode has poor c-axis crystallinity. To overcome this weakness of bottom electrode, SiN_x buffer layer is introduced prior to the deposition of bottom electrode. An amorphous SiN_x film which thickness is 1000\AA was fabricated by Plasma Enhanced Chemical Vapor Deposition (PECVD) and served as a buffer layer between bottom electrode and piezoelectric layer. [40] An AlN film was then fabricated on top of the buffer layer through pulsed reactor DC magnetron sputtering and the substrate temperature (300°C) was kept. The thickness of AlN is about 11000\AA . The fourth layer of an aluminum film which thickness is 3500\AA was fabricated by electron beam evaporation and patterned by photolithography as a top electrode. The active area of FBAR is only about $70 \times 70\mu\text{m}$ to reduce the parasitic capacitance from electrodes for the purpose of high frequency operation. The copper temporary support which thickness is 5000\AA was removed by wet etching using ASP100 and leaving a membrane resonator supported at the edges. The die photo is shown in Fig. 2-15.

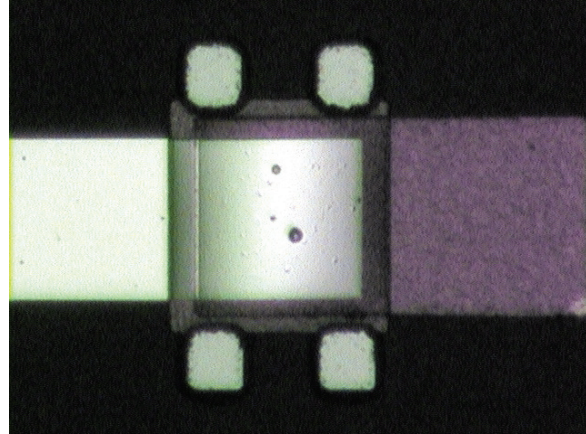
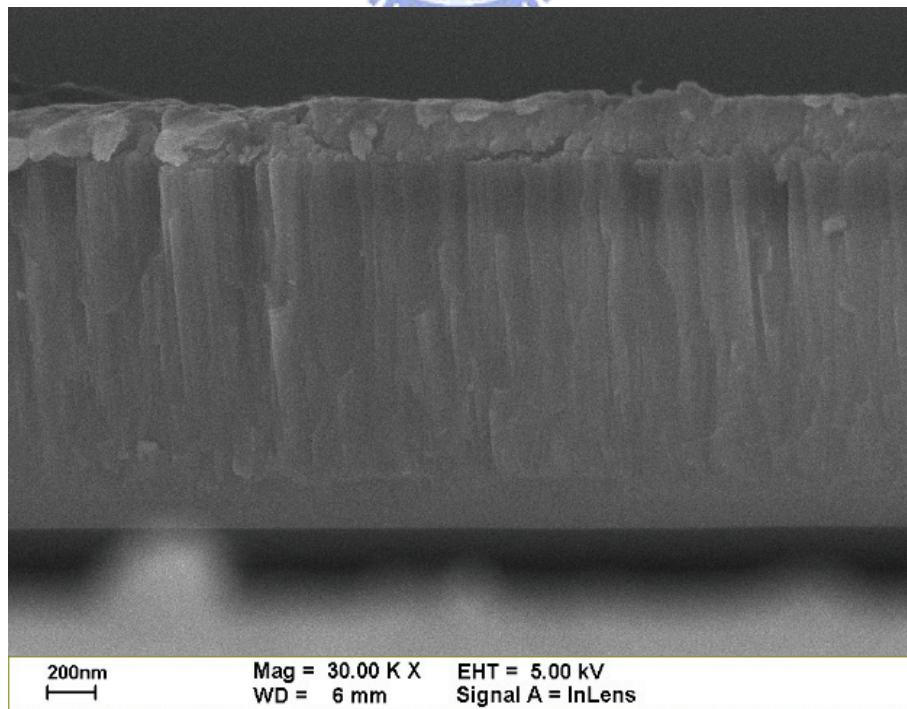
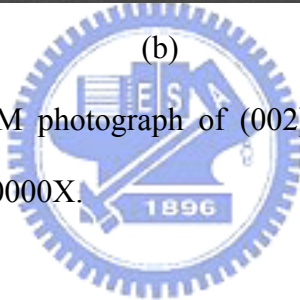
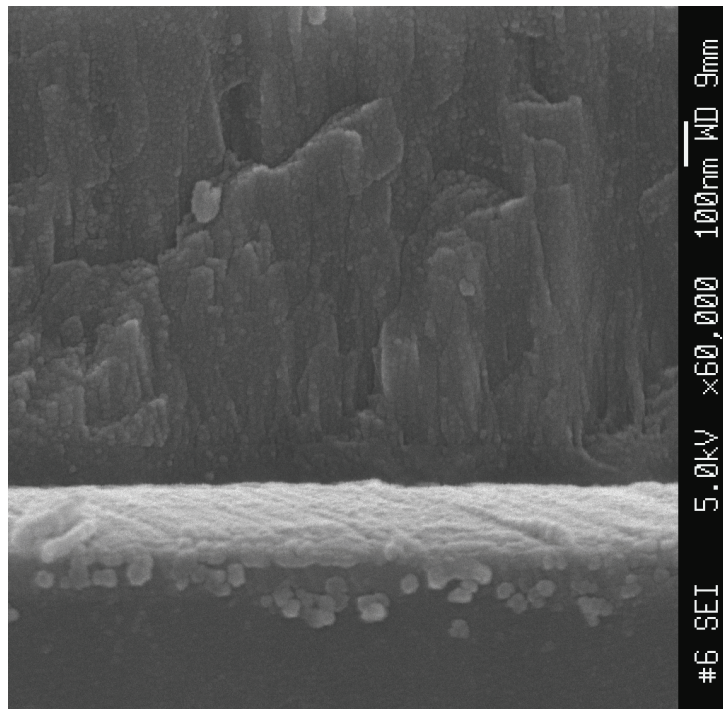


Fig. 2-15 Picture for the Film Bulk Acoustic Resonator

Fig. 2-16(a) and (b) show the cross-sectional SEM photograph of (002)-oriented AlN film, lie on SiN_x buffer layer and bottom electron. The cross section view of the thin film shows an AlN film with a highly aligned columnar structure was formed. The sharp boundaries of interface between the SiN_x layer and AlN film from a smooth surface.



(a)



(b)
 Fig. 2-16 Cross-sectional SEM photograph of (002)-oriented AlN film with SiN_x buffer layer (a) 30000X, (b) 60000X.

The FBAR sensors were probed at wafer level to measure the resonant behavior. The Agilent 8510C Vector Network Analyzer, controlled automatically by program, was employed to acquire the S-parameters. Fig. 2-17 shows the Z-parameter impedance characteristics calculated from the measured S-parameters. The resonator reveals two resonant frequencies characterized by a zero phase shift. One is a series resonance frequency (denoted by f_s) with minimum impedance and zero phase shift, which occurs as piezoelectric coupling is in phase with an applied voltage. The other is a parallel resonance frequency (denoted by f_p) with maximum impedance and zero phase shift, which occurs as piezoelectric coupling is 180 degrees out of phase with an applied voltage.

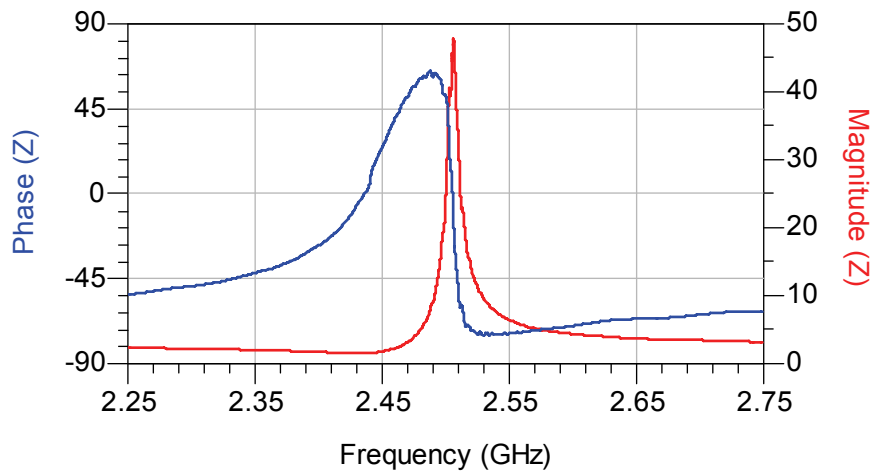


Fig. 2-17 Z-parameters of the FBAR.

2.3.2 Oscillator Design

With the success of FBAR, an oscillator was designed and fabricated. Its functional block is illustrated in Fig. 2-18. The architecture with FBAR forms a feedback loop. It consists of a single loop amplifier, a Wilkinson power splitter, a phase adjusting, and a FBAR resonator. The HBT monolithic amplifier is selected as the loop amplifier because of low noise figure and high dynamic range. The P1dB is at +17dBm and the bandwidth is 4 GHz. Its bandwidth was properly selected to prevent high 2nd harmonics. The nominal gain of 17dB is much greater than that required to overcome the total loop losses to insure the stable oscillation. The magnitude of gain variation over temperature is approximately 0.005dB/°C and this feature can prevent the temperature variation of oscillator. The power divider and phase shift were made of lumped elements. The resonator acts as a short circuit with zero phase-shift at the desired frequency. The oscillation occurs as the closed loop gain satisfies Barkhausen criteria.[41] During design phase, the open loop gain (S_{21}) is

actually evaluated by breaking the loop at the appropriate plane with equal input and output impedance, such as line AB noted in Fig. 2-18. The linear simulation is performed by using Agilent Advance Design System (ADS) software and shown in Fig. 2-19. The oscillation starts when the phase of S_{21} equal to zero and $|S_{21}| > 1$, which in turn implies the equivalent resistance is negative. The Barkhausen criteria are satisfied simultaneously.

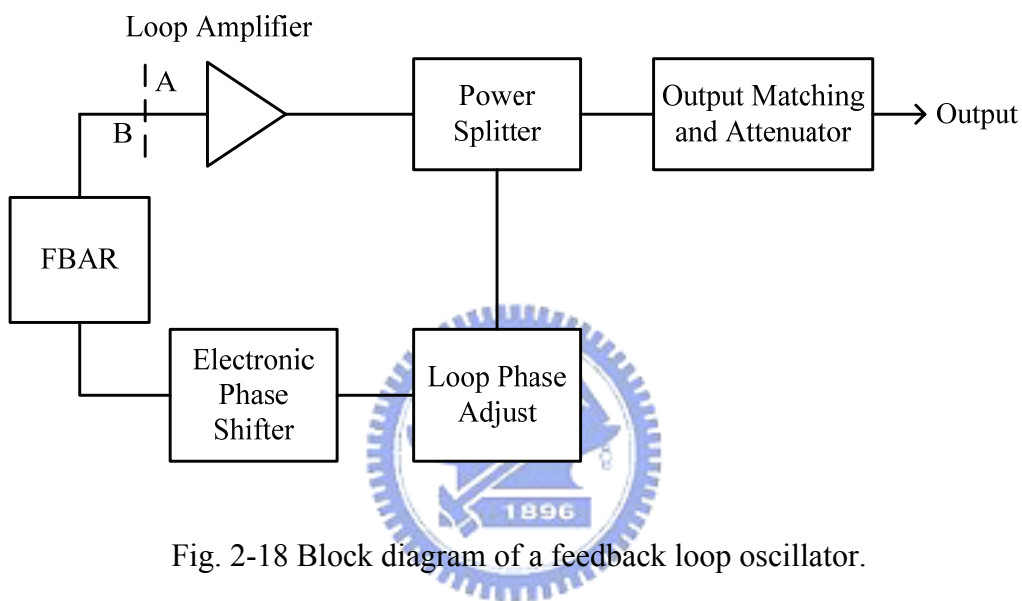


Fig. 2-18 Block diagram of a feedback loop oscillator.

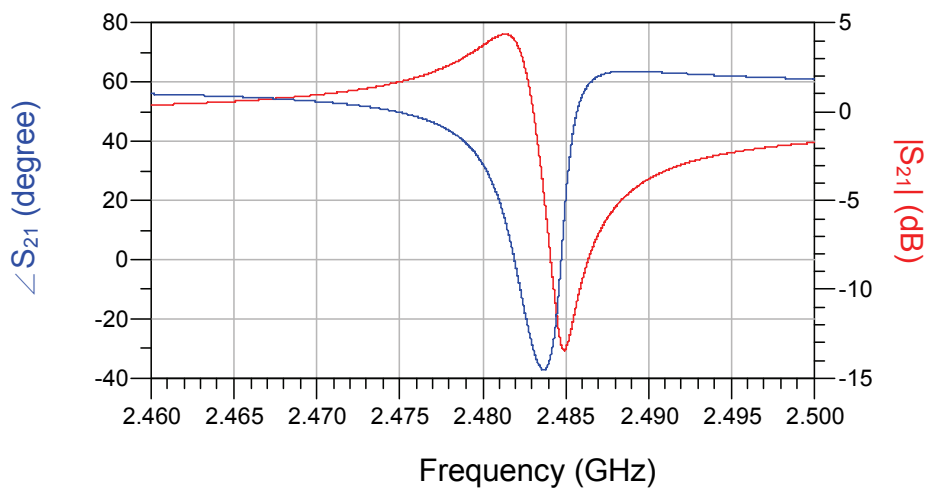


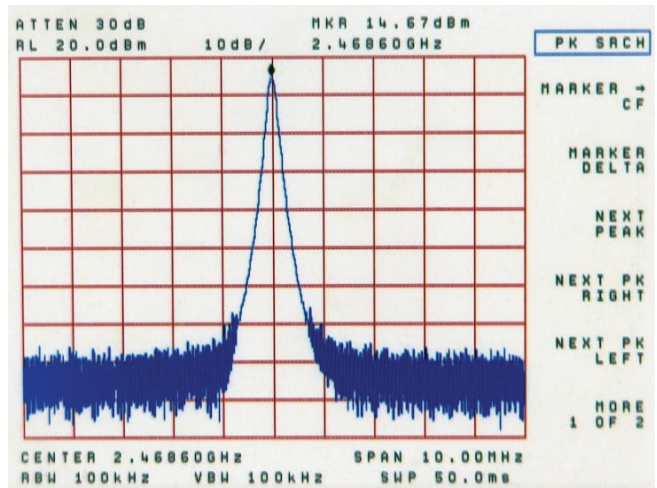
Fig. 2-19 Results of linear simulation using ADS.

2.3.3 Measurement and Discussion

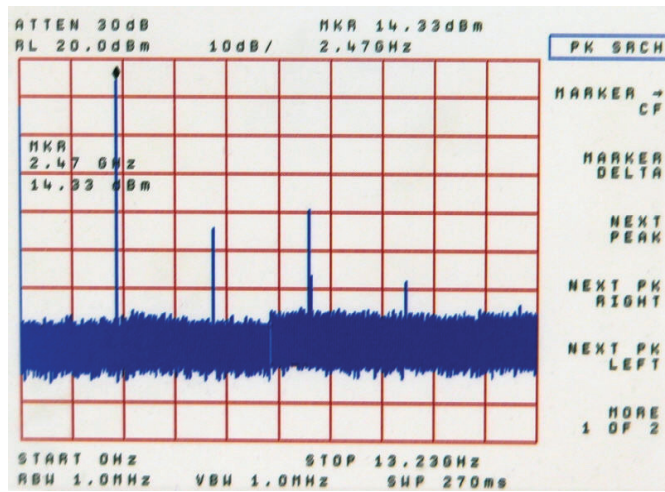
The fundamental and higher harmonics oscillation spectrums were measured and shown in Fig. 2-20 (a) and (b), respectively. The 2nd harmonics of oscillator is suppressed below 40 dB as shown in Fig. 2-20(b). The oscillation frequency is slightly higher than the series resonance frequency f_s of FBAR because of the parasitic capacitance from package effect. The variation of fundamental frequency with temperature was also measured and shown in Fig. 2-21. The TC of oscillator is about -34.5ppm/°C and seems to be equal to that of FBAR. It implies that the effective tank of the oscillator is dominated by the FBAR resonator. The tuning characteristic is shown in Fig. 2-22 with $\pm 6\%$ range. The performances of the oscillator with FBAR resonator are measured and summarized in Table 2.3.

Table 2.3: Measured Results for the FBAR oscillator.

Item	Value
Supply Voltage (Volts)	+5.0
Supply Current (mA)	65
Output Power (dBm)	+14.5
Tuning Voltage (Volts)	0-5
Tuning Range	$> \pm 6\%$
Sub Harmonics (dBc)	-40



(a)



(b)

Fig. 2-20 (a) Output fundamental spectrum, and (b) harmonics spectrum for the oscillator.

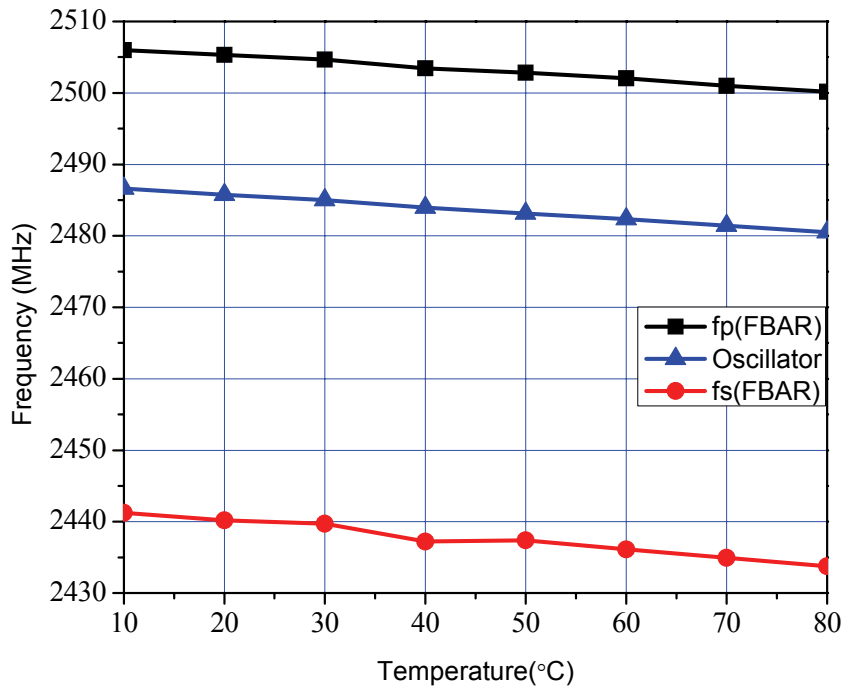


Fig. 2-21 Measured variation of fundamental frequency with temperature for FBAR and oscillator.

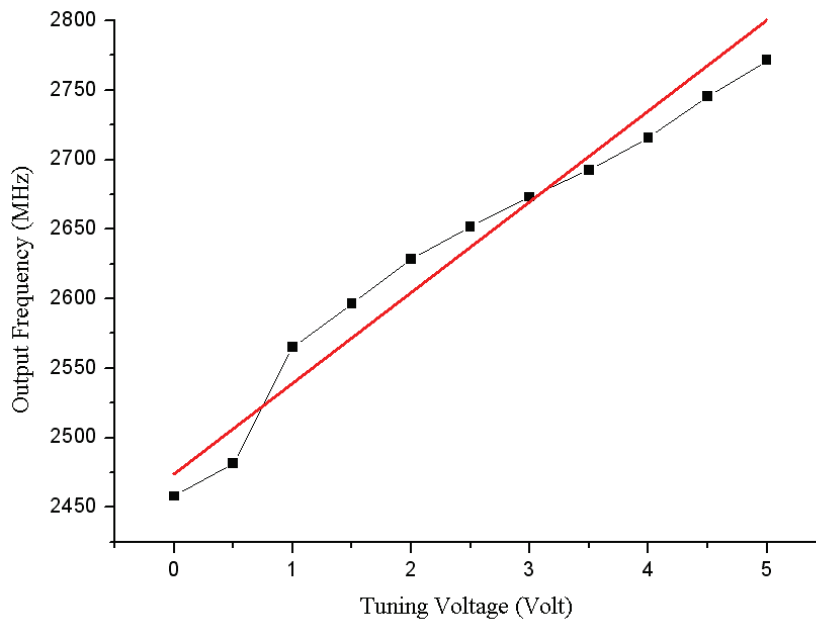


Fig. 2-22 Output frequency vs. tuning voltage

Chapter 3

Measurement and Prediction of Phase Noise in Oscillator with STW Resonator

3.1 Introduction

Frequency stability can be defined as the degree to which an oscillating source produces the same frequency throughout a specified period of time. Every RF and microwave source exhibits some amount of frequency instability. This stability can be broken down into two components: one is long-term stability, the other is short-term stability. Long-term stability describes the frequency variations that occur over long time periods, expressed in parts per million per hour, day, month, or year. Short-term stability contains all elements causing frequency changes about the nominal frequency of less than a few seconds duration. Here, we just focus on the short-term stability.

Phase noise is the important specification for an oscillator. The absolute phase noise of an oscillator is set by the residual noise of the active devices, the residual noise of the resonator and the bandwidth of the resonator. Generally the active devices in the oscillator are the major noise contributors. In the design phase, we found that the active devices with lower noise figure could not always lead to the oscillator with lower phase noise. After examining the residual phase noise of the major components in the oscillator, we found the residual phase noise of the STW resonator dominates the phase noise of the oscillator instead of the active devices and the lower noise figure of active devices do not relate to the lower residual phase noise.

Here, the Agilent's E5503B phase noise measurement system is used for residual phase noise and absolute phase noise measurements. A phase noise prediction method based on residual phase noise of devices in oscillators is presented in this chapter.

3.2 Residual Phase Noise of Devices

3.2.1 Residual Noise

Residual noise (or two-port noise) is the noise added to signal when the signal is processed by a two-port device. Such devices include: amplifiers, dividers, filters, mixers, multipliers, phase-lock loop synthesizers, or any other two-port electronic networks. Residual noise contains both AM and PM components. [42-44]

There are two basic noise mechanisms in residual noise: one is additive noise, the other is multiplicative noise. Residual noise is the sum of additive and multiplicative noise. Additive noise, as shown in Fig. 3-1, is generated by the two-port device at or near the signal frequency and added in a linear fashion to the signal. Multiplicative noise has two known causes. One is an intrinsic, direct phase modulation with $1/f$ spectral density and the exact origin of this noise component is unknown. The other is noise may modulate an RF signal by multiplying baseband noise with the signal, as shown in Fig. 3-2. This mixing is due to any non-linearities in the two-port network. The baseband noise may be produced by the active devices active devices of the internal network, or may come from low-frequency noise on the signal or power supply.

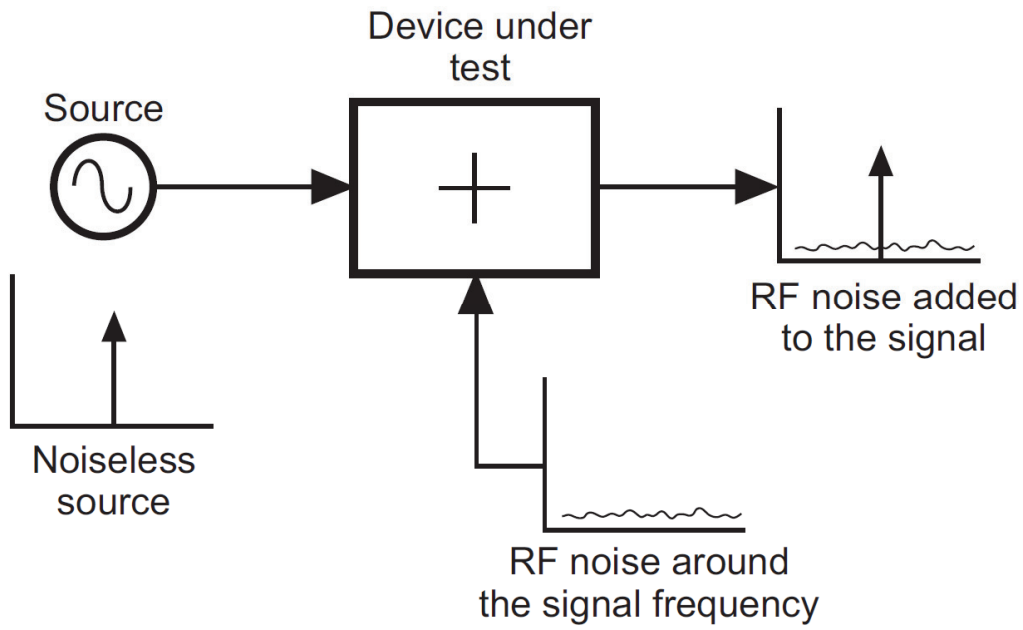


Fig. 3-1 Additive noise component.

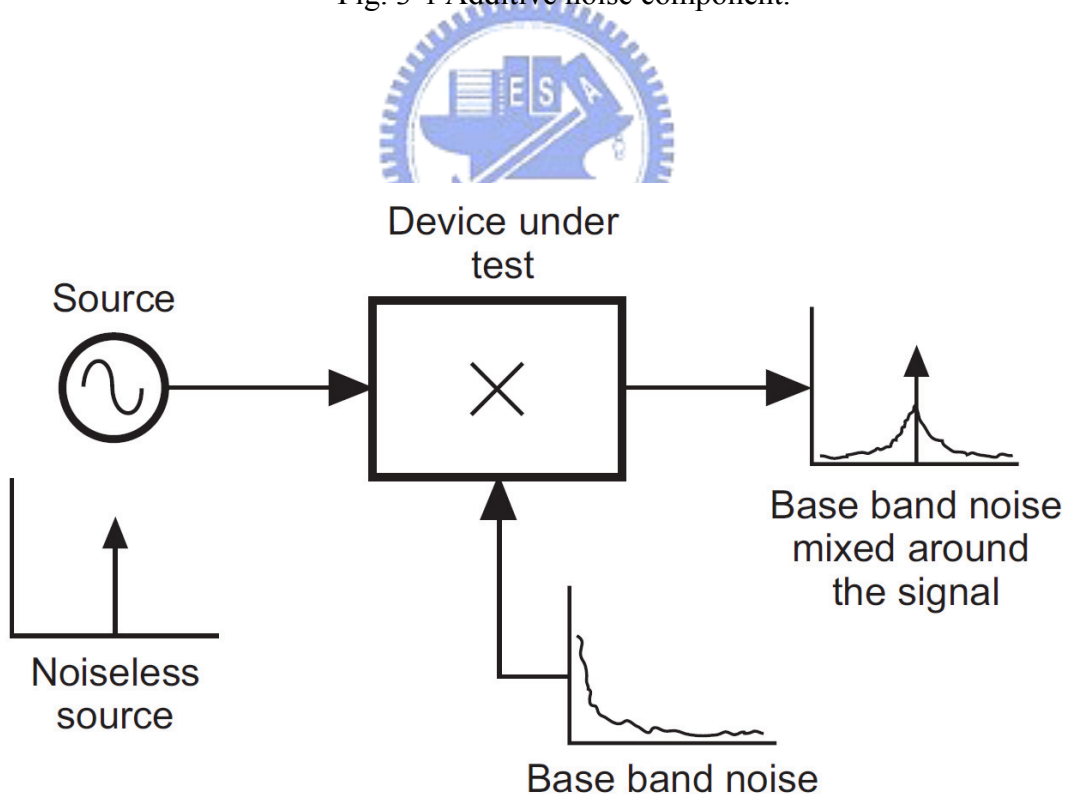


Fig. 3-2 Multiplicative noise component.

3.2.2 Measurement Process of Residual Phase Noise

The basic residual phase noise measurement setup is shown as Fig. 3-3. An unmodulated signal source with low AM noise is necessary. The AM noise of the source which used for residual phase noise measurement must be comparatively small because the mixer type phase detector has only 20 to 30 dB of AM noise rejection. If the AM component of the source is greater than 20 to 30 dB above the residual phase noise of the device-under-test (DUT), it will contribute to the residual phase noise measurement and show the residual phase noise as being greater than it really is. The noise floor of measurement system is established by replacing the DUT with a feed-through and adjusting the total insertion loss in the device test path to maintain the proper RF signal power level to the R-port (LO-port) of the phase detector. Phase quadrature for two input ports of the phase noise detector is established by using a mechanical line stretcher. The electronic phase shifter is not proper because of its high residual noise. A critical point is to maintain the constant RF power level to the L-port (device test path) and R-port for the phase detector during calibration as well as during the actual measurement. The source noise in each of the two phase detector paths is correlated at the phase detector for frequency offset range of interest. When the source noise is correlated at the phase detector, the source phase noise cancels, leaving only the residual phase noise of the DUT. Agilent E5503B noise measurement system is used for the residual phase noise measurement. Fig. 3-4 shows the E5503B connection diagram for residual phase noise measurement and the system noise floor is shown in Fig. 3-5. The spurious signals which closed to the carrier are the system spurious, primary 60 Hz (and harmonics) power line spurs.

A bandpass filter type response will cause the source noise to be decorrelated at the edge of the filter. This decorrelation of noise causes the system to measure the source noise level directly at the offsets beyond the filter bandwidth.

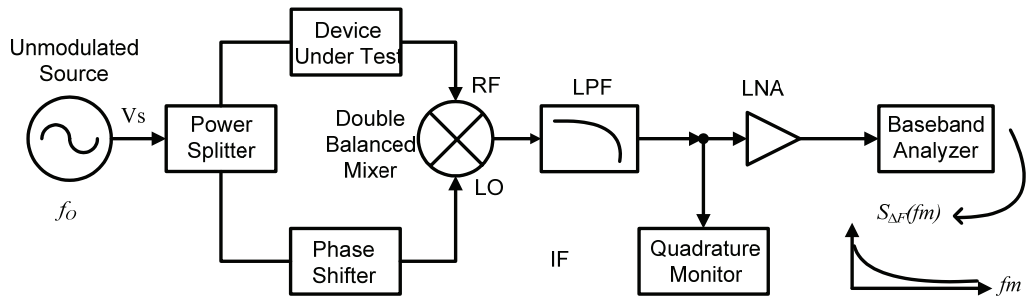


Fig. 3-3 The basic setup for residual phase noise measurement.

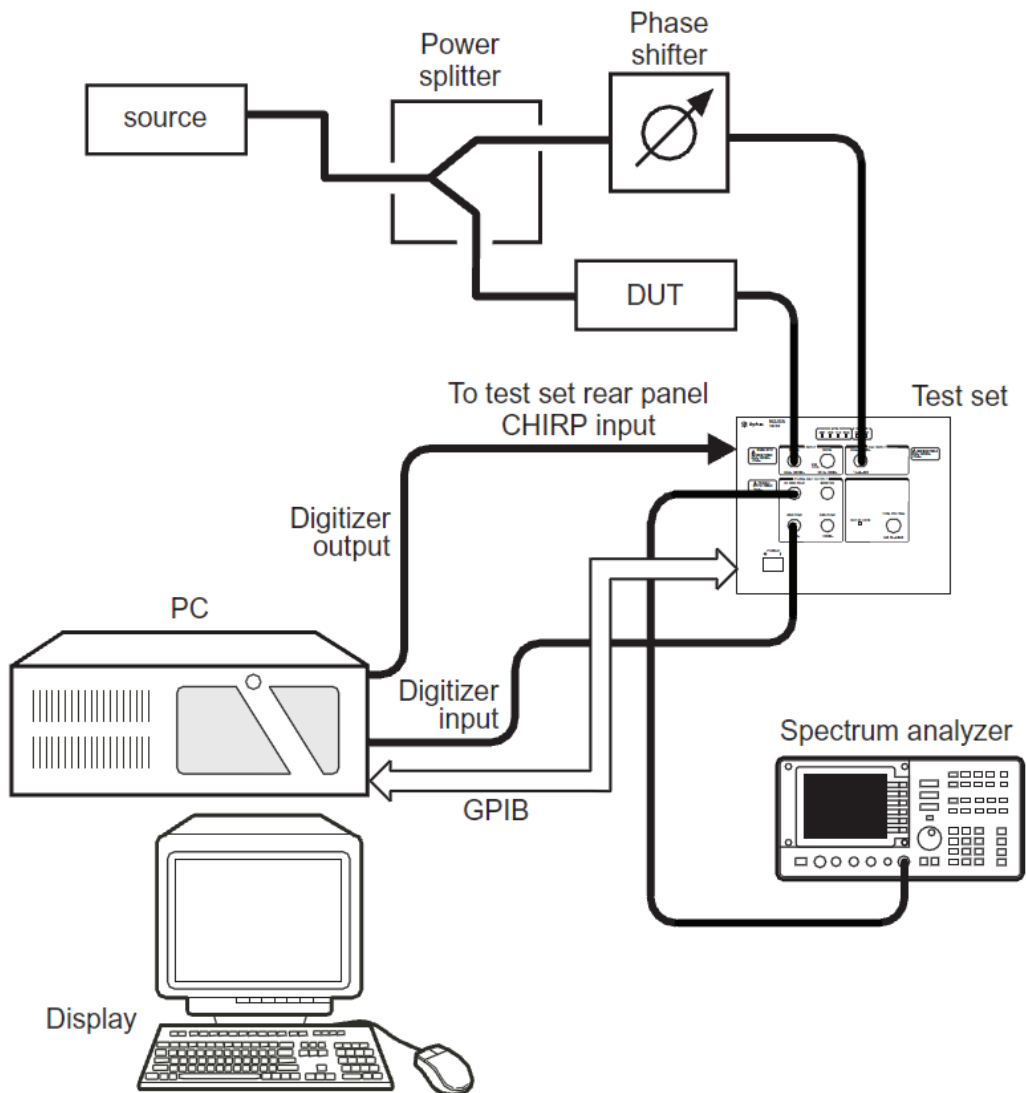


Fig. 3-4 The E5503B connection diagram for residual phase noise measurement. [44]

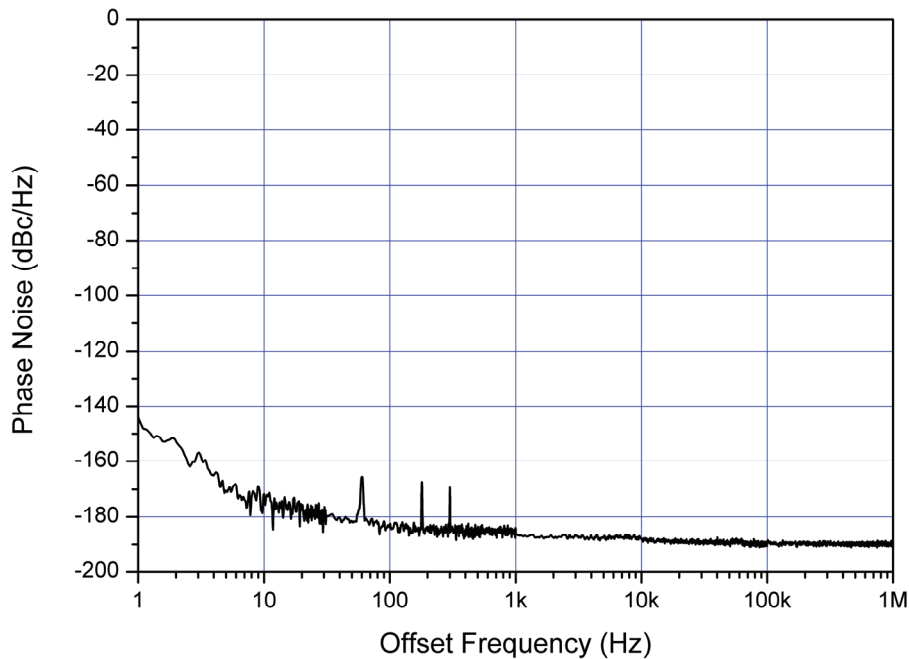


Fig. 3-5 Measured noise floor for residual phase noise measurement system.

3.2.3 Residual Phase Noise of Main Components in Oscillator

There are three major noise contributors in this feedback loop oscillator: STW resonator, loop amplifier and electronic phase shifter.

Residual phase noise in a SAW or STW resonator occurs when an unmodulated carrier is passed through the acoustic device. In this process, phase fluctuations which occur in the resonator cause a direct phase modulation of the carrier so that it appears with PM modulation noise sideband at the device output.[43] The residual phase noise of the STW resonator is shown in Fig. 3-6. It is measured by applying the power approximately the same power level in the steady state oscillation condition. The corner of the flick noise is out of the scope of this measurement.

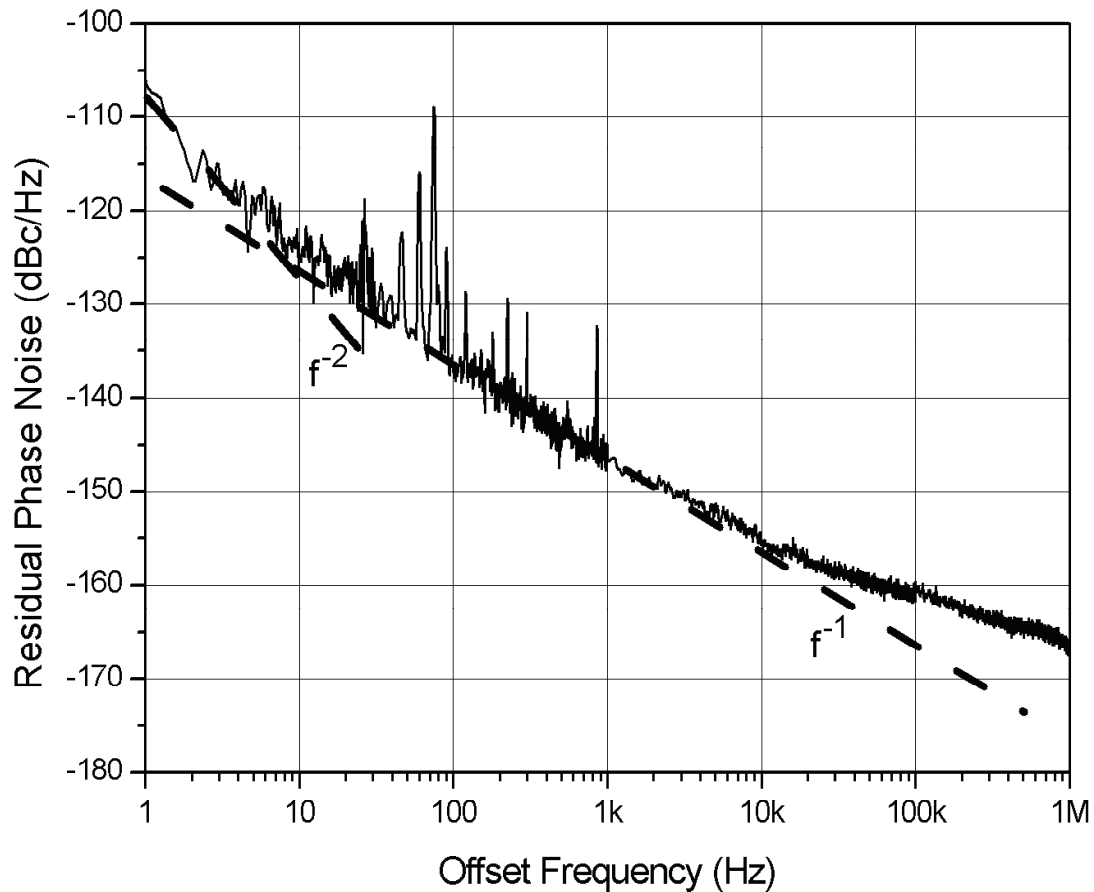


Fig. 3-6 Residual phase noise of STW resonator.

The residual phase noise of the loop amplifier is shown in Fig. 3-7. The noise floor is approximately -170dBc/Hz with a 1/f flicker noise corner at 17 kHz. Noise figure is the ratio of the output noise of an amplifier referred back to the input divided by the thermal noise floor. Noise figure is a common specification that is used to calculate the noise at Fourier frequencies f that are far from the carrier frequency. The noise figures listed in the data sheets of active devices are small signal noise figures, not dynamic noise figure. The dynamic noise figures are measured under actual large signal conditions and may differ from the small signal noise figures. It includes the multiplicative noise produced by the non-linearities of active device, in the presence of a large signal. In the presence of a carrier signal, the noise level is no longer

constant but often increases as f decreases. This increase usually changes at a rate of at least $1/f$, “flicker” behavior, which often significantly dominates over the white-noise level given by the NF, which in practice is measured in the absence of an actual signal through the amplifier. Furthermore, the flicker- noise level depends on the amplifier’s linearity and input power. Because of this signal induced rise in amplifier noise, many systems do not achieve the performance predicted by using the no-signal NF characterization. The dynamic noise figure can be expressed as:[45]

$$NF_D = L(f) - N_{TH} + P_{in}$$

Where NF_D is the dynamic noise figure in dB, N_{TH} is the thermal noise, P_{in} is the input signal power in dBm, and the $L(f)$ is the residual phase noise in dBc/Hz.

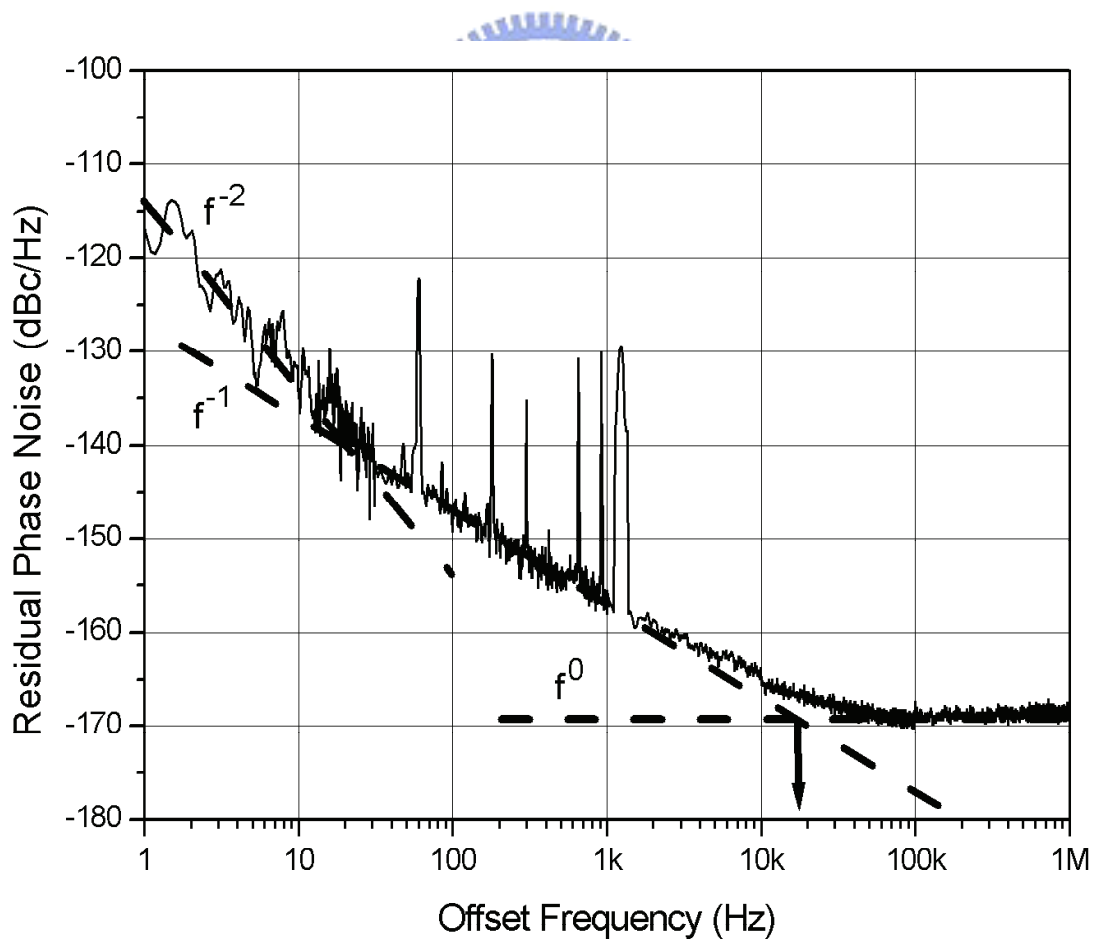


Fig. 3-7 Residual phase noise of loop amplifier.

The electronic phase shifter is mainly constructed varactors and inductor. The varactors are the noise contributors. The residual phase noise performance for the electronic phase shifter is measured and shown in Fig. 3-8.

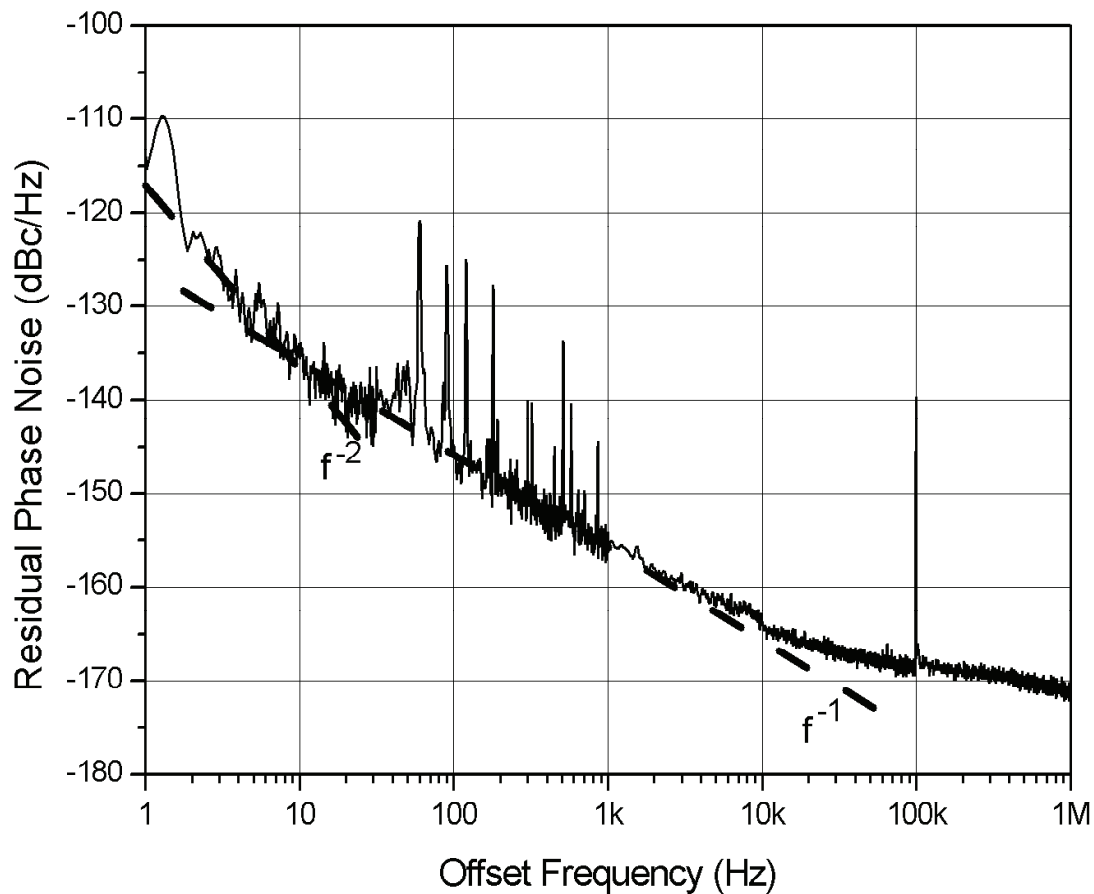


Fig. 3-8 Residual phase noise of electronic phase shifter.

3.3 Absolute Phase Noise of Oscillators

The phase noise test characterizes the output spectral purity of an oscillator by determining the ratio of desired energy being delivered by the oscillator at the specified output frequency to the amount of undesired energy being delivered at neighboring frequencies. This ratio is usually expressed as a series of power measurements performed at various offset frequencies from the carrier. The power measurements are normalized to a 1 Hz bandwidth basis and expressed with respect to

the carrier power level.

3.3.1 Phase techniques of absolute phase noise measurements

There are three dominant techniques used to measure the phase noise of oscillators: the direct spectrum analyzer approach, the phase-lock-loop (PLL) techniques, and the discriminator techniques.[46] The most direct and probably the oldest method used to measure the phase noise of oscillators is the direct spectrum analyzer method. Here the signal from the device-under-test (DUT) is input to a spectrum analyzer tuned to the DUT frequency. The sideband noise power can be directly measured and compared to the carrier signal power to obtain the phase noise spectrum. This method actually measures the total sideband noise, including AM noise and phase noise. If AM noise is much less than the phase noise, the measurement can be considered as to be the phase noise. The sensitivity of this method is limited by the internal local oscillator (LO) noise of the spectrum analyzer, and the inability to track any signal drift limits the close-to-carrier noise measurement capability of the analyzer.

When the AM noise is relatively high to the phase noise, a phase detector is required to separate the phase noise from the amplitude noise. The phase detector converts the phase difference of the two incident signal in to a voltage at the output of the detector. When the phase difference between the two input ports of the detector is set to 90 degree, the voltage output will be zero volts. Any phase fluctuation from quadrature will result in a voltage fluctuation at the output. When the quadrature is not maintained, an error can be introduced into results based on the amount of the phase delta from quadrature. The error is $20 \log [\cos (\text{phase deviation from quadrature})]$ (dB). Phase detectors are usually constructed by the double balanced mixers, and typically required large power signals at the input port to operate properly.

One of the signals must be of high power to switch the diodes in the detector, allowing the other signal to be of lower power.

There are two different measurement techniques which use a phase detector, along with associated filters, low noise amplifier, and baseband analyzer: one is the PLL with reference source measurement technique, and the other is FM discriminator measurement technique. Within the PLL with reference source measurement technique, another source is used to provide the reference phase signal for the phase detector. This is the standard measure of phase fluctuations described in NIST Technical Note 1337. Fig. 3-9 shows a block diagram of the method suggested by NIST.

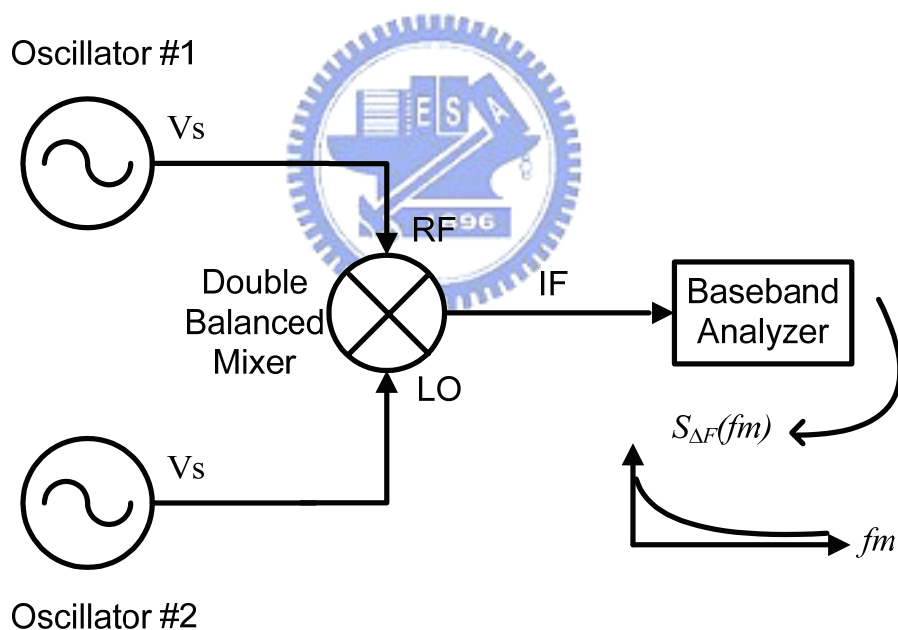


Fig. 3-9 General block diagram described in NIST technical note 1337.

Signals from two oscillators at the same nominal frequency are applied to the mixer inputs. The PLL is used to controlled either of the two sources and establish phase quadrature at the input ports of the phase detector. This means that one of the two sources used in this method must have DC voltage control capability for phase

locking. A very narrow band PLL is used to maintain a 90 degree phase difference between these two sources. The phase detector operation is such that when the input signals are 90 degrees out of phase (in quadrature), the output of the mixer is a small fluctuating voltage proportional to the phase difference between the two oscillators. By examining the spectrum of this error signal on the spectrum analyzer, the phase noise performance of this pair of oscillators may be measured. If the noise of one oscillator dominates, its phase noise is measured directly. A useful and practical approximation when the two test oscillators are electrically similar is that each oscillator contributes one-half the measured noise power. When three or more oscillators are available for test, the phase noise of each oscillator may be accurately calculated by solving simultaneous equations expressing data measured from the permutations of oscillator pairs. The frequency difference between the two sources at the phase detector must be less than 10% of the peak-tuning-range (PTR) for PLL to close. High PTR will cause the increase in the system noise floor. This feature makes this technique is not suitable for measuring the high-drift-rate low phase noise sources which requires high PTR. Lower power from the DUT or the reference source can cause the phase detector noise floor to rise or the phase detector to not operate. Low noise amplifier prior to the phase detector can help to solve this problem, but the residual noise of the amplifiers will add to the phase detector phase noise floor. The increase in the system noise floor will degrade the sensitivity of the phase detector. The residual noise of the amplifier becomes a limiting factor in the overall system measurement noise floor.

The oscillators with SAW or STW resonators have both low phase noise and high drift rate characteristics. So, the direct spectrum techniques and the PLL with reference source measurement techniques are not fulfilling the requirement while measuring the low phase noise oscillator with piezoelectric resonator. FM

discriminator technique is the hopeful candidate for measuring these low phase noise SAW oscillator. The theory and design consideration are describe as follows.

3.3.2 Theory of FM discriminator [46,47]

The basic block diagram for frequency discriminator is shown as Fig. 3-10. Unlike the PLL phase detector method, the frequency discriminator method does not require a second reference source phase locked to the source under test. This makes the frequency discriminator method extremely useful for measuring sources those are difficult to phase lock, including sources those are microphonic or drift quickly. It can also be used to measure sources with high-level, low-rate phase noise, or high close-in spurious sidebands, conditions with can pose serious problems for the phase detector method. A wide-band delay line discriminator can be implemented using a low loss coaxial cable. A resonator can also be applied for the narrow-band delay line discriminator. Delay line discriminators are only capable of measuring phase type random noise and are in fact insensitive to AM noise. Typically AM rejection for the delay line discriminator is greater than 20dB.

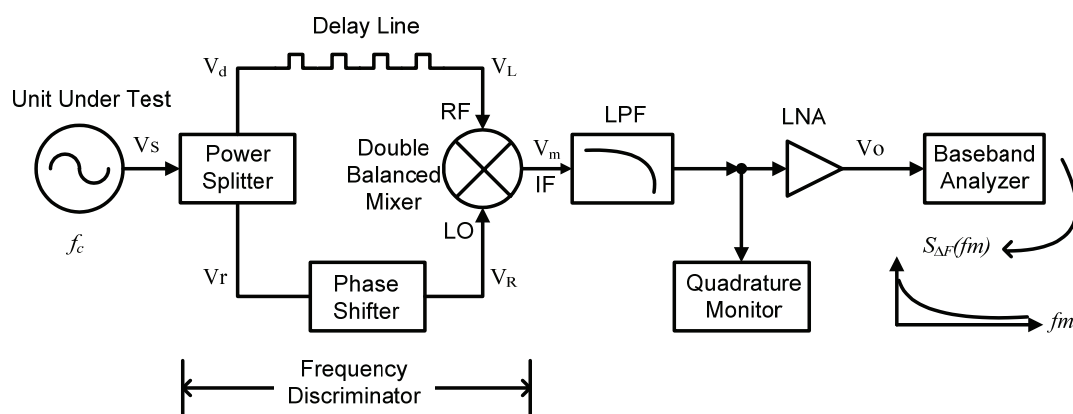


Fig. 3-10 Basic block diagram for frequency discriminator.

A delay line and a mixer operating as a phase detector have the combined effect of a frequency discriminator. The delay line transforms any frequency fluctuation into phase fluctuation and the mixer with L and R inputs at 90 degree offset linearly converts the phase fluctuations into voltage fluctuations at the IF port. Fig. 3-10 shows the basic block diagram of frequency discriminator. The theory can be derived as follows:

The source under test can be represented as

$$V_s(t) = A_o \cos[\omega_c t + \phi(t)] \quad (3.1)$$

Where A_o is the signal magnitude, ω_c is the carrier frequency, and $\phi(t)$ is the function describing the phase fluctuation with time.

Equation (1) can be expanding as:

$$V_s(t) = A_o [\cos \omega_c t \cos \phi(t) - \sin \omega_c t \sin \phi(t)] \quad (3.2)$$

When the phase noise is treated as narrow band phase modulation, the magnitude of $\phi(t)$ is small and the maximum phase variation from $\phi(t)$ is much less than one radian. Since $\phi(t)$ is very small, the approximation $\cos \phi(t) \approx 1$ and $\sin \phi(t) \approx \phi(t)$ can be made. Equation (2) can be rewritten as

$$V_s(t) = A_o [\cos \omega_c t - \phi(t) \sin \omega_c t] \quad (3.3)$$

$$V_d(t) = L_s A_o \cos[\omega_c t + \phi(t)]$$

$$V_r(t) = L_s A_o \cos[\omega_c t + \phi(t)]$$

Where L_s is the insertion loss of power splitter.

We can get $V_L(t)$ and $V_R(t)$ which are the input signals of the L-port and R-port for the mixer type phase detector respectively,

$$V_L(t) = L_s L_D A_o \cos[\omega_c (t - \tau) + \phi(t - \tau)]$$

$$V_R(t) = L_s A_o \cos[\omega_c t + \phi(t) + \phi_p]$$

Where L_D is the insertion loss of delay line.

The mixer output signal $V_m(t)$ can be express as:

$$V_m(t) = L_s L_D L_m A_o \left\{ \cos[2\omega_c t - \omega_c \tau + \phi_p + \phi(t) + \phi(t - \tau)] + \cos[\phi_p + \omega_c \tau + \phi(t) - \phi(t - \tau)] \right\}$$

After passing through the low pass filter and low noise amplifier, the output signal $V_o(t)$ is,

$$V_o(t) = L_s L_D L_m G A_o \cos[\phi_p + \omega_c \tau + \phi(t) - \phi(t - \tau)]$$

Where L_m is transfer gain of the mixer, and G is the sum of insertion loss of low pass filter and the gain of the low noise amplifier.

If $\phi_p + \omega_c \tau = \frac{\pi}{2}$, than

$$\begin{aligned} V_o(t) &= L_s L_D L_m G A_o \cos\left[\frac{\pi}{2} + \phi(t) - \phi(t - \tau)\right] \\ V_o(t) &= -L_s L_D L_m G A_o \sin[\phi(t) - \phi(t - \tau)] \\ V_o(t) &= -L_s L_D L_m G A_o [\phi(t) - \phi(t - \tau)] \end{aligned} \quad (3.4)$$

Here, the output signal $V_o(t)$ is proportional to the phase difference $\phi_o(t) = [\phi(t) - \phi(t - \tau)]$.

Let $\phi(t) = \phi_m \sin \omega_m t$

Than $\phi(t) - \phi(t - \tau) = \phi_m [\sin \omega_m t - \sin \omega_m (t - \tau)]$

$$\begin{aligned} \phi_o(t) &= 2\phi_m \sin \frac{\omega_m \tau}{2} \cos(\omega_m t - \frac{\tau}{2}) \approx 2\phi_m \sin \frac{\omega_m \tau}{2} \cos \omega_m t \\ V_o(t) &= -2L_s L_D L_m G A_o \phi_m \sin \frac{\omega_m \tau}{2} \cos \omega_m t \end{aligned} \quad (3.5)$$

Therefore the sensitivity to the phase noise of the source is:

$$Sensitivity = 2 \sin \pi f_m \tau \quad (3.6)$$

where f_m is the offset frequency, and τ is the delay time.

3.3.3 Frequency Discriminator System Setup

The frequency discriminator is used to measure the phase noise of the oscillator with STW resonator. The delay line frequency discriminator is implemented with Agilent's E5503B phase noise measurement system and a delay line. The connect diagram for this system is shown in Fig. 3-11. The key element in the design of delay line discriminator is the delay line itself. For accurate phase noise measurements, it was shown that the delay time τ must be chosen such that $f_M \ll \frac{1}{2\pi\tau}$, where f_M is the maximum frequency of the components to be measured. A 312ns delay line implemented by an ANDREW LDF5-50A low-loss coaxial cable is used in this measurement. Long enough delay time is needed to ensure the sensitivity of the measurement system. In Fig. 3-12, it reveals the system noise floor and the null points of the frequency discriminator. The sensitivity of the discriminator techniques is approximately equal to the phase detector system sensitivity at the offset frequency $f_m = \frac{1}{2\pi\tau}$ and tipped up by 20dB/decade for $f_m < \frac{1}{2\pi\tau}$. The noise floor is set by the LNA noise and therefore does not have $\frac{\sin x}{x}$ -type response. Increasing the length of the delay time improve the close-to-carrier noise floor but reduces the power to the phase detector. It also reduces the maximum offset frequency that can be measured with no $\frac{\sin x}{x}$ correction.

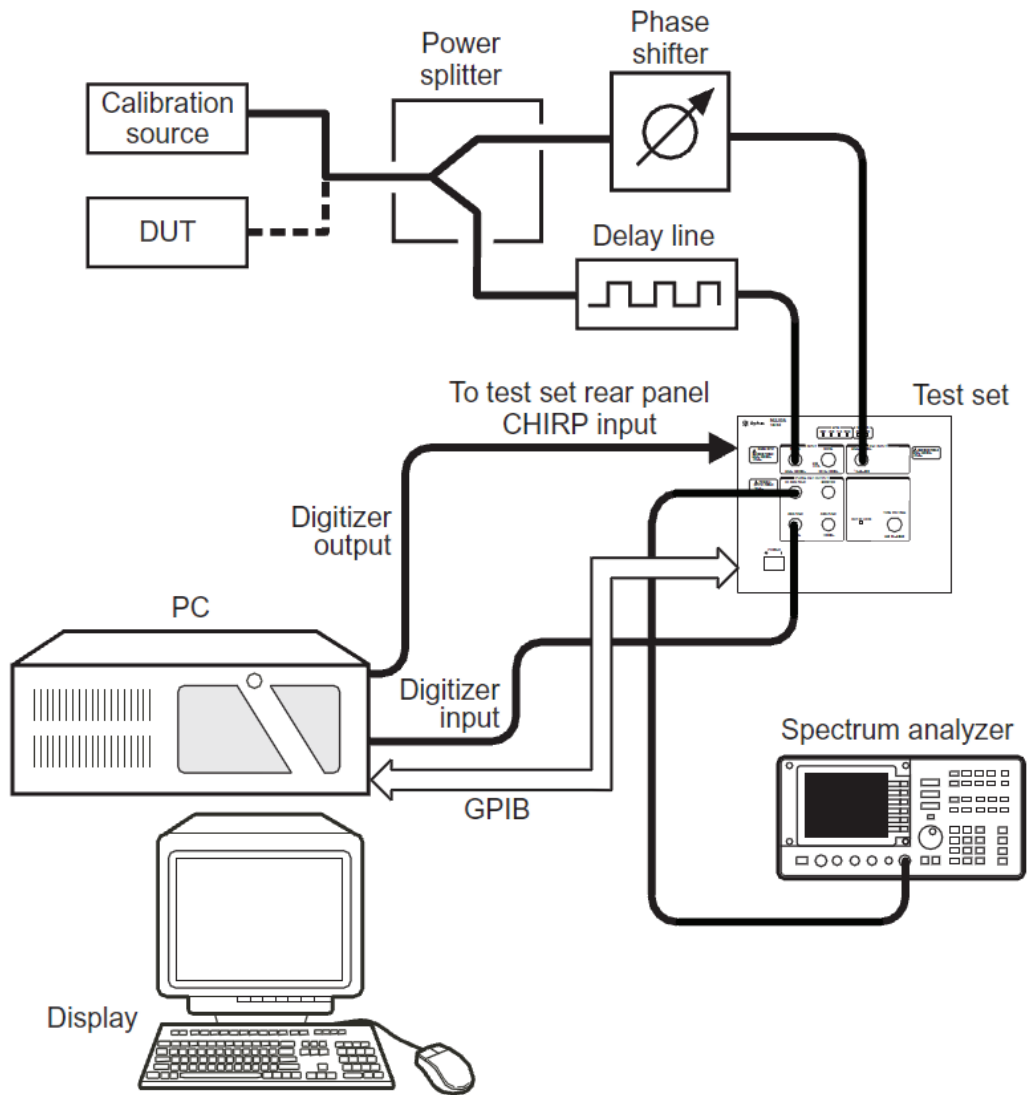


Fig. 3-11 Connect diagram of Agilent E5503B for FM discriminator technique. [44]

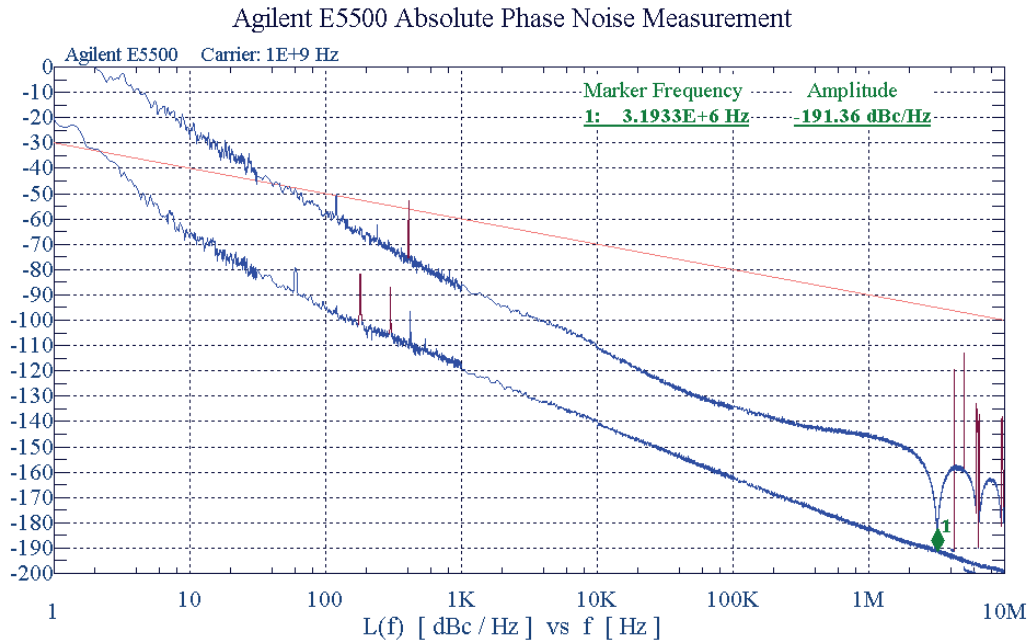


Fig. 3-12 The measured system noise floor and the null points for FM discriminator.

3.4 Prediction of Phase Noise

A feedback loop oscillator with STW resonator is presented in section 2.2. For comparison, the measured absolute phase noise of the oscillator and the residual phase noise of main components for the oscillator, including loop amplifier, electronic phase shifter, and STW resonator, are shown in Fig. 3-13. The spectral shape of the oscillator (curve 1) indeed arrears $1/f^3$ near the carrier. The intersection point with $1/f$ curve is around 50 kHz offset. The magnitude at 100 kHz offset is -153dBc/Hz.

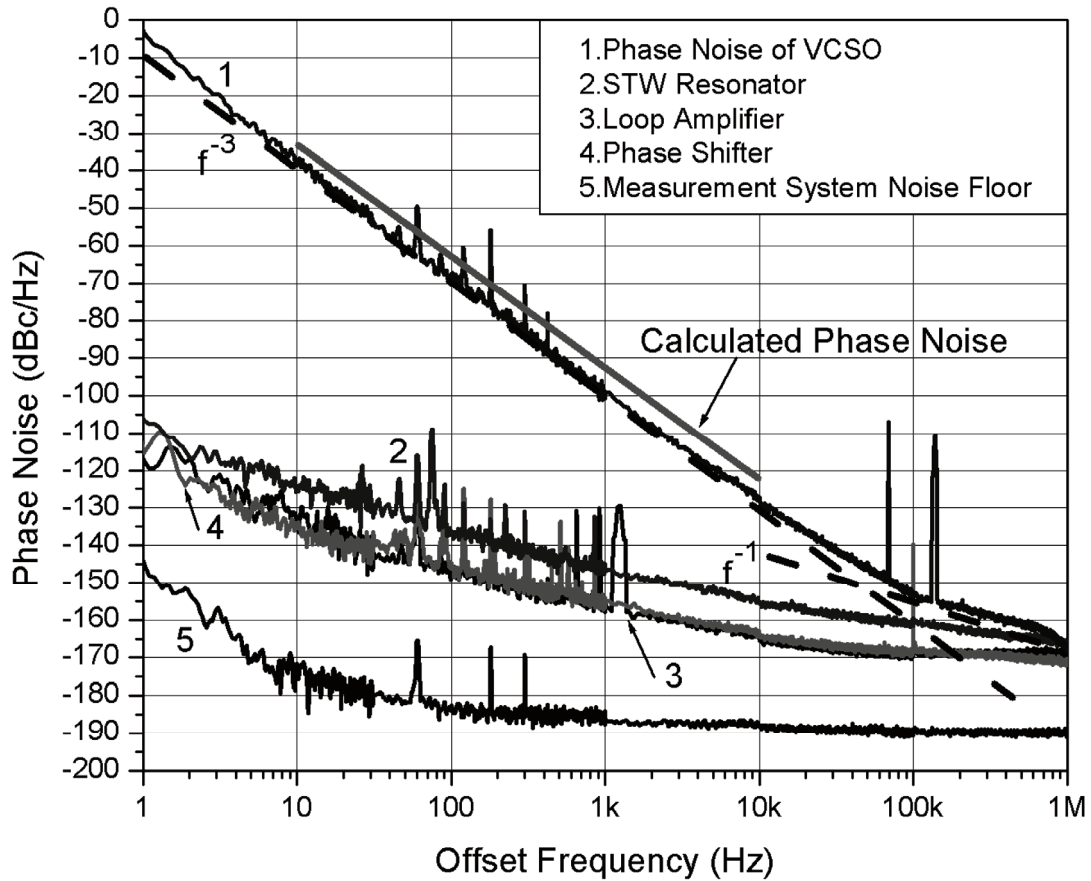


Fig. 3-13 Measured phase noise for the 2488.32 MHz STW oscillator.

To analyze the shaping behavior of the close loop, the residual phase noises are examined. In Fig. 3-13, it reveals that the noise n_r from the STW resonator (curve 2) is dominant about 10dB above those from the amplifier n_g (curve 3) and the phase shifter n_p (curve 4). The phase shifter has the same order of magnitude as that in amplifier. The system's floor is also indicated as in curve 5, which is much lower than the measured items.

As referred to Fig. 3-14, the magnitude of the loop gain under steady state is assumed to one with a rather wide bandwidth, at least ± 500 kHz at 2488.32 MHz. The STW resonator looks like a pure resistor not a inductor at the oscillation frequency. In the Lesson's model the transfer function is consider to be a symmetrical one on each side of the carrier frequency.

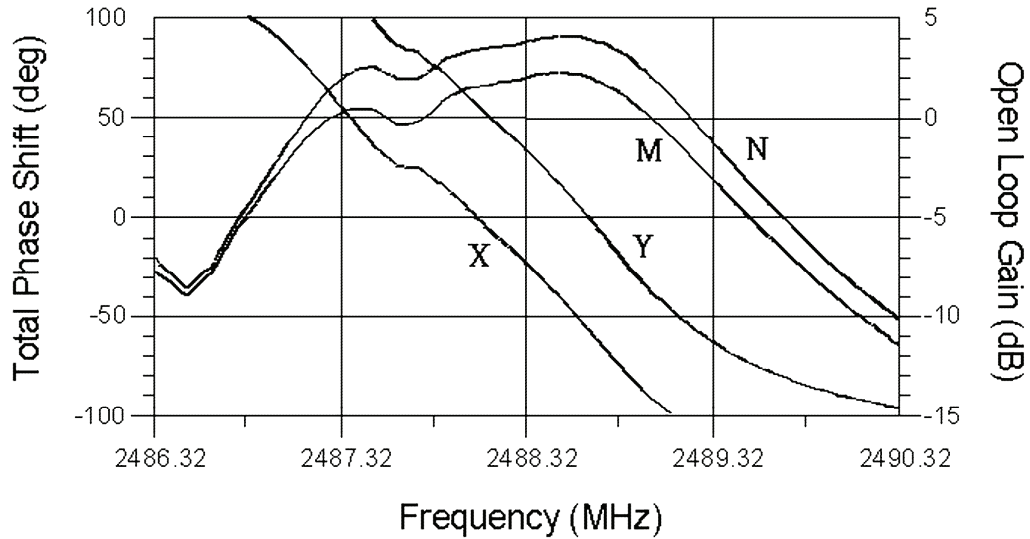


Fig. 3-14 The open loop gain and phase shift of the STW oscillator at the oscillation frequency.

As shown in Fig. 3-15, the basic open loop circuit is divided to four components, phase shifter, STW resonator, amplifier, and power splitter, whose transfer functions are $P(\omega)$, $R(\omega)$, $G(\omega)$, and $D(\omega)$, respectively.

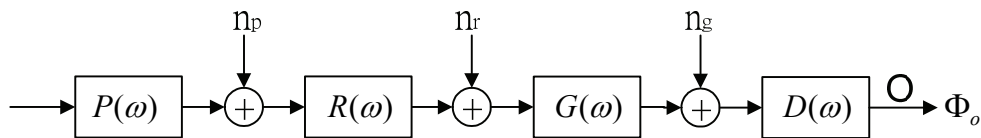


Fig. 3-15 Transfer functions in open loop circuit.

The power spectral density (PSD) at output point o is as follows:

$$\Phi_o = (n_g + n_r \cdot |G(\omega)| + n_p \cdot |R(\omega)| \cdot |G(\omega)|) \cdot |D(\omega)|$$

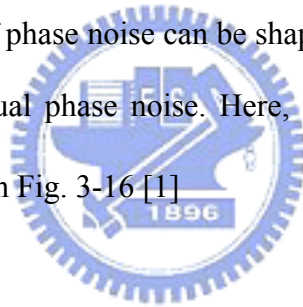
Because of n_r is greater than n_g and n_p , the output noise is further simplified as

$$\Phi_o \cong n_r \cdot |G(\omega)| \cdot |D(\omega)|$$

The product $|G(\omega)| \cdot |D(\omega)|$ is approximately 8~9dB in this work. The phase shift as a function of frequency is assumed linear with slope or group delay τ_g , which is roughly equal to 1.74×10^{-6} rad/Hz in our case, within the limited bandwidth. Hence, the normalized open loop gain is written as $e^{-j\Delta\omega\tau_g}$, where $\Delta\omega$ is the offset frequency from the center frequency. Then the closed loop gain is obtained as

$$\begin{aligned} \text{Closed Loop gain} &= \frac{1}{1 - e^{-j\tau_g\Delta\omega}} \\ &= \frac{1}{2 \sin\left(\frac{\tau_g\Delta\omega}{2}\right)} \end{aligned}$$

According to [43], the PSD of phase noise can be shaped by multiplying the square of closed-loop gain to the residual phase noise. Here, the shaping factor for the PSD is $\left[2 \sin(\Delta\omega\tau_g / 2)\right]^{-2}$ as shown in Fig. 3-16 [1]



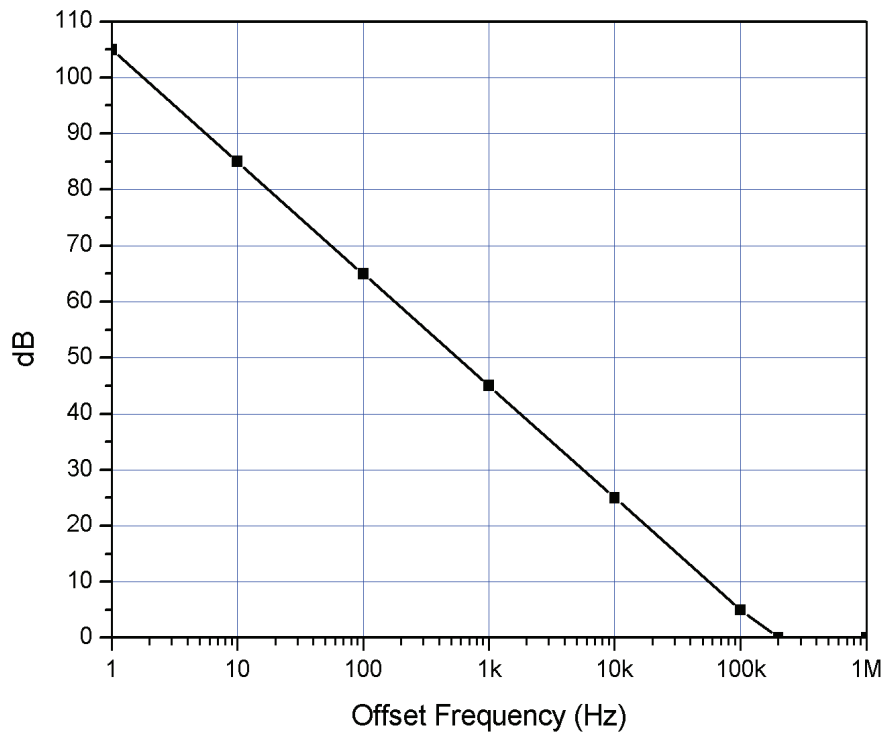


Fig. 3-16 The transfer function vs. Fourier frequency.

For the close-in noise with $\Delta\omega$ which is smaller than $\frac{\pi}{4}$, the shaping appears as $(\Delta\omega\tau_g)^{-2}$. It is concluded that the phase noise is indeed shaped from the residual noise by the $(\Delta\omega)^{-2}$ term, which is originated from the high Q resonator. The calculated results are in good agreement with the measurements.

Chapter 4

Modified Pierce Oscillator with One-port SAW

Resonator

4.1 Introduction

The Pierce oscillator, as shown in Fig. 4-1, is one of the more popular circuits for the crystal oscillators used today. It has very low power consumption with high stability. The Pierce oscillator is a series resonant circuit for fundamental mode crystal, and oscillates just above the series resonant frequency of the crystal. [48] But the crystal resonator with fundamental frequency higher than 200 MHz is hard to be available. The one-port SAW resonator has the same topology with bulk crystal resonator. It is the hopeful candidate to replace the crystal resonator in Pierce oscillator, and make Pierce oscillator be able to work at the frequency from 200 MHz to 1 GHz. The main advantage of the use of SAW resonator is the high quality factor (unloaded quality factor: $Q = 8000$). Although the fundamental frequency of SAW resonator is up to 1 GHz, the shunt capacitance is similar to the low frequency crystal resonator. The relative large shunt capacitor makes the insertion loss of π -feedback network in conventional Pierce oscillator too large to overcome.

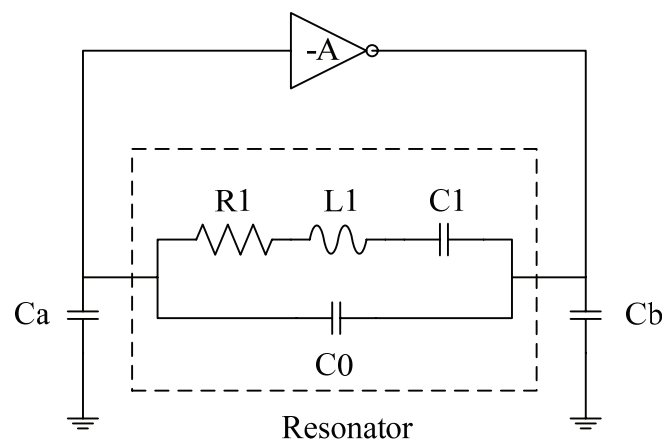


Fig. 4-1 Conventional Pierce oscillator.

In this section, a modified Pierce oscillator for SAW resonator is proposed to prevent the large insertion loss caused by shunt capacitor of SAW resonator. A low phase noise voltage controlled Pierce oscillator with SAW resonator at 622 MHz is presented. The active part of oscillator is designed and fabricated with Taiwan Semiconductor Manufacturing Company (tsmc) 0.18 μ m CMOS process. The core oscillation circuit consumes 10.2mA from +1.2V DC power supply. The measured white phase noise floor is -175dBc/Hz for carrier offset frequency greater than 1 MHz. The oscillator's phase noise level at 10 kHz carrier offset frequency is approximately -136dBc/Hz .

4.2 One-port SAW Resonator

In conventional Pierce oscillator circuits, the crystal resonator is effectively inductive and forms a highly frequency selective π network with two capacitors which provides the additional phase shift necessary to sustain oscillation. But crystal resonator is hard to be available which fundamental frequency is higher than 200 MHz. For this reason, one-port SAW resonator is chosen to replace crystal resonator for high frequency application. One-port SAW resonator is good for frequency from 200 MHz to 1 GHz and the same topology with bulk crystal resonator. The typical equivalent circuit model used for one port SAW resonator is shown in Fig. 4-2. This models the motional arm as series R-L-C in parallel with a static capacitor C_0 . The static capacitor C_0 is due to the inter-digital transducers (IDTs) of SAW resonator and the stray capacitor of package between the terminals of SAW resonator. The typical values at 622 MHz are given as $L_1 = 42.22 \mu\text{H}$, $C_1 = 1.55 \text{ fF}$, $R_1 = 20.2 \text{ Ohm}$, $C_0 = 2.11 \text{ pF}$. Although the topology is similar to that in low frequency crystal resonator,

the shunt capacitance C_0 has a serious bad effect on the oscillation because of high frequency operation. [49] This point is detailed in the following paragraph. The reactance characteristics with frequency are shown in Fig. 4-3. F_r is called the resonant frequency and is where L_1 and C_1 are in series resonance and the resonator looks like a small resistance R_1 . The frequency F_a is the anti-resonant frequency and is the point the where L_1 - C_1 look inductive and resonate with C_0 to form the parallel resonance frequency F_a .

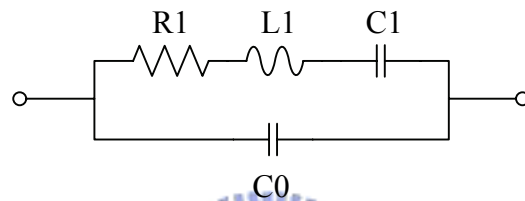


Fig. 4-2 Equivalent circuit for one-port SAW resonator.

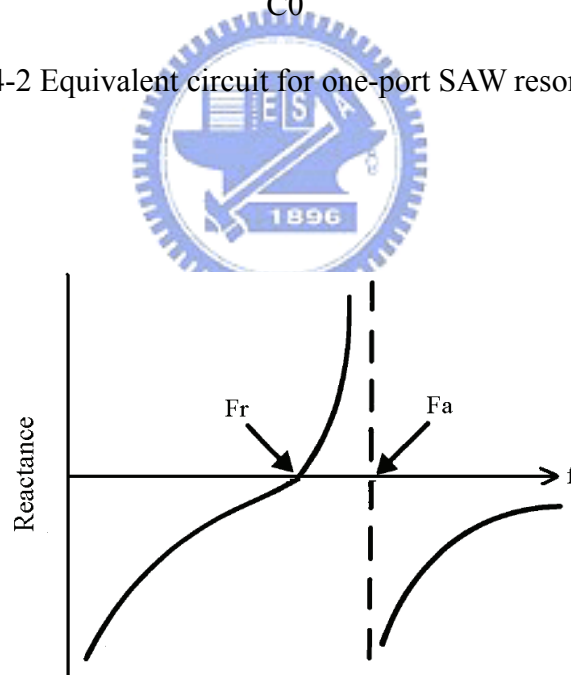


Fig. 4-3 Reactance of SAW resonator.

4.3 Oscillator Design

The Pierce oscillator is designed to look into the lowest possible impedance across the resonator terminals. The oscillation satisfies the Barkhausen criterion with

closed loop gain ≥ 1 and phase shift equal 360 degrees. [48] As shown in Fig. 4-1, the signal from the input to the output of the amplifier is phase shift 180 degrees. The resonator appears as a large inductance since it is operating in the parallel mode between F_r and F_a . In conjunction with C_a and C_b , the passive circuit forms a pi network that provides an additional 180 degrees of phase shift from output to the input. C_a in series with C_b plus any additional stray capacitance forms the load capacitance for the resonator. However, there exists some shunt capacitance in the SAW resonator itself, which is often ignored by the SAW vendors. [49] The implications are illustrated in the followings. The insertion loss and the phase shift of the SAW resonator in conjunction C_a and C_b are shown in Fig. 4-4. The line A and the line C are the insertion loss and phase shift respectively obtained without C_a and C_b . The initial phase at 621 MHz is negative rather than positive as often observed in crystal resonator. With increasing C_a and C_b , the phase shift downward and reaches finally the requirement of 180 degrees as shown in the line D. Unfortunately, the minimum insertion loss also degrades from -1 dB to -8 dB as shown in the line B. This implies the amplifier needs to draw more DC power to overcome the insertion loss. Accordingly, the efficiency of the oscillator is degraded.

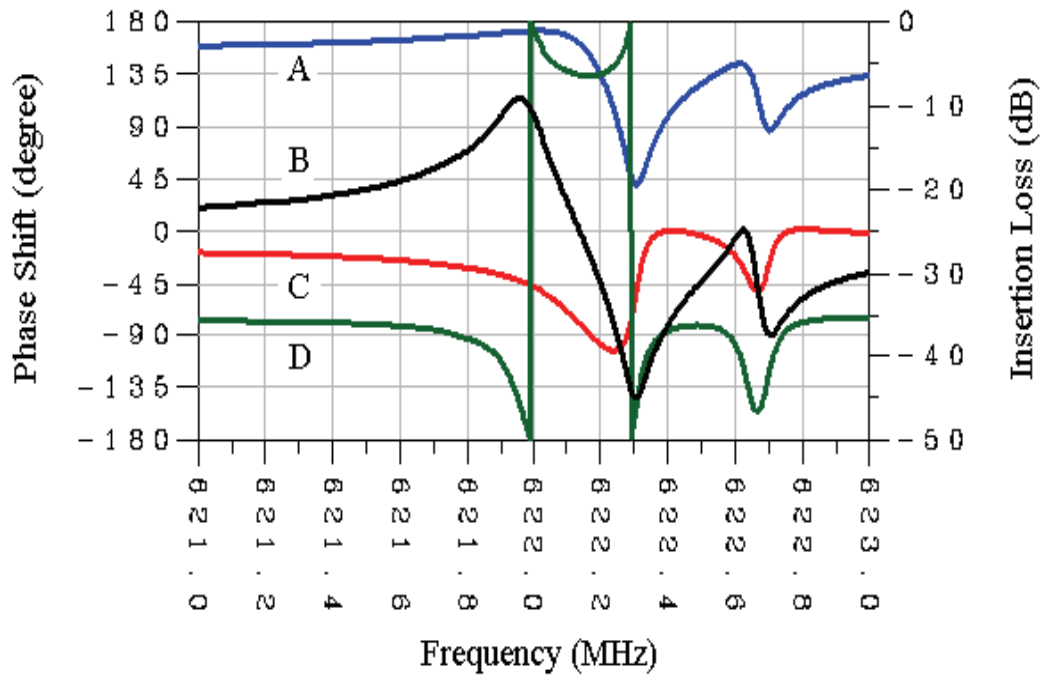


Fig. 4-4 Phase shift and insertion loss of open-loop simulation for conventional Pierce oscillator.



To prevent the degradation of efficiency, we modify the Pierce oscillator as shown in Fig. 4-5. An additional phase shift is inserted in series with the SAW resonator. The insertion loss and the phase shift in the π feedback network in modified circuit are shown in Fig. 4-6. In the beginning, the capacitances of C_a and C_b were trimmed until the phase shift of 180 degrees at 622.2 MHz as shown in the line III. In this moment, the insertion loss of π network as shown in line II is about 15dB too high to be overcome. To achieve the Barkhausen's criterion, the resonance phase shifter is trimmed to have the minimum insertion loss coincidence with the frequency of 180 degrees as shown in line IV. We can see the minimum insertion loss before (line II) and after (line I) adding the phase shift is almost the same. No larger power amplifier is needed. The efficiency of oscillator is improved.

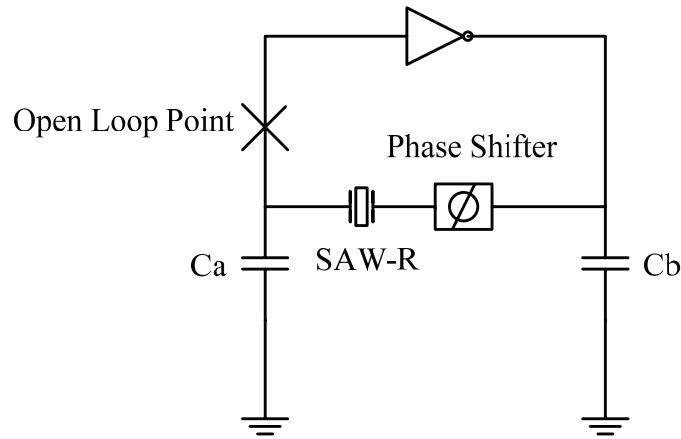


Fig. 4-5 Modified Pierce oscillator.

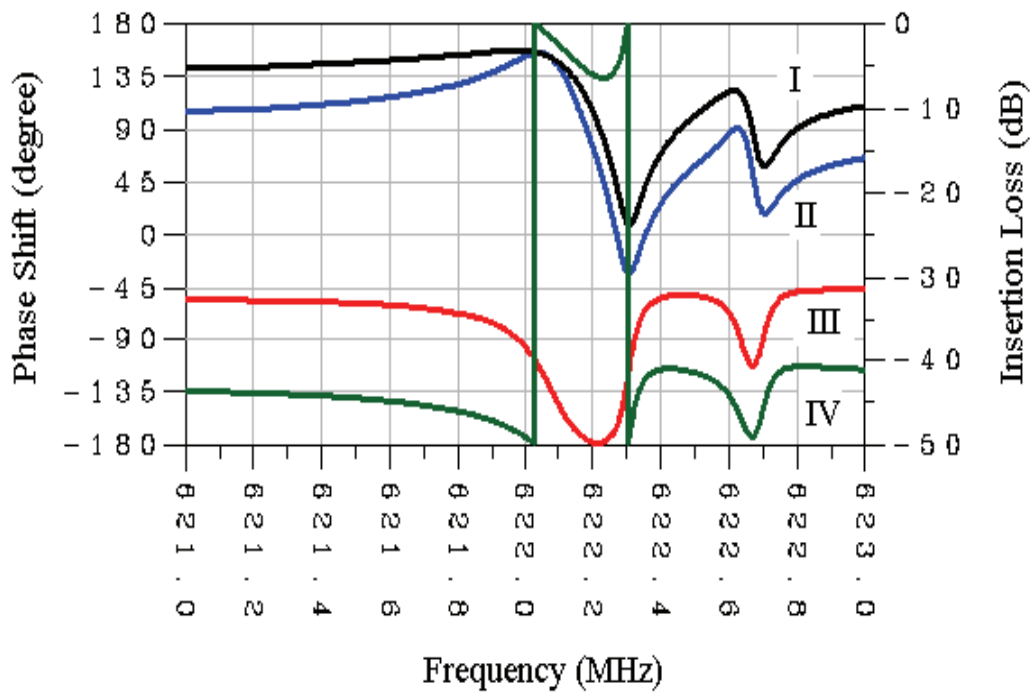


Fig. 4-6 Phase shift and insertion loss of open-loop simulation for modified Pierce oscillator.

In Fig. 4-6, we can find an extra 90 degree phase shifter is required. The phase shifter can be implemented in different types, including transmission line, and lump LC components. The 90 degree phase shifter can be implemented with a $\frac{\lambda}{4}$ transmission line. While applied in the frequency of 622.08 MHz, the phase shifter

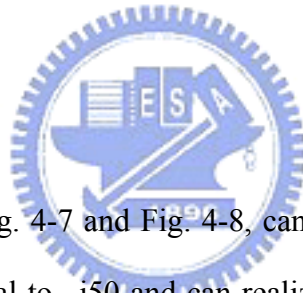
constructed by lump LC circuits is the better choice because of the wave length in this frequency is about 48 cm. The size of the transmission line phase shifter is unacceptable. Here, we will discuss the method to design phase shifter with lump LC components.

The After we decide the impedance Z_o and phase shift θ for the phase shifter we need, the 2 x 2 transmission (ABCD) matrix can describe the two-port phase shifter as follows:[50]

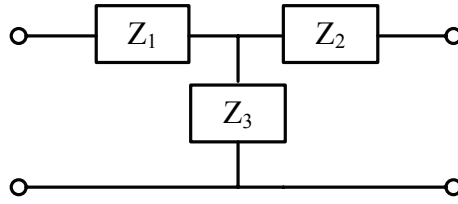
$$\begin{bmatrix} A & B \\ C & D \end{bmatrix} = \begin{bmatrix} \cos \theta & jZ_o \sin \theta \\ j \frac{\sin \theta}{Z_o} & \cos \theta \end{bmatrix}$$

Since Z_o is 50Ω and $\theta = 90^\circ$, the ABCD matrix of the phase shifter can be expressed as:

$$\begin{bmatrix} A & B \\ C & D \end{bmatrix} = \begin{bmatrix} 0 & j50 \\ j0.02 & 0 \end{bmatrix}$$

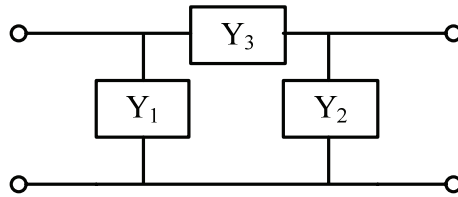


T or π circuit, as shown in Fig. 4-7 and Fig. 4-8, can achieve the requirement of the matrix. In T-circuit, Z_3 is equal to $-j50$ and can realized with a capacitor $C=5.11$ pF. For symmetric, Z_1 and Z_2 is the same value and equal to $-Z_3$. Z_1 and Z_2 can be realized with inductors $L=12.79$ nH. In π -circuit, Y_3 is equal to $-j0.02$ and can be realized with an inductor $L=12.79$ nH. For symmetric, Y_1 and Y_2 is the same value and equal to $-Y_3$. Y_1 and Y_2 can be realized with capacitors $C=5.11$ pF. Finally, we choose the π -circuit, as shown in Fig. 4-9, for the phase shifter in the oscillator. By using π -circuit, the C_2 and combined with C_b and C_1 can absorb some parasitic capacitance from SAW resonator. The final modified Pierce oscillator just has one more inductor and one more capacitor than conventional Pierce oscillator.



$$A = 1 + \frac{Z_1}{Z_3} \quad B = Z_1 + Z_2 + \frac{Z_1 Z_2}{Z_3} \quad C = \frac{1}{Z_3} \quad D = 1 + \frac{Z_2}{Z_3}$$

Fig. 4-7 The ABCD matrix for T-circuit.



$$A = 1 + \frac{Y_2}{Y_3} \quad B = \frac{1}{Y_3} \quad C = Y_1 + Y_2 + \frac{Y_1 Y_2}{Y_3} \quad D = 1 + \frac{Y_1}{Y_3}$$

Fig. 4-8 The ABCD matrix for π -circuit.

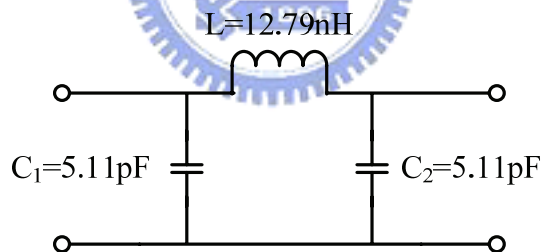


Fig. 4-9 The 90 degree phase shifter at 622.08 MHz.

The active part of this SAW oscillator is designed with tsmc 0.18um CMOS process. The oscillator circuit is shown in Fig. 4-10. Because of the RF signal is input from the gate and amplified after passing through the output drain terminal, the dominant noise source is from the gate input terminal. This is because the noise source in an amplifier system is due to following equation [51]:

$$NF_T = NF_1 + \frac{NF_2 - 1}{G_1} + \dots + \frac{NF_n - 1}{G_1 G_2 \dots G_{n-1}}$$

Thus, the noise of the system with amplification is governed by the input stage, where G_i is the gain of each stage amplifier. In core oscillation circuit, drive power into the resonator should be kept at a safe minimum level to assure proper start up. Excessive drive power will result in resonator fracture or long term frequency drift. If multi-stage amplifier is used, the G_1 is not large enough to suppress the noise caused by 2nd or 3rd stage amplifier. To achieve the low phase noise, only one active transistor is used in the core circuit.

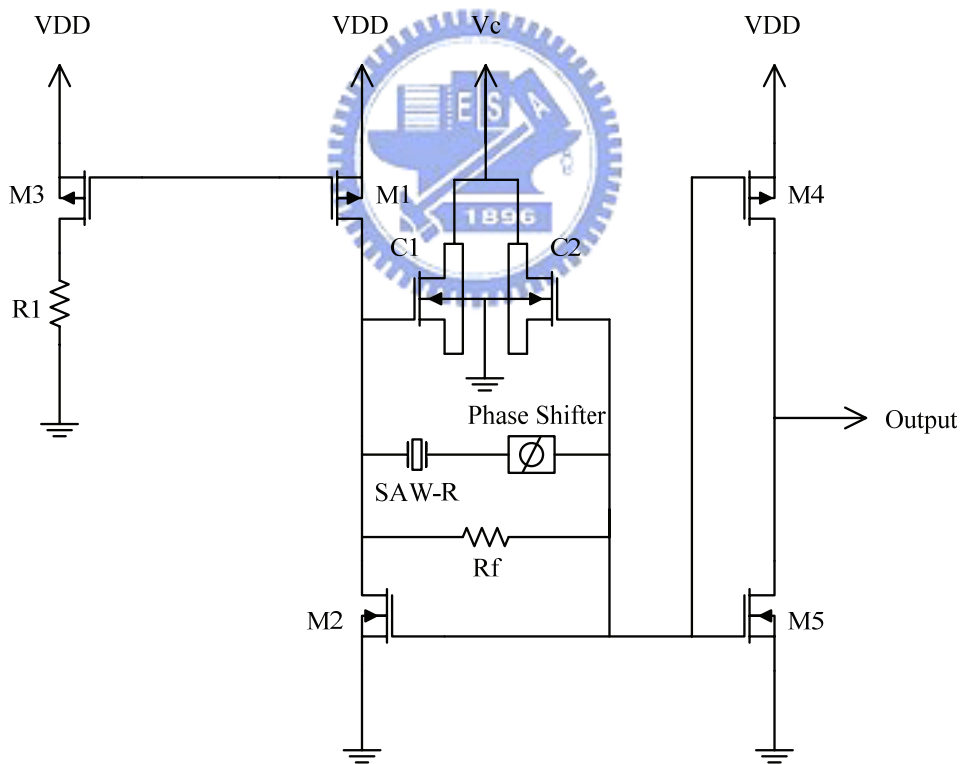


Fig. 4-10 Circuit diagram of active device of SAW oscillator.

Negative resistance is created by using the RF-NMOS device M2 in the common source configuration. The device size of M2 is $W/L = 192/0.18$ (um). PMOS M1 and

M3 are used as the current mirrors. M1 acts as the active load of M2. R_f is the feedback resistor of M2. The chosen value of R_f is sufficiently large so that the input impedance of the inverter and the resonator can be matched. The SAW resonator in series with phase shifter is used as a frequency-determining element between the drain and the gate of M2. The output power is coupled from the gate of M2 to the limiter buffer amplifier constructed by M4 and M5.

Fig. 4-11 shows the linear simulation of open-loop frequency response using the osc-port function of Agilent Advance Design System (ADS) software in order to insure that negative resistance is large enough ($|S_{11}| > 1$) in the desired frequency. The open-loop point is shown in Fig. 4-5. The oscillation starts when the phase of S_{11} equals to zero and amplitude of S_{11} is larger than one. The Barkhausen criteria are also satisfied in this moment.

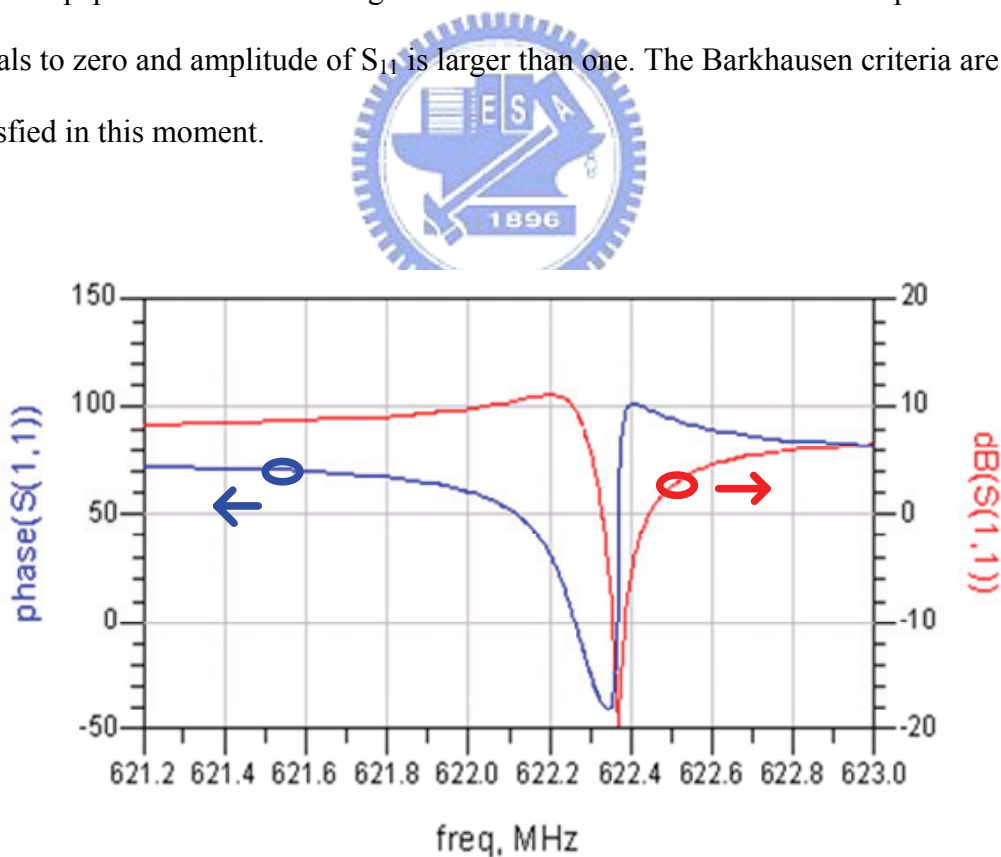


Fig. 4-11 Results of linear simulation using ADS.

4.4 Oscillator Performance

The photograph of chip is shown in Fig. 4-12. The chip was fabricated by tsmc 0.18um CMOS process. Chip size is 850 x 465 μm^2 . Table 4.1 is the summary of SAW oscillator performance. The spectrums of oscillation in narrow and broadband band scan are shown in Fig. 4-13 (a) and (b), respectively. The oscillator provides 4.0dBm of output power. Agilent E5052A Signal Source Analyzer was used to measure the phase noise of the oscillator. The measured phase noise is shown in Fig. 4-14 at 622 MHz. Phase noise of -136dBc/Hz at 10 kHz offset represents the excellent phase noise of this work.

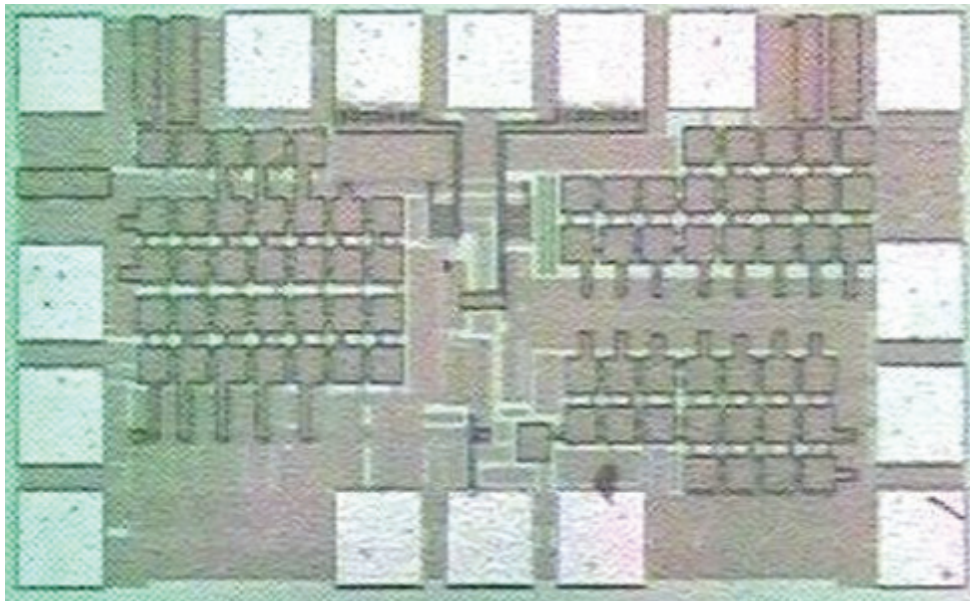
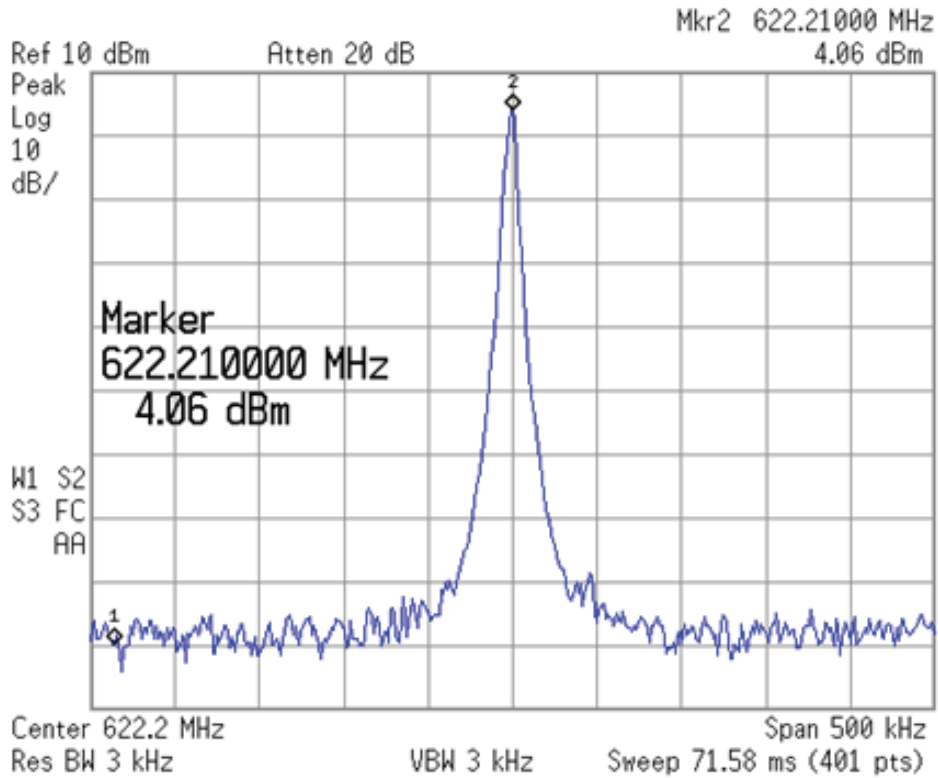


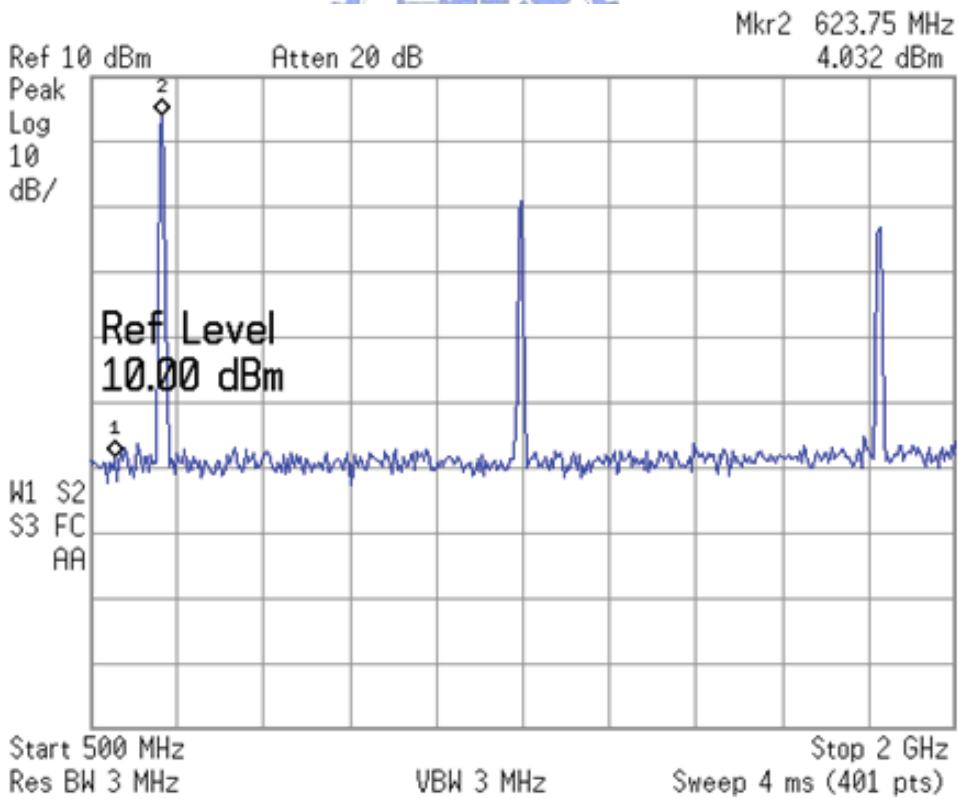
Fig. 4-12 Picture of the active part of the SAW oscillator.

Table 4.1: Measurement results for the SAW oscillator.

Output Frequency	622 MHz
Output Power	4.0dBm
Phase Noise	-136 dBc/Hz @ 10 kHz offset
DC Power Supply	1.2V, 15mA



(a)



(b)

Fig. 4-13 (a) Fundamental spectrum and (b) harmonics spectrum of oscillator.

The comparisons of phase noise with other works are shown in Fig. 4-14. [52] We can see the phase noise of this work is much lower than those in Vectron VS700 and the product of TXC. The reasons may be from the low noise process of device in our work. As indicated in [53], the noise figure of the device by circuit-theory-derived equation was given as

$$NF_{\min} = 1 + 2\gamma \frac{f}{f_t} \sqrt{\gamma + g_m R_g}$$

Where R_g is the gate resistance, f_t is the unit gain frequency, f is the oscillation frequency, and γ is the proportional constant of the drain current noise. In the above equation, we can see larger f_t can reduce the NF_{\min} .

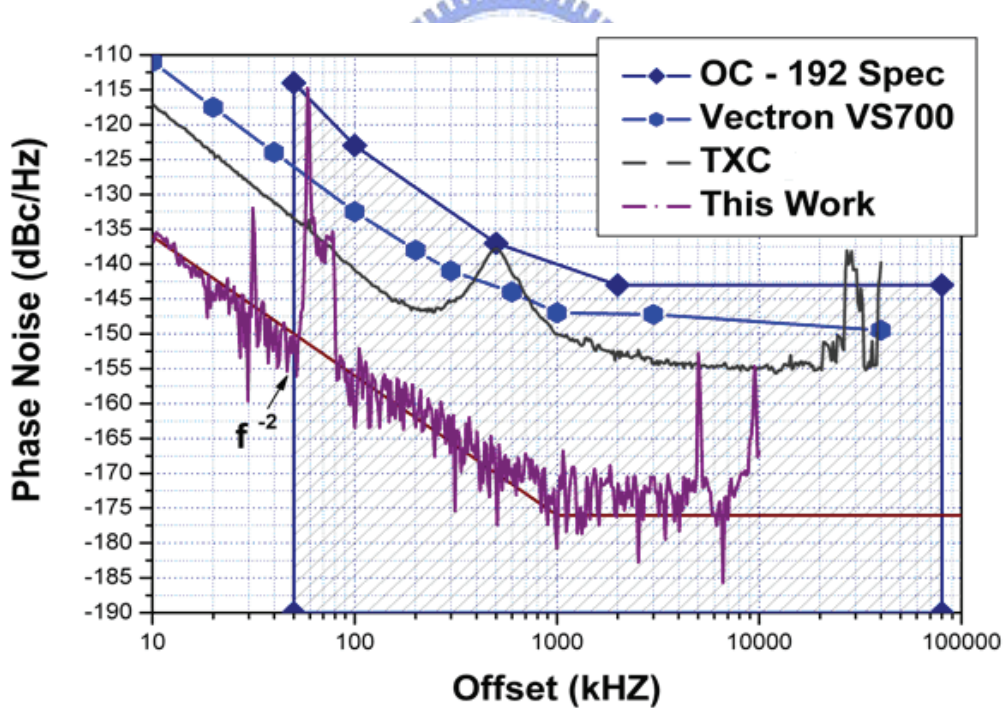


Fig. 4-14 Phase noise comparison for different SAW oscillators.

The product of TXC is fabricated by 0.35um CMOS process and this work is fabricated by 0.18um CMOS process. The gate resistance is about $8\Omega/\text{sq}$ at 0.18um

CMOS process and $35 \text{ } \Omega/\text{sq}$ in $0.35\mu\text{m}$ CMOS process. The f_i of $0.35\mu\text{m}$ CMOS process is about 13 GHz and the f_i of $0.18\mu\text{m}$ CMOS process is about 34 GHz. The large difference of f_i and gate resistance between two different processes makes the low phase noise of this work. Another reason is only one transistor is used as active device.



Chapter 5

Balanced Oscillator with One-port SAW Resonator

5.1 Introduction

Balanced circuit topologies are widely used to enhance circuit's performance, such as differential amplifier and balance mixer. But how to generate accurate antiphase signals is the most difficult part of circuit design. Traditionally, balanced signals are obtain by the use of passive or active baluns. Several oscillator circuits have been reported that have two identical oscillators operating in antiphase. The resonators may be in the form of dielectric resonators [12], hairpin resonator[13], microstrip patch resonators[14], or 180 degree phase shifter[15].

A technique for generating accurate antiphase signals is presented in this work. A simplified analysis of the balance oscillator and measurement results of two identical oscillators with one-port SAW resonator at 433 MHz are presented to demo this technique. Based on this balanced SAW oscillator, a push-push oscillator can be constructed. By using the feature of the accurate antiphase signals, the phase noise and the even harmonics of the push-push oscillator can be improved.

5.2 Oscillator Design

The core circuit of this balanced oscillator is a Colpitts oscillator stabilized with one-port SAW resonator and is shown as Fig. 5-1. The base-to-emitter capacitors cause each device to exhibit negative resistance, as well as some reactance. In the SAW resonator, the surface waves are trapped between the two reflectors of Fig 2-1(a), making multiple transits between them and creating a standing wave, like

electromagnetic waves in a cavity resonator. This one-port SAW resonator serves as the tank of the SAW oscillator and acts like a short-circuited $\frac{\lambda}{2}$ cavity, which the zero node voltages and maximum node currents are at both of the terminals of the resonator. Some important parameters of the transistor are listed in the Table 5.1 and the equivalent circuit model of the one-port SAW resonator used in this oscillator is shown as Fig. 5-2.

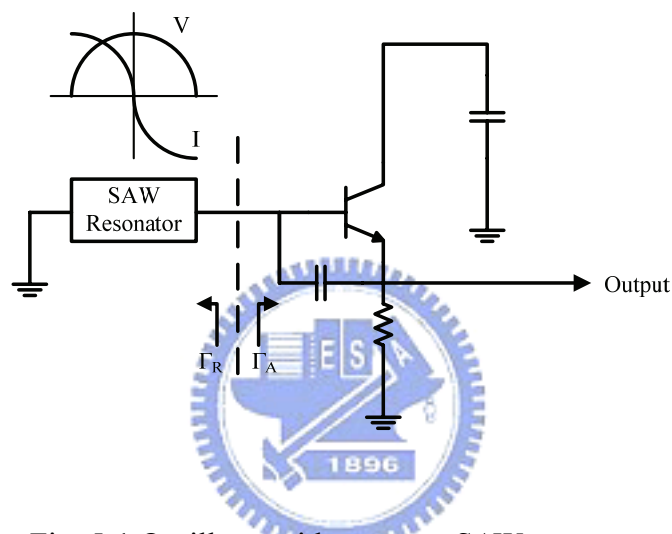
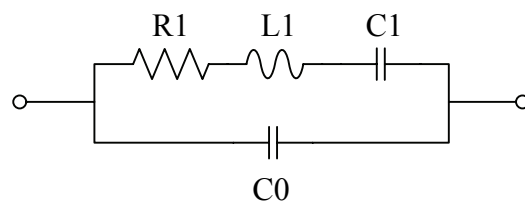


Fig. 5-1 Oscillator with one-port SAW resonator.



$$L1 = 72\mu\text{H}$$

$$C1 = 1.9 \text{ fF}$$

$$R1 = 13 \Omega$$

$$C0 = 2.7\text{pF}$$

Fig. 5-2 Equivalent circuit model for one-port SAW resonator.

Table 5.1: Parameters of the transistor.

Characteristic	Typical Value
DC Current Gain (h_{FE})	75 to 150
Gain Bandwidth Product (f_T)	12.0 GHz
Feed-Back Capacitance (C_{re})	0.4pF
Noise Figure (NF)	1.5dB

The oscillation condition can be expressed as:

$$\Gamma_A \cdot \Gamma_R = 1$$

This equation implies amplitude and phase conditions:

$$|\Gamma_A| \cdot |\Gamma_R| = 1$$

$$\theta_A + \theta_R = 0$$

Based on this core circuit, the balanced oscillator is constructed by two identical SAW oscillators and shown in Fig. 5-3. The one-port SAW resonator acts as the tank of the SAW oscillator and is also applied for the coupling network between two identical oscillators. The oscillation frequency is the resonant frequency of the SAW resonator which is under fundamental vibration mode. Under fundamental vibration mode, the RF currents of the opposite plates of the resonator is out of phase, which leads to the corresponding outputs of two identical oscillators 180° out of phase. Both of the terminals of the resonator in the balanced oscillator are virtual ground because the SAW resonator acts like a short-circuited $\frac{\lambda}{2}$ cavity, which the node voltages are zero. The oscillation condition for the oscillator can be expressed as:

$$\Gamma_{A1} \cdot \Gamma_{R1} = 1 \quad \text{and} \quad \Gamma_{A2} \cdot \Gamma_{R2} = 1$$

For the balanced structure,

$$\Gamma_{A1} = \Gamma_{A2} = \Gamma_A$$

$$\Gamma_{R1} = \Gamma_{R2} = \Gamma_R$$

Where Γ_A and Γ_R are the same as the half-circuit shown in Fig. 5-2.

This equation implies amplitude and phase conditions as follows:

$$|\Gamma_A| \cdot |\Gamma_R| = 1$$

$$\theta_A + \theta_R = 0$$

So, we can make sure the behavior of the half circuit of balanced SAW oscillator is the same as that of the one-side SAW oscillator.

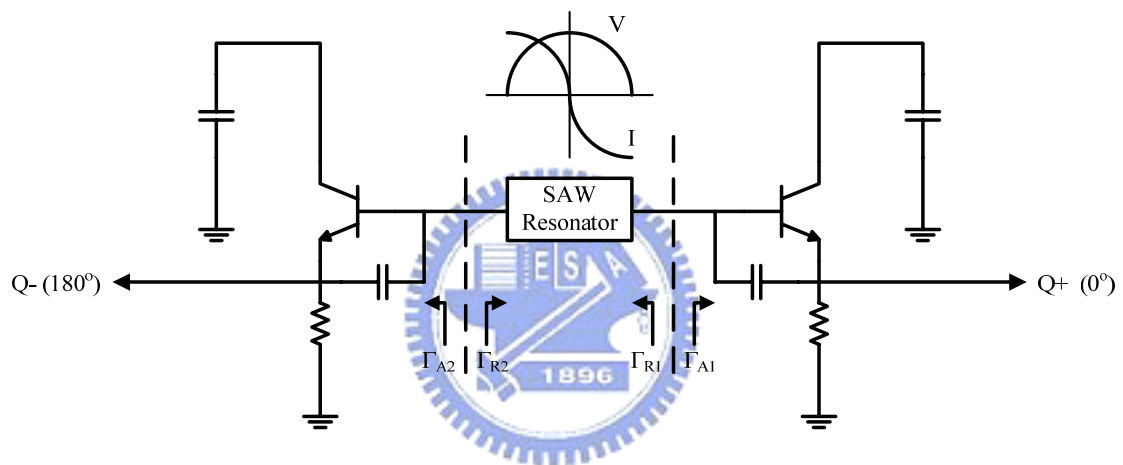


Fig. 5-3 Balanced oscillator with one-port SAW resonator.

The outputs of the balanced oscillator possess inherently in phase in even harmonics and 180° out of phase in odd harmonics. The differential outputs are fed to a output coupling network (0° or 180° power combiner) and a push-push oscillator will be available as shown in Fig. 5-4.

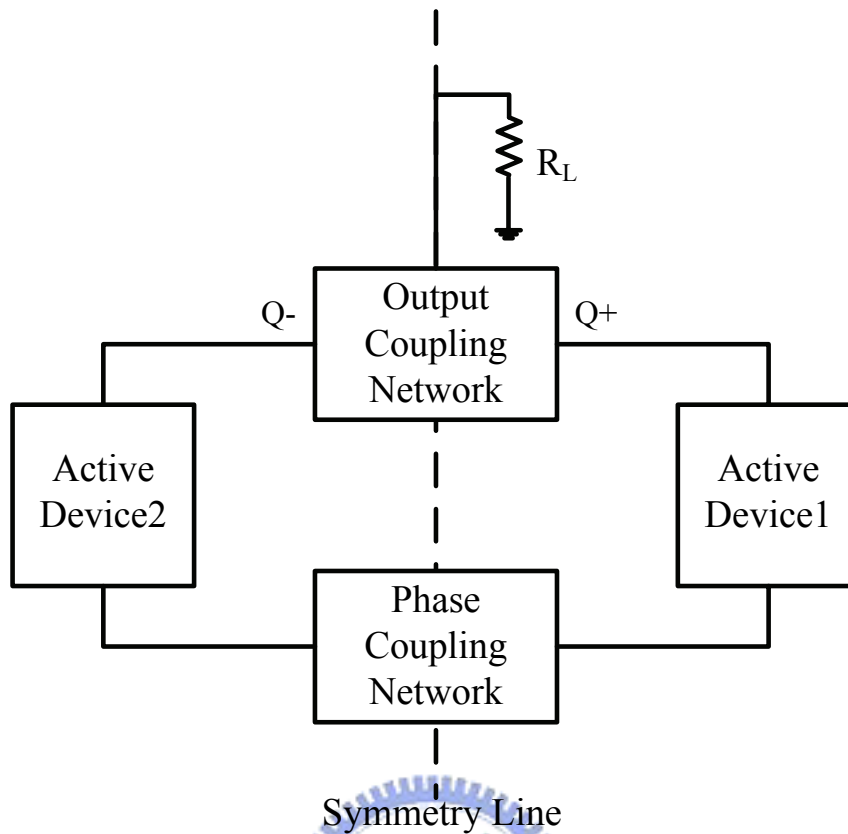


Fig. 5-4 Principle of push-push oscillator.

Since the even harmonics responses for SAW resonator, as shown in Fig. 2-1, is very weak, the push-push SAW oscillator is not suitable for operating at the twice fundamental frequency. For fundamental frequency operation, the push-push SAW oscillator can be used to suppress the even harmonics and improve the phase noise of the oscillator when the resonators with higher quality factors are not available. The strategy is using the 180° power combiner to cancel the undesired even harmonics and add the correlated fundamental oscillation carriers. All even harmonics are in phase in the balanced outputs and can in principle be completely cancelled. When the two outputs are combined using an 180° power combiner, the balanced RF output voltages are correlated and therefore to produce a 6-dB-higher combined output power. The increase in combined output power will lead to the improvement in phase noise of push-push oscillator.

5.3 Measurement and Discussion

The balanced SAW oscillator has been fabricated on FR4 substrate and its photograph is shown in Fig. 5-5. The detail circuit is shown in Fig. 5-6. The size of the pc board is 25mm x 25mm for the convenience of measurement. The oscillation starts when the DC voltage supplies to the transistor is 3.0V and the ASK input is also set to “High” (3.0V). Table 5.2 summarizes the data measured for the oscillator.

Table 5.2: Performance of balanced SAW oscillator.

Characteristic	Measured Results
Frequency	433 MHz
DC Voltage (Vcc)	3.0V
DC Current	17mA
Power Consumption	51mW
Output RF Power	3.0dBm

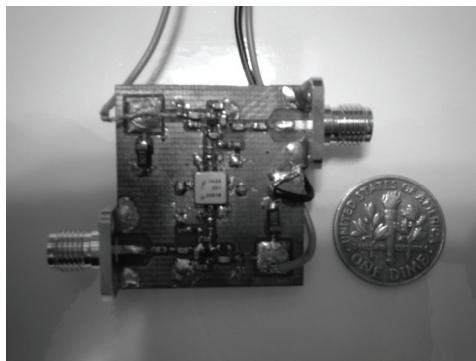


Fig. 5-5 Photograph of balanced SAW oscillator.

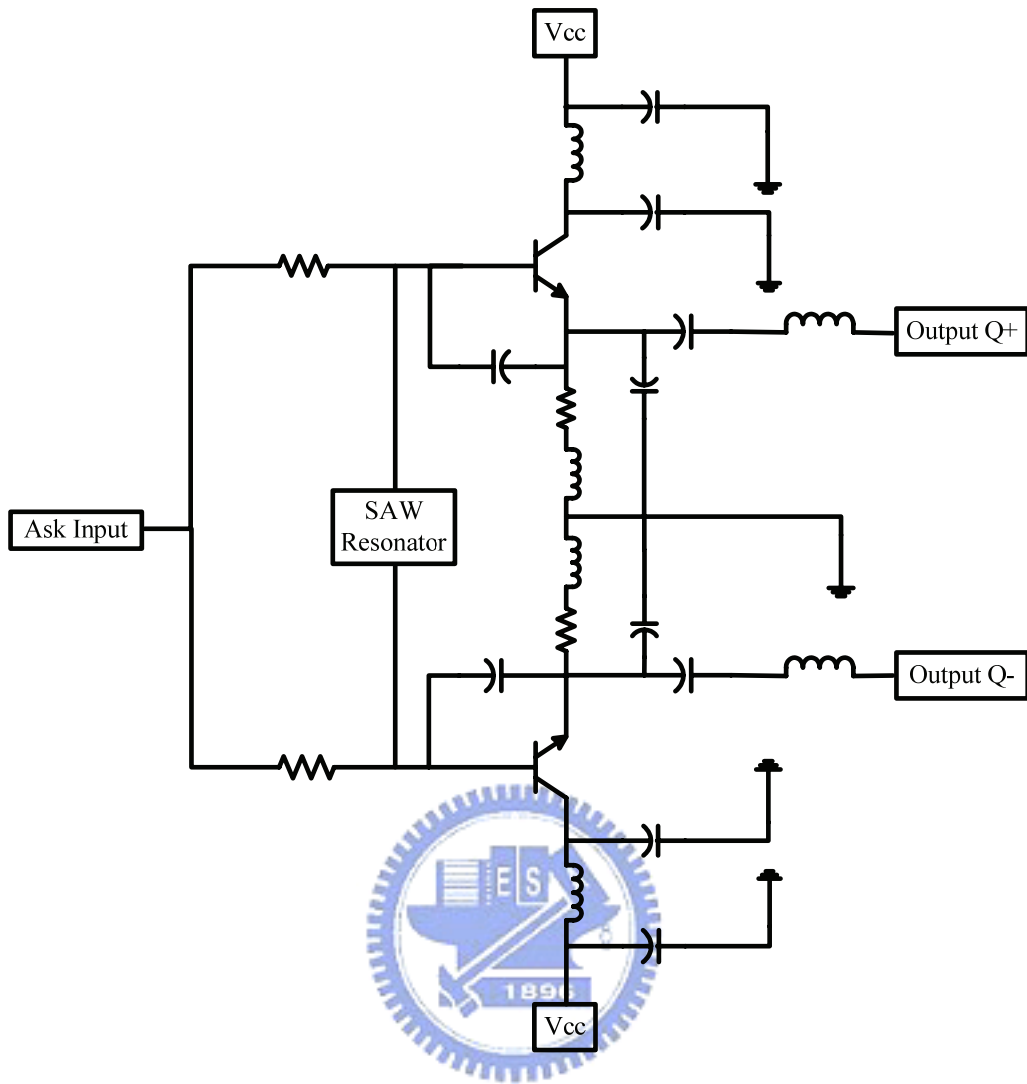


Fig. 5-6 Circuit diagram of balanced SAW oscillator with ASK switch.

Lecroy WAVE pro 954 oscilloscope is used to measure the output waveforms of the balanced oscillator. Fig. 5-7 shows the output waveforms of Q+ and Q-. We can see the two outputs are almost the same amplitude and indeed 180° out of phase.

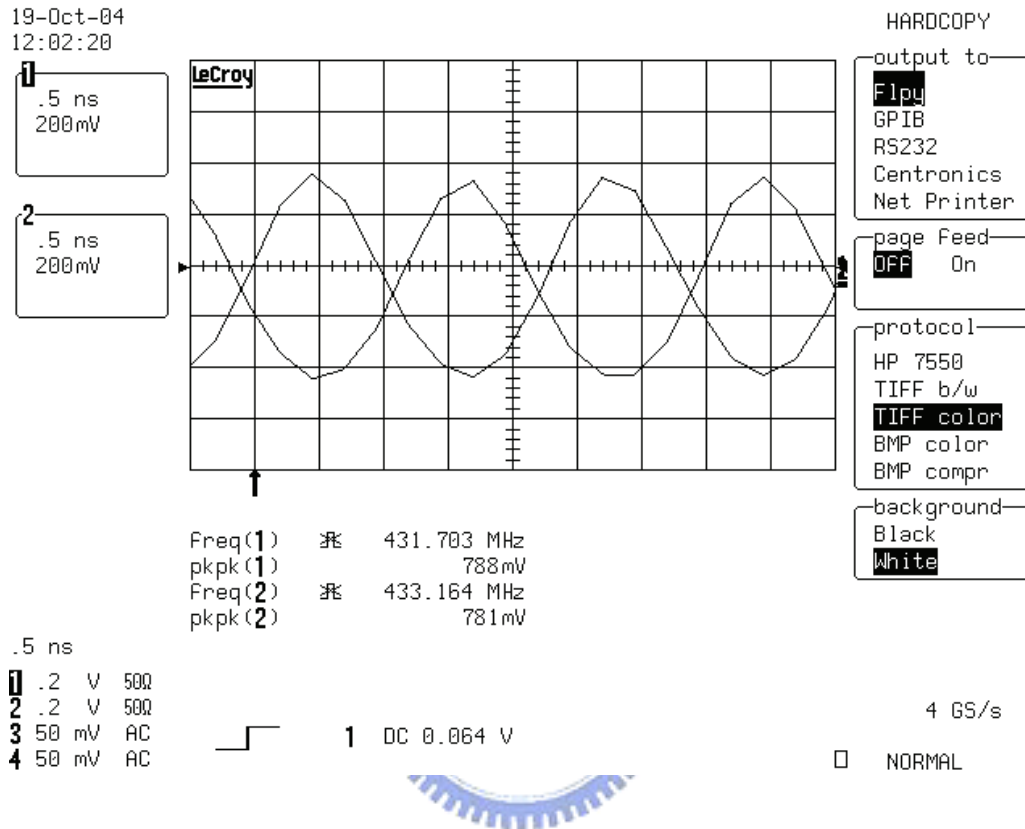


Fig. 5-7 Measured output waveforms of the balanced SAW oscillator.

HP 8561EC spectrum analyzer is used for the measurement of the oscillation frequency and harmonic spectrum for this oscillator. Fig. 5-8~11 present measurement results for the balanced oscillator. Fig. 5-8 and Fig. 5-9 show the harmonic spectrums for the output Q+ and Q-.

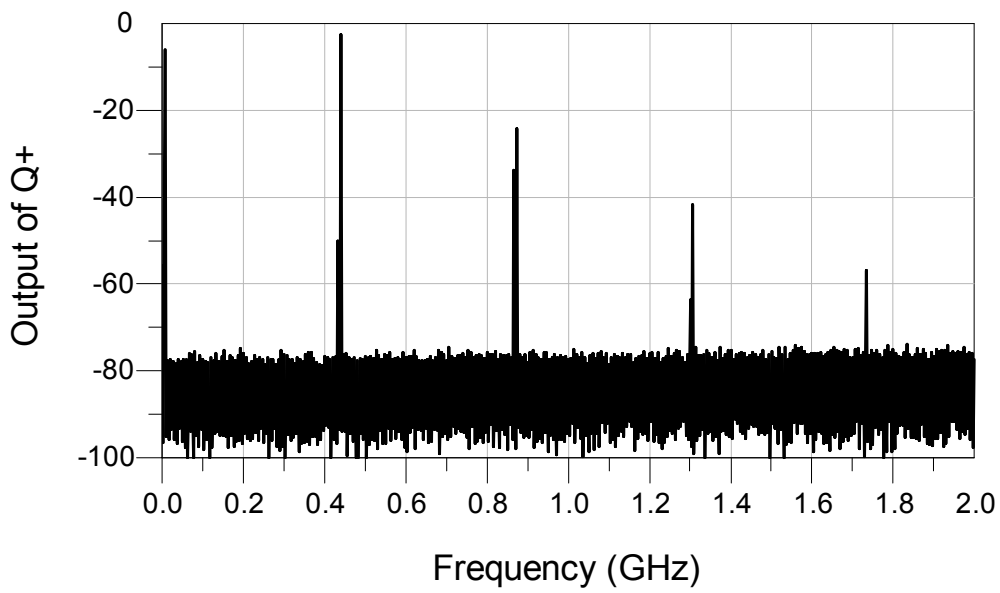


Fig. 5-8 Harmonic spectrum of the output Q+.

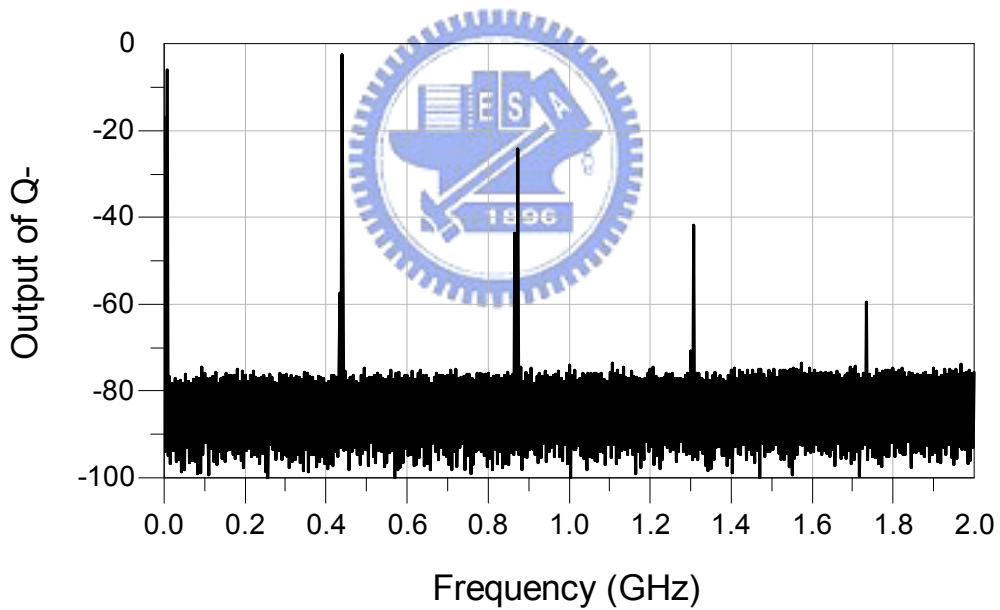


Fig. 5-9 Harmonic spectrum of the output Q-.

The harmonics spectrum of the balanced oscillator after the 180° power combiner is shown as Fig. 5-10. The suppression of even harmonics is achieved by feeding output signals to the 180° power combiner. Because even harmonics are in phase, they can in principle be totally cancelled. By replacing 180° power combiner with 0° power

combiner, Fig. 5-11 shows the suppression of odd harmonics and we can sure that the fundamental outputs of the oscillator are nearly exactly 180° out of phase.

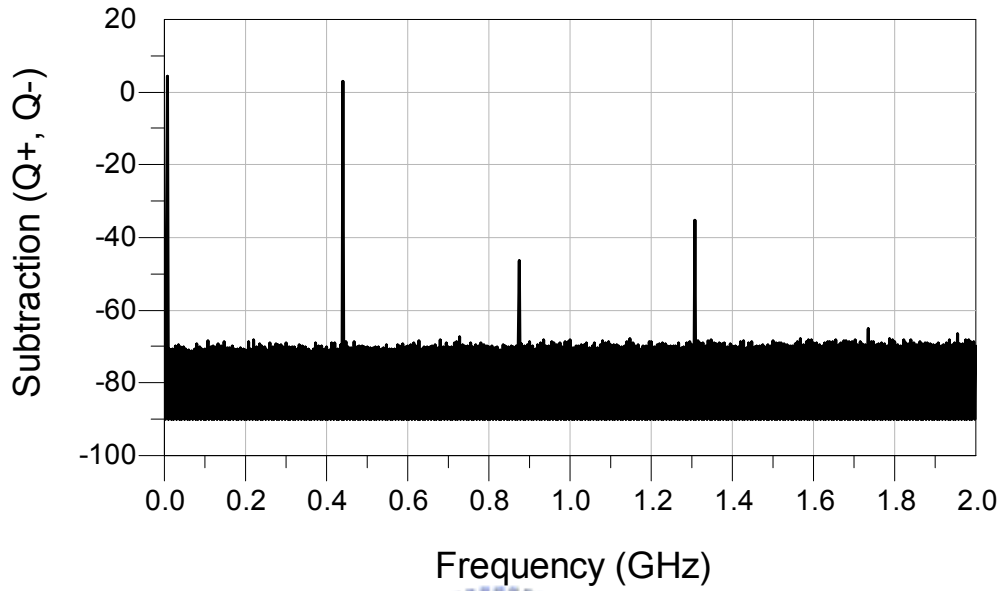


Fig. 5-10 Harmonic spectrum of the subtraction (Q+, Q-).

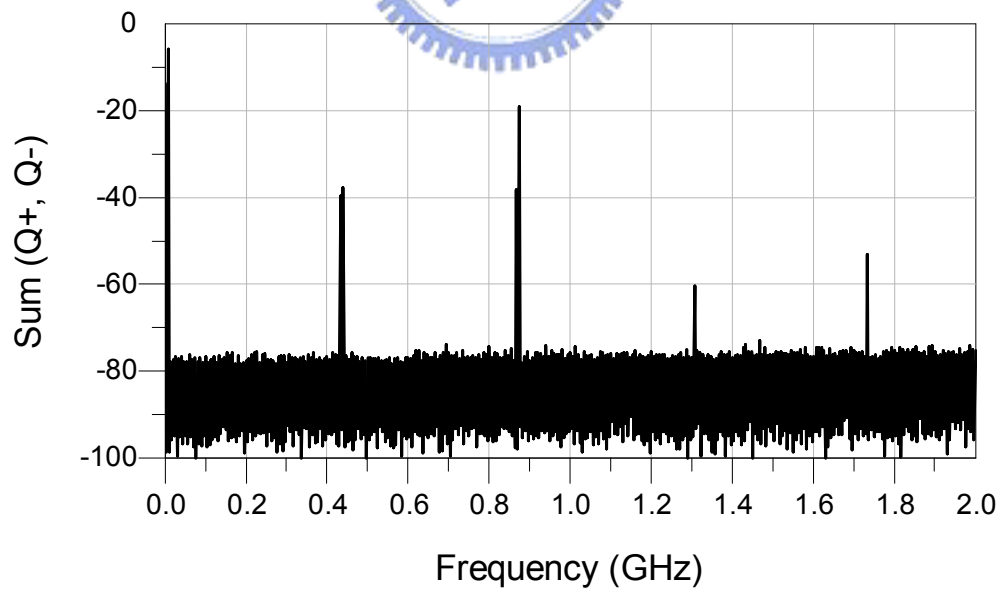


Fig. 5-11 Harmonic spectrum of the sum (Q+, Q-).

Table 5.3 reveals the harmonics before and after the 0° or 180° power combiners. The 22dB reduction factor in the second harmonic after 180° power combiners is remarkable. In the meantime, the degradation in third harmonic is negligible. It is noted that the cancellation of second harmonic is limited by the difference between these two identical oscillators, including the features of the transistors, circuit layout and other passive components.

Table 5.3: Harmonics before and after the 0° or 180° power combiner.

Harmonics	1st	2nd	3rd
Output of Q+	-2.50 dBm	-24.17 dBm	-41.83 dBm
Output of Q-	-2.50 dBm	-24.33 dBm	-41.83 dBm
Subtraction (Q+,Q-) (180° power combiner)	3.00 dBm	-46.33 dBm	-35.17 dBm
Sum (Q+,Q-) (0° power combiner)	-37.67 dBm	-19.00 dBm	-60.50 dBm

Agilent E5052A Signal Source Analyzer was used to measure the phase noise of the oscillator. The measured phase noise spectrum for this circuit is shown in Fig. 5-12. At 100 kHz offset from the carrier, the phase noise is about -158 dBc/Hz for balanced outputs and -164 dBc/Hz for the output combined with 180° power combiners. Beside an increase in output power level by about 6 dB, a significant reduction in phase noise was also observed. Since the noise voltage perturbations associated with the two identical active devices are uncorrelated with each other, the noise voltage will keep the same level at the linearly combined output. Thus, a 6 dB reduction in phase noise is expected, which is in good agreement with the measurement results.

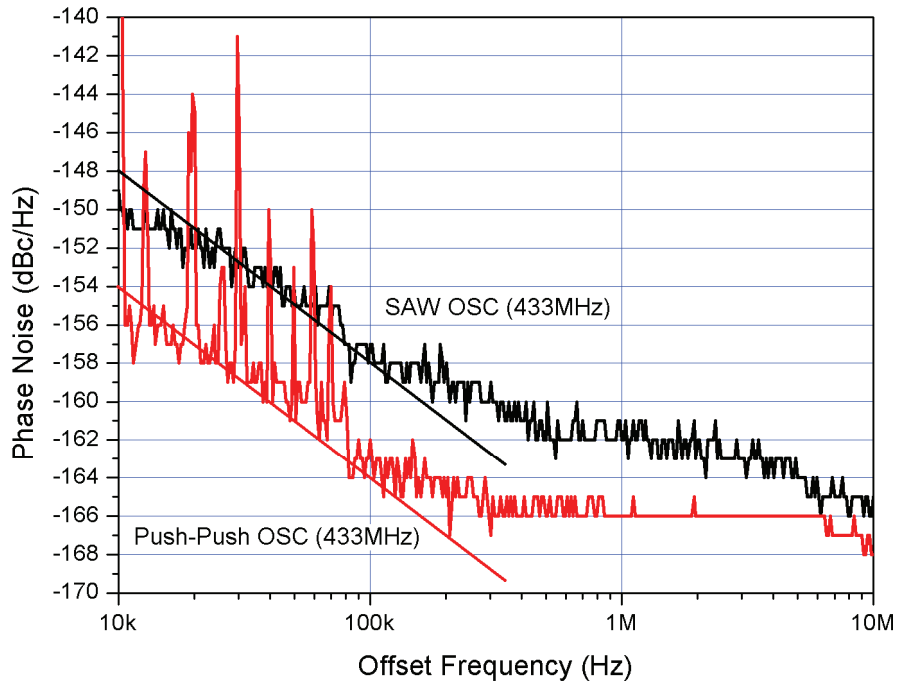


Fig. 5-12 Measured phase noise of SAW oscillator at 433 MHz.



Chapter 6

Conclusions

In this thesis, we introduce the basic structure of piezoelectric resonators, including SAW resonators and FBAR, and applied these different resonators for the oscillators in UHF band. There are four types of oscillators with piezoelectric resonators presented in this thesis: 2488 MHz voltage-controlled oscillator with STW resonator, 2488 MHz voltage-controlled oscillator with FBAR, 622 MHz modified Pierce oscillator with one-port SAW oscillator, and 433 MHz balanced oscillator with one-port SAW resonator.

The tuning ability of the 2488 MHz voltage-controlled oscillator with STW resonator achieves ± 200 ppm and its phase noise performance is 8dB better than the other commercial products at offset 100 kHz frequency. The white phase-noise floor is about -170dBc/Hz. In the design phase of this oscillator, we found that the lower phase noise of the oscillator can not be achieved by using the active devices with lower noise figure. By examining the residual phase noises of the main components in the oscillator, we found that the residual phase noise of the STW resonator dominates the phase noise of the oscillator, instead of active devices and the behavior of the phase noise is shaped by the important factor of group delay.

For developing the voltage-controlled FBAR oscillator, a FBAR is designed and fabricated with AlN thin film process. Using this resonator, a 2488 MHz voltage-controlled oscillator was designed and constructed with lump circuit components. The resonator is operated directly at the specific frequency 2488 MHz to avoid the degradation of phase noise due to frequency multiplication. The tuning capability achieves $\pm 6\%$. The 2nd harmonics of oscillator is suppressed below 40 dB. The oscillator provides 14.5dBm of output power and consumes 65mA from +5V DC

power supply. The temperature coefficients factor of the oscillator is about $-34.5\text{ppm}/^{\circ}\text{C}$ which dominated by the FBAR.

The modified Pierce oscillator is studied. The active part of the oscillator is designed and fabricated by tsmc 0.18um CMOS integrated circuit. With only one NMOS transistor and an extra phase shifter, the oscillation can be easily obtained than the conventional Pierce oscillator. The oscillator provides 4.0dBm of output power and the core circuit consumes 10.2mA from +1.2V DC power supply. The total current consumption is about 15mA from +1.2V DC power supply. The measured white phase noise floor is $-175\text{dBc}/\text{Hz}$ for carrier offset frequency greater than 1 MHz. The phase noise level of the oscillator is approximately $-136\text{dBc}/\text{Hz}$ at 10 kHz carrier offset.

With a popular commercial one-port SAW resonator, the behavior of the balanced SAW oscillator is presented. The balanced SAW oscillator can provide pure antiphase signals without using passive or active balun. The antiphase signals are verified by feeding to a 0° or 180° power combiner and the measurement results have good agreements to that expected. By using an 180° power combiner, we can construct a push-push topology oscillator and improve the phase noise by 6dB in comparison with the single-end output.

References

- [1] D. B. Leeson, "A simple model of feedback oscillator noise spectrum," *Proc. IEEE*, vol. 54, no. 2, pp. 329-330, Feb. 1966.
- [2] L. Rayleigh, "On Waves Propagating along the Plane Surface of an Elastic Solid," *Proc. London Math. Soc.*, vol. 7, pp. 4-11, 1885.
- [3] R. M. White and F. W. Volmer, "Direct Piezoelectric Coupling to Surface Elastic Waves," *Appl. Phys. Lett.*, vol. 17, pp. 314-316, 1965.
- [4] K. Hashimoto, *Surface Acoustic Wave Devices in Telecommunications*. Berlin, Germany: Springer-Verlag, 2000.
- [5] 台南科學工業園區創新技術研究發展計畫獎助執行成果報告, "以表面聲波共振器為振盪源之高性能壓控振盪器的開發" 立朗科技股份有限公司, 計畫編號: 92-1001-B062-001.
- [6] O. Ishii, H. Iwata, M. Sugano, and T. Ohshima, "UHF AT-CUT crystal resonators operating in the fundamental mode", in *IEEE Int. Freq. Control Symp.*, 1998, pp. 975-980.
- [7] N. Nomura, M. Itagaki, and Y. Aoyagi, "Small packaged VCSO for 10Gbit Ethernet application", in *IEEE Int. Ultrason., Ferroelectr., Freq. Control Symp.*, 2004, pp. 418-421.
- [8] B. Fleischmann, A. Roth, P. Russer, and R. Weigel, "A 2.5 GHz Low Noise Phase Locked Surface Transverse Wave VCO," in *IEEE Int. Ultrason., Ferroelectr., Freq. Control Symp.*, 1989, pp. 65-69.
- [9] I. D. Avramov, "Very Wide Tuning Range, Low-Noise Voltage Controlled Oscillators using Ladder Type Leaky Surface Acoustic Wave Filters", in *IEEE Ultrason., Ferroelectr., Freq. Control Symp.*, 1998, pp. 489-496.

- [10] C. E. Hay, M. E. Harrell, and R. J. Kansy, "2.4 and 2.5 GHz Miniature, Low-Noise Oscillators Using Surface Transverse Wave Resonators and a SiGe Sustaining Amplifier," in *IEEE Int. Ultrason., Ferroelectr., Freq. Control Symp.*, 2004, pp. 174-179.
- [11] T. L. Bagwell and R. C. Bray, "Novel Surface Transverse Wave Resonators with Low Loss and High Q," in *Proc. IEEE Ultrason. Symp.*, 1987, pp. 319-324.
- [12] A. M. Pavio and M. Smith, "Push-push dielectric resonator oscillator," in *IEEE MTT-S Int. Microw. Symp. Dig.*, 1985, pp. 188-195.
- [13] J. Birkeland, and T. Itoh, "Spatial power combining using push-pull FET oscillators with microstrip patch resonators," in *IEEE MTT-S Int. Microw. Symp. Dig.*, 1990, pp. 1217-1220.
- [14] H. Yabuke, M. Sagawa, and M. Makimoto, "Voltage controlled oscillators using the miniaturized hairpin resonators," in *IEEE MTT-S Int. Microw. Symp. Dig.*, 1991, pp. 1175-1178.
- [15] X. Zhou and A. S. Daryoush, "An injection locked push-pull oscillator at Ku-band," *IEEE Microw. Guide Wave Lett.*, vol. 3, pp. 244-246, Aug. 1993.
- [16] K. S. Ang, M. J. Underhill, and I. D. Robertson, "Balanced Monolithic Oscillators at K- and Ku-band," *IEEE Trans. Microw. Theory and Tech.*, vol. 48, no. 2, pp. 187-193, Feb. 2000.
- [17] T. W. Grudkowski, J. F. Black, T. M. Reeder, D. E. Cullen, and R. A. Wagner, "Fundamental Mode UHF/VHF Miniature Resonators and Filters," *Applied Physics Lett.*, vol. 39, no. 11, pp. 993-995, Nov. 1980.
- [18] K. M. Lakin and J. S. Wang, "Acoustic Bulk Wave Composite Resonators," *Applied Physics Lett.*, vol. 39, no. 3, pp. 125-128, Feb. 1981.

- [19] C. Vale, J. Rosenbaum, S. Horwitz, S Krishnaswamy, and R. Moore, "FBAR Filters at GHz Frequencies," in in *Proc. IEEE, 45th. Annual Freq. Control Symp*, 1991, pp. 332-336.
- [20] M. Kitayama, T. Fukuichi, T. Shiosaki, and A. Kawabata, "VHF/UHF Composite Resonator on a Silicon Substrate," *J. J. Appl. Phys.* vol. 22, Suppl. 22-3, pp. 139-141, 1983.
- [21] K. Nakamura, Y. Ohashi, and H. Shimizu, "UHF Bulk Acoustic Wave Filters Utilizing Thin ZnO/SiO₂ Diaphragms on Silicon," *J. J. Appl. Phys.* vol. 25, no. 3, pp. 371-375, 1986.
- [22] K.M. Lakin, G.R. Kline and K.T. McCarron, "Thin Film Bulk Acoustic Filters for GPS," in *Proc. IEEE Ultrason. Symp.*, 1992, pp. 471-476.
- [23] K.M. Lakin, "Modeling of Thin Film Resonators and Filters," in *IEEE MTT-S Int. Microw. Symp. Dig.*, June 1992, pp. 149-152.
- [24] Q. X. Su, P/B. Kirby, E. Komuro, and R.W. Whatmore, "Edge Supported AnO Thin Film Bulk Acoustic Wave Resonators and Filter Design", in *Proc. IEEE/EIA Int. Freq. Control Symp. and Exhibition*, 2000, pp 434-440.
- [25] R. Ruby, P. Bradley, J. D. Larson III, and Y. Oshmyansky, "PCS 1900 MHz duplexer using thin film bulk acoustic resonator (FBARS)," *Electron. Lett.*, vol. 35, no.10, May. 1999.
- [26] J. D. Larson III, P. Bradley, S. wartenberg, and R. Ruby, "Modified butterworth-Van Dyke Equivalent Circuit for FBAR Resonators and Automated Measurement System," in *IEEE Int. Ultrason. Symp.*, 2000, Paper 3H-5.
- [27] J. D Larson, S.M. Ruby, P. Bradley, and Y. Oshmyansky, "A BAW Antenna Duplexer for the 1900 PCS Band," in *Proc. IEEE Ultrason. Symp.*, 1999, pp. 887-890.

- [28] P. Osbond, C. M. Beck, D. J. Brierley, M. R. Cox, S. P. Marsh, and N. M. Shorrocks, "The Influence of ZnO and Electrode Thickness on the Performance of Thin Film Bulk Acoustic Wave Resonators," in *Proc. IEEE Ultrason. Symp.*, 1999, pp. 911-914.
- [29] R. Ruby, J. D. Larson III, J. Wen, S. L. Kok, R. Buted, and D. Figueredo, "Power Handling and Temperature Coefficient Studies in FBAR Duplexers for the 1900 MHz PCS Band," in *IEEE Int. Ultrason. Symp.*, 2000, Paper 3H-6.
- [30] H. Satoh, Y. Ebata, H. Suzuki, and C. Narahara, "An Air Gap Type Piezoelectric Composite Resonator," in *Proc. IEEE, 39th. Annual Freq. Control Symp*, 1985, pp. 361-366.
- [31] C. W. Seabury, J. T. Cheung, P. H. Korbin, and R. Addison, "High Performance Microwave Air-Bridge Resonators," in *Proc. IEEE, Ultrason. Symp.*, 1995, pp. 909-911.
- [32] W. E. Newell, "Face-Mounted Piezoelectric Resonators," in *Proc. IEEE*, vol. 53, pp. 575-581, June 1965.
- [33] T. E. Parker and G. K. Montress, "Precision Surface Acoustic Wave (SAW) Oscillator," *IEEE Trans. Ultrason., Ferroelectr., Freq. Control*, vol. 35, no. 3, pp. 342-364, May 1988.
- [34] R. S. Naik, J. J. Lutsky, R. Reif, C. G. Sodini, A. Becker, L. Fetter, H. Huggins, R. Miller, J. Pastalan, G. Rittenhouse, and Y.H. Wong, "Measurements of the bulk, c-axis electromechanical coupling constant as a function of AlN film quality," *IEEE Trans. Ultrason., Ferroelectr., Freq. Control*, vol. 47, pp. 292-296, 2000.
- [35] H. Lee, J. Park, K. Lee, Y. Ko, and J. Bu, "Silicon Bulk Micromachined High Q Film Bulk Acoustic Resonator Devices with Mo/AlN/Mo Structures," *Integrated Ferroelectrics*, vol. 69, pp. 323-332, 2005.

- [36] R. Aigner, L. Elbrecht, T. R. Herzog, H. Siegertsbrunn, S. Marksteiner, and W. Nessler, "Bulk-Acoustic-Wave Filters: Performance Optimization and Volume Manufacturing," in *IEEE MTT-S Int. Microw. Symp. Dig.*, 2003, pp. 2001-2004.
- [37] G. S. Kino, *Acoustic Waves: Devices, Imaging, and Analog Signal Processing* New Jersey: Prentice-Hall, 1987 pp. 549.
- [38] W. Pang, H. Yu, H. Zhang, and E. S. Kim, "Temperature-Compensated Film Bulk Acoustic Resonator above 2 GHz," *IEEE Electron Device Lett.*, vol. 26, no. 6, pp. 369-371, June 2005.
- [39] G.F. Iriarite, Dr. Thesis, Faculty of Science and Technology, Uppsala University, Sweden, 2003.
- [40] R. Aigner, L. Elbrecht, T. R. Herzog, H. Siegertsbrunn, S. Marksteiner, and W. Nessler, U.S. Patent 6878604B2, 2005.
- [41] G. D. Vendelin, A. M. Pavio, and U. L. Rohde, *Microwave Circuit Design Using Linear and Nonlinear Techniques*, 2nd ed., New Jersey: Wiley, 2005, p.550.
- [42] G. K. Montress, T. E. Parker, and M. J. Loboda, "Residual Phase Noise Measurements of VHF, UHF, and Microwave Components," *IEEE Trans. Ultrason., Ferroelectr., Freq. Control*, vol. 41, no. 5, pp. 664-679, Sep. 1994.
- [43] T. E. Parker and G. K. Montress, "Precision Surface Acoustic Wave (SAW) Oscillator," *IEEE Trans. Ultrason., Ferroelectr., Freq. Control*, vol. 35, no. 3, pp. 342-364, May 1988.
- [44] *Agilent E5505A Phase Noise Measurement System User's Guide*, 1st ed., Agilent Technology, Jun. 2004.
- [45] A. Hati, D. A. Howe, F. L. Walls, and D. Walker, "Noise Figure vs. PM Noise Measurement: A Study at Microwave Frequency," in *Proc. IEEE Int. Freq. Control Symp. and PDA Exhibition*, 2003, pp. 516-520.
- [46] D. Scherer, "Design Principles and Measurement of Low Phase Noise RF and Microwave Sources," presented at the Hewlett-Packard RF and Microw. Meas. Symp. and Exhibition, Hasbrouck Heights, NJ, 1979.

- [47] C. Schiebold, "Theory and Design of the Delay Line Discriminator for Phase Noise Measurement," *Microw. Journal*, pp.103-112, December 1983.
- [48] R. W. Rhea, *Oscillator Design and Computer Simulation*, 2nd ed., Atlanta, GA : Nobel Publishing, 1995.
- [49] M. Cavin, N. Eisenhauer, and D. C. Malocha, "Parameter Extraction of SAW Resonator Equivalent Circuit Parameters and Package Parasitics," in *Proc. IEEE Freq. Control Symp.*, 1992, pp. 384-390.
- [50] David M. Pozar, *Microwave Engineering*, 2nd ed., John/Wiley & Sons, Inc. 1998, pp. 206-213.
- [51] R. Pettai, *Noise in Receiving System*, New York: Wiley, 1984, pp. 132.
- [52] <http://www.vectron.com>, accessed April 2007.
- [53] M.C. King, Z. M. Lai, C. H. Huang, C. F. Lee, M. W. Ma, C. M. Huang, Y. Chang, and Albert Chin, "Modeling Finger Number Dependence on RF Noise to 10 GHz in 0.13um Node MOSFETs with 80nm Gate Length," in *IEEE Radio Freq. Integrated Circuits Symp.*, 2004, pp. 171-174.